UNIVERSITY OF NAIROBI
FACULTY OF SCIENCE AND TECHNOLOGY
DEPARTMENT OF CHEMISTRY

PHYTOCHEMICAL INVESTIGATION OF FIVE *PENTAS* SPECIES FOR LEISHMANICIDAL PRINCIPLES
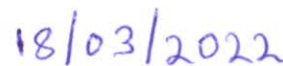
By

Vicent Kamya

I56/15292/2018

A Thesis Submitted in Partial Fulfilment of the Requirements for the Award of the Degree of Master of Science in Chemistry of the University of Nairobi

2022

DECLARATION

I declare that this thesis is my original work and has not been submitted elsewhere for examination, award of a degree or publication. Where other people's work or my work has been used, this has properly been acknowledged and referenced following the University of Nairobi requirements.

_____   18/03/2022

Kamya, Vicent   Date
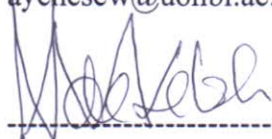
(I56/15292/2018)

Department of Chemistry

University of Nairobi

This thesis has been submitted with our approval as research supervisors:

_____   18/3/2022

Professor Abiy Yenesew   Date

Department of Chemistry

University of Nairobi

P.O. Box 30197-00100

Nairobi Kenya

ayenesew@uonbi.ac.ke

_____   18/03/2022

Dr Albert Ndakala   Date

Department of Chemistry

University of Nairobi

P.O. Box 30197-00100

Nairobi Kenya

andakala@uonbi.ac.ke

DEDICATION

I dedicate this thesis to my parents, Mr Anatooli Mulindwa and Ms Scovia Tebitondwa.

ACKNOWLEDGEMENTS

ABSTRACT

Leishmaniasis is a disease complex instigated by a protozoan parasite of the genus *Leishmania*. Contemporary chemotherapies for leishmaniasis employ pentamidine (**1**), amphotericin B (**2**) and pentavalent antimonials (**3**). The efficacy of these drugs has deteriorated due to drug resistance. The drugs also pose unbearable side effects owing to their toxicity. Some metabolites from the genus *Pentas* (family Rubiaceae) have been reported to show antiprotozoal activity against *Plasmodium* species, but no studies on antileishmanial activity have been done. The study was focused on investigating five *Pentas* species for antileishmanial principles. The CH_2Cl_2/CH_3OH (1:1) extracts of the roots and/or stems of *Pentas bussei, P. longiflora, P. micrantha, P. parvifolia* and *P. zanzibarica* were subjected to a combination of chromatographic separations resulting in the isolation of 14 compounds. The pure compounds were characterized by utilizing ^1H NMR, ^{13}C NMR, ^1H-^1H COSY, HMBC, HSQC and MS. The crude extract from the roots of *Pentas parvifolia* yielded busseihydroquinone B (**51**). The stem bark of *Pentas parvifolia* yielded β-stigmasterol (**50**) and β-amyrin (**95**). The aerial parts of *P. parvifolia* yielded vanillic acid (**96**), *p*-hydroxybenzoic acid (**97**) and protocatechuic acid (**98**). The aerial part of *P. bussei* yielded β-stigmasterol (**50**), a homoprenylated naphthoquinone (**55**), busseihydroquinone A (**7**), busseihydroquinone B (**51**), busseihydroquinone C (**52**) and methyl-8-hydroxy-1,4,6,7-tetramethoxy-2-naphthoate (**47**), which is a new compound. The aerial parts of *P. micrantha* yielded 2-methoxy-3-methyl-anthracene-9,10-dione (**72**). The stem bark of *P. zanzibarica* yielded rubiadin-1-methyl ether (**65**) and rubiadin (**64**). The roots of *Pentas longiflora* yielded pentalongin (**74**). Pentalongin (**74**) showed antileishmanial activity (IC_{50} = 11 µM) against the antimony sensitive strain of *Leishmania donavani* (MHOM/IN/83/AG83). It also generated a substantial amount of nitric oxide in the cell culture (IC_{50} = 1.08 µM) relative to the positive control, miltefosine (**4**), (IC_{50} = 1.11 µM). Busseihydroquinone A (**7**) was oxidized with silver (I) oxide to yield 1-hydroxy-4,6-dimethoxy-7,8-dioxo-7,8-dihydro-naphthalene-2-carboxylic acid methyl ester (**99**). Through computational modelling, the inhibitory potential of phytochemicals from the genus *Pentas* for *Leishmania infantum* trypanothione reductase was studied using UCSF Chimera 1.15. Among the studied compounds, schimperiquinone A (**92**) exhibited the highest affinity for the binding site of the receptor; with a binding energy of -10.9 kcal/mol. Anthraquinones generally showed superior inhibitory potency for *Leishmania infantum* trypanothione reductase than naphthoquinones. Overall, the phytochemicals from the genus *Pentas* showed sustained hydrogen bonds with Thr335, Lys60 and Cys52; these amino acid residues assist FAD to achieve a proper orientation towards the catalytic site of the enzyme. Therefore, the quinones from the genus *Pentas* have the potential to guide the development of antileishmanial drug agents. Given the distinctive binding mode of some of the anthraquinones and naphthoquinones observed here, the compounds should be subjected to *in vitro* and *in vivo* studies.
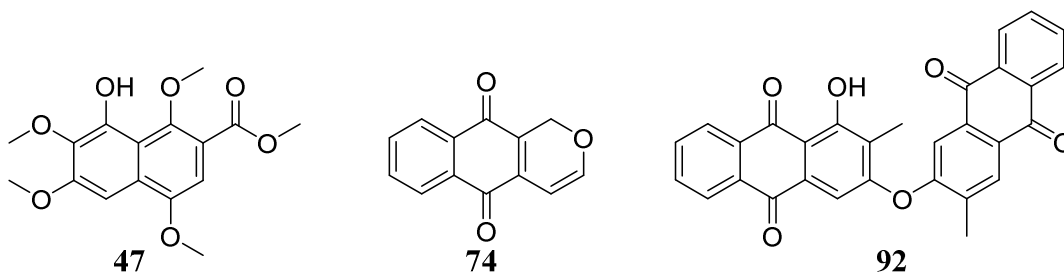
47

74

92

TABLE OF CONTENTS

LIST OF TABLES

LIST OF FIGURES

LIST OF SCHEMES

LIST OF APPENDICES

LIST OF ACRONYMS AND SYMBOLS

CADD	Computer Aided Drug Design
CFR	Case Fatality Rate
ESI-MS	Electron Spray Ionisation Mass Spectrometry
FAD	Flavin-adenine dinucleotide
GCG	Bis(gamma-glutamyl-cysteinyl glycinyl)spermidine
HMG-CoA	3-Hydroxy-3-methylglutaryl coenzyme A
HMBC	Heteronuclear Multiple Bond Correlation
HSQC	Heteronuclear Single Quantum Coherence
IC_{50}	50% Inhibition Concentration
*Li*TR	*Leishmania infantum* trypanothione reductase
MMFF	Merck Molecular Force Field
NMR	Nuclear Magnetic Resonance
NOESY	Nuclear Overhauser Effect Spectroscopy
PTLC	Preparative Thin Layer Chromatography
QSAR	Quantitative Structural Activity Relationship
UV	Ultraviolet
WHO	World Health Organization

CHAPTER ONE

INTRODUCTION

1.1   Background Information

Leishmaniasis is a set of protozoan-based infections with numerous clinical indicators: destructive mucosal inflammation and ulcerative skin lesions; it is caused by over 20 species of *Leishmania* parasite (Kaye *et al*., 2020). Worldwide, two (2) million cases of leishmaniasis occur annually, and three hundred fifty million people are at risk of getting infected (Jawed and Majumdar, 2018). According to WHO (2017), over 95% of the new cases of visceral Leishmaniasis were reported to occur in four Asian and five African countries. In July 2019, a total of 1,564 leishmaniasis cases were reported by WHO (2019) in Marsabit and Wajir, Counties of Kenya. WHO (2021) reported 873 cases of visceral leishmaniasis in Marsabit, Garissa, Kitui, Baringo, West Pokot, Mandera and Wajir since January 2020 which accounted for 9 deaths (CFR 1.0%).

Leishmaniasis is one of the neglected tropical diseases; it affects mainly the marginalised communities that cannot afford to pay for the medication even when it is made available. Consequently, pharmaceutical companies, which are primarily profit-oriented do not find it cost effective to invest in the manufacture of drugs for such diseases (de Menezes *et al*., 2015).

To date, an effective vaccine against leishmaniasis has not been found. Leishmaniasis is largely treated using chemotherapeutic agents, usually entailing the use of antimony-based compounds administered by injection. In addition to the antimony-based drugs, pentamidine (**1**), amphotericin B (**2**) and Pentostam (sodium stibogluconate, **3**) are used (Jawed and Majumdar, 2018).

Pentamidine and pentostam are employed in East Africa to treat visceral leishmaniasis (Marlet *et al*., 2003). However, these drugs are highly toxic and relatively expensive. The current therapies for leishmaniasis are also faced with drug resistance, which significantly compromises their efficacy in combating the disease (Tiuman *et al*., 2011).

1

3

2
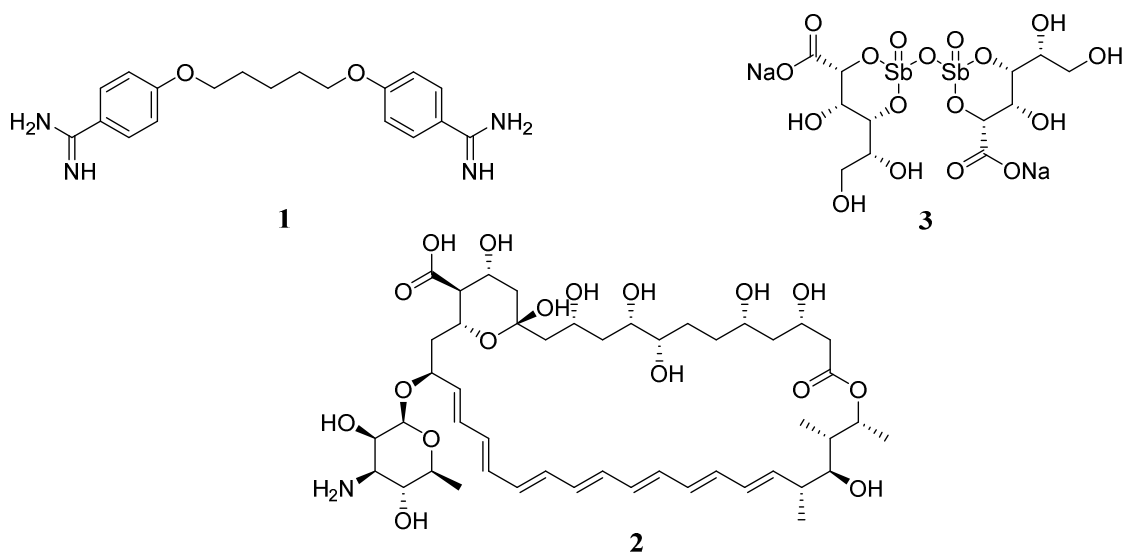
Nature-derived therapies have for millennia been irrefutably fundamental in the fight against protozoan based infections such as malaria, amoebiasis and leishmaniasis. Phytochemicals belonging to the classes of alkaloids, terpenoids, saponins, phenolics and quinones were reported to exhibit antileishmanial activity (Manuel and Luis, 2001). Some natural products from the Rubiaceae family, most notably quinine, have been reported to exhibit significant antiprotozoal activity. Endale (2012) reported substantial antiplasmodial activities for some phytochemicals in the genus *Pentas*.

1.2 Statement of the Problem

The available knowledge on leishmania has not yet translated into successful antileishmanial drug agents (de Menezes *et al*., 2015). Many of the therapies used for treating leishmaniasis such as pentamidine (**1**), miltefosine (**4**) and paromomycin (**5**) exhibit species-specific activity; they are only effective against particular strains of the pathogen (Arevalo *et al*., 2001 ; *Alvar et al*., 2006 ; Reithinger *et al*., 2007 ; Miranda-Verastegui *et al*., 2009). Furthermore, the conventional therapies for leishmaniasis widely involve the application of pentavalent antimony compounds which are associated with agonizing secondary side effects such as muscular-skeletal pains, renal failure, hepatotoxicity and cardiotoxicity (Reithinger *et al*., 2007; de Menezes *et al*., 2015; Jawed

2

and Majumdar, 2018). Consequently, this has dramatically lessened drug tolerability and resulted in treatment noncompliance and abandonment. Ultimately, the emergence of drug-resistant strains of leishmania is prevalent, this accounts for the remarkable decline in the efficacy of the conventional therapies. There is, therefore, an urgent need for interventions that include exploration of alternative drug molecules. The study was focused on the investigation of natural products for antileishmanial compounds. Particularly, the study was anchored on the phytochemical investigation of *Pentas* species; *P. parvifolia, P. bussei, P. micrantha, P. longiflora* and *P. zanzibarica* in the pursuit of safer and affordable leishmaniasis therapies.
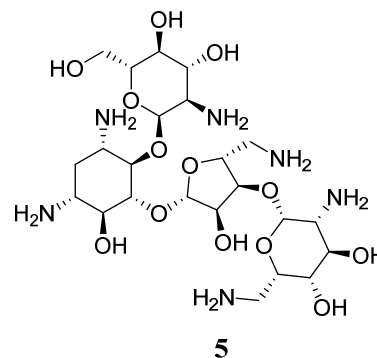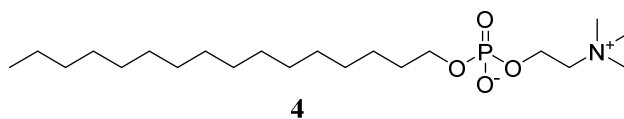
1.3   Objectives of the Study

1.3.1   General Objective

The general objective of this study was to identify antileishmanial principles from five *Pentas* species.

1.3.2 Specific Objectives

The specific objectives of this study were:

i. To isolate and characterize secondary metabolites from *P. parvifolia, P. bussei, P. micrantha, P. longiflora* and *P. zanzibarica*.

ii. To determine the antileishmanial activity of secondary metabolites isolated from *P. parvifolia, P. bussei, P. micrantha, P. longiflora* and *P. zanzibarica*.

iii. To predict the inhibitory potency of phytochemicals in the genus *Pentas* for *Leishmania infantum* trypanothione reductase through computational modelling.

iv. To enhance the antileishmanial activities of promising phytochemicals through structural modification.

1.4 Justification of the Study

Naphthalene derivatives such as plumbagin (**6**), a naphthoquinone isolated from *Plumbago rosea* (Kapadia *et al.*, 2005), were reported to show antileishmanial activity with IC_{50} of 0.42 and 1.10 μgmL^{-1} against the amastigotes of *Leishmania donovani* and *Leishmania amazonensis*, respectively (Manuel and Luis, 2001). Endale (2012) reported naphthalene derivatives such as busseihydroquinone A (**7**), from the genus *Pentas* with antiprotozoal activity against *Plasmodium falciparum*; D6 clone (IC_{50} 11.10 μgmL^{-1}) and W2 clone (IC_{50} 44.50μgmL^{-1}). Leishmaniasis, like malaria, is caused by a protozoan parasite. In addition, quinone derivatives were reported to bind effectively in the FAD binding cavity of *Leishmania infantum* trypanothione reductase (Venkatesan *et al*., 2010). Therefore, compounds from *Pentas* species are attractive candidates for designing antileishmanial drugs.

6   7

4
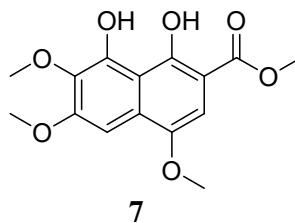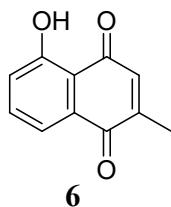
CHAPTER TWO

LITERATURE REVIEW

2.1   Leishmaniasis

Leishmaniasis is a set of ailments endemic to tropical and sub-tropic areas; its transmission is by female sand-flies of the genera *Lutzomyia* and *Phlebotomus*. Epidemiologically, leishmaniasis is classified into two depending on the life cycle: zoonotic leishmaniasis, for which animals (wild and domestic) are the reservoir hosts and anthroponotic for which humans are the reservoir hosts (Alvar *et al*., 2006; Lévêque *et al*., 2020). Leishmaniasis is clinically categorised into cutaneous, mucocutaneous, and visceral leishmaniasis, Table 2.1 (WHO, 2021). The protozoan parasites from the genus *Leishmania* are known to cause leishmaniasis; they attack both man and lower vertebrates (Manuel and Luis, 2001). The pathogen exists in the form of promastigotes in the vector's gut. When the vector takes a blood meal, it deposits these promastigotes in the host's blood. Macrophages of the host's immune system transform the promastigotes to amastigotes during phagocytosis. The amastigotes multiply in the cells of various tissues and are transferred to the vector when it takes a blood meal from the infected host (Monzote, 2009). These amastigotes transform to the promastigotes in the Sand fly's gut and can be spread to several other hosts.

Leishmaniasis has been reported to be one of the most neglected diseases generally distressing the deprived communities, especially in the developing world (de Menezes *et al*., 2015). It is an important public health concern in Eastern Africa, being endemic to Eritrea, Ethiopia, Kenya, Sudan, Somalia and Uganda (Jones & Welburn, 2021). According to the weekly bulletin on outbreaks and other emergencies published by WHO (2019), from January to June 2019, a total of 1,564 leishmaniasis cases were reported from Marsabit and Wajir counties of Kenya, with the highest peak being observed on 19th May 2019 in Marsabit county where 1,387 suspected cases were reported with 15 deaths (CFR 1.08%), Wajir county reported 261 suspected cases with seven deaths (CFR 2.68%).

Table 2.1: Clinical forms of leishmaniasis and their causative agents

Clinical form	Cause
Cutaneous	*L. major*
	L. aethiopica
	L. Mexicana
	L. tropica
Mucocutaneous	*L. braziliensis complex*
	L. donovani
Visceral	*L. chagasi*
	L. infantum

Note: Adopted from Kiprotich (2006)

2.1.1   Visceral Leishmaniasis

Visceral leishmaniasis is a fatal form of leishmaniasis caused by *L. donovani* which is transmitted by *Phlebotomus orientalis*, *P. martini* and *P. celiae*; it is characterized by anaemia, spleen and liver enlargement, irregular bouts of fever, and weight loss, and if left untreated, it results in the death of the mammalian host (Jawed and Majumdar, 2018). According to WHO (2019), over 90% of the cases of visceral leishmaniasis reported in 2019 occurred in Ethiopia, Eritrea, Brazil, Iraq, Nepal, South Sudan, Sudan, Iraq, India and Kenya; high prevalence was reported in Brazil, South-East Asia and East Africa; with an approximate incidence of 90,000 new cases annually worldwide. In Eastern Africa, South Sudan has the highest prevalence of leishmaniasis followed by Ethiopia (Al-Salem *et al.*, 2016; Jones and Welburn, 2021). At the WHO (2015) bi-regional consultation (Addis Ababa, Ethiopia 2015), it was noted that between 2,000 to 4,500 cases of visceral leishmaniasis occur in Ethiopia annually. The report also dubbed the states; Upper Nile, Jonglei, Unity and Eastern Equatoria of South Sudan as highly endemic with visceral leishmaniasis, putting 2.7 million people at risk annually. In Kenya, 4000 cases of visceral leishmaniasis, transmitted by *Phlebotomus orientalis* and *Phlebotomus martini* were reported to occur annually, mostly affecting Baringo, Isiolo, Marsabit, Turkana, Wajir and West Pokot Counties (WHO, 2015).

In August 2021, WHO (2021) reported a Case Fatality Rate of 1.0%, (873 cases, 9 deaths), associated with visceral leishmaniasis in seven counties of Kenya; Marsabit, Garissa, Kitui, Baringo, West Pokot, Mandera and Wajir since January 2020. The outbreak of visceral leishmaniasis was declared to be active in Mandera, West Pokot and Wajir (WHO, 2021). In Uganda, visceral leishmaniasis is prevalent in the North-Eastern region, devastating four districts of the Karamoja region; Amarut, Moroto, Kotido, and Nakapiripirit (Jones and Welburn, 2021).

2.1.2 Cutaneous Leishmaniasis

Cutaneous leishmaniasis is the most frequent of the three clinical forms; significant clinical indicators include lesions on the exposed body parts, which appear after 2 weeks of incubation (Hernández-Bojorge *et al*., 2020). Vulnerability to cutaneous leishmaniasis has been linked to malnutrition, immunosuppression and the host genetic setting (Reithinger *et al*., 2007). Out of the new cases of cutaneous leishmaniasis reported by the World Health Organisation in 2019, more than 87% ensued in Afghanistan, the Syrian Arab Republic, Brazil, Algeria, Colombia, the Islamic Republic of Iran, Libya, Pakistan, Iraq and Tunisia. Estimates reveal between 600,000 to 1 million new cases worldwide every year (WHO, 2019). In Kenya, cutaneous leishmaniasis is caused by *L. tropica*, *L. major* and *L. aethiopica* which infest the Rift Valley region, low lands (Kitui and Baringo) and high-altitude areas such as Mt. Elgon, respectively (Jones and Welburn, 2021).

2.1.3 Mucocutaneous Leishmaniasis

Mucocutaneous leishmaniasis is a metastatic form of cutaneous leishmaniasis with an incubation period ranging from one to three months; it destroys nasal mucous membranes, throat and mouth (Hernández-Bojorge *et al*., 2020). More than ninety per cent of the cases ensue in Bolivia, Ethiopia, Brazil, and Peru (WHO, 2019).

2.2 Prevention and Treatment of Leishmaniasis

To date, there is no vaccine for leishmaniasis (Jawed and Majumdar, 2018). The control strategy for leishmaniasis is anchored on early diagnosis and treatment, control of animal reservoir hosts and vector control strategies, such as treating bed nets (WHO, 2021). The contemporary treatment strategies for leishmaniasis are predominantly grounded on chemotherapy. Traditionally, drastic methods such as the use of battery acid, hot plate and copper (II) sulphate have been employed (Manuel and Luis, 2001). Such approaches, however, leave long-lasting and unbearable side effects such as burns on the patient's body due to the hot plate therapy. Antiprotozoal agents, pentavalent antimony compounds and systematic antifungal agents predominate the chemotherapeutic treatment of leishmaniasis. With the rising need to avert drug resistance and minimise toxicity, combination therapies of these agents have been employed (Sundar and Singh, 2018).

2.2.1 Use of Antiprotozoal Agents, Antifungal Agents and Antibiotics

Antiprotozoal agents like miltefosine (**4**) and pentamidine (**1**) kill parasites by directly attaching to one of the parasite's cellular parts to inhibit its normal functions (Jawed and Majumdar, 2018). Pentamidine (**1**) is currently used to treat numerous protozoal infections, including leishmaniasis. It inhibits the growth of the *Leishmania* parasite through hindering oxidative phosphorylation or inhibition of protein and phospholipids biosynthesis (Scala *et al*., 2018). The use of pentamidine (**1**) however, is limited by its unsettling side effects that include renal toxicity, hypertension and diabetes mellitus (Singh *et al*., 2012).

Miltefosine (**4**) (Trade name – Miltex) is administered orally and used to treat visceral leishmaniasis, particularly that which is instigated by *L. donovani* (de Menezes *et al*., 2015); Its mode of action involves interfering with the functions of membrane lipids, thereby compromising the integrity of the membrane hence destroying the activity of mitochondrial cytochrome C oxidase leading to cell death (Villa-Pulgarín *et al*., 2017). This drug is not suitable for expectant mothers because it instigates teratogenesis (Croft and Olliaro, 2011).

Fluconazole (**8**), an antifungal agent with antileishmanial activity, inhibits the cytochrome 450 enzyme, 14α-demethylase and blocks ergosterol synthesis (Jawed and Majumdar, 2018). In some instances, paromomycin (**5**), an antibacterial agent, has been used to treat leishmaniasis because of its antiprotozoal activity (Neal, 1968, Monzote, 2009). Paromomycin (**5**) has been reported to cure 89% of the cases of antimony-resistant visceral leishmaniasis in India (Berman, 2003).

8
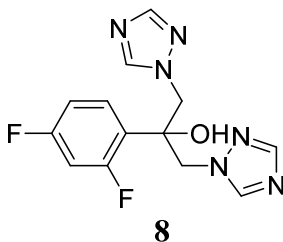
2.2.2 Use of Pentavalent Antimonials

Antimony (Sb^{5+}) compounds such as sodium stibogluconate (**3**) are the most widely used therapeutic agents for the treatment of leishmaniasis (Murray *et al*., 2005). These drugs act by interfering with the parasite's nucleotide metabolism (Jawed and Majumdar, 2018).

In East Africa, visceral leishmaniasis is treated mainly using a combination therapy that involves the use of paromomycin (**5**) with pentavalent antimonials to minimize the toxicity of the antimonials and minimise the susceptibility to drug resistance (Jawed and Majumdar, 2018). However, acute secondary effects are attributed to antimony toxicity such as musculoskeletal pains, renal failure, hepatotoxicity and cardiotoxicity (Reithinger *et al*., 2007); hence their usage requires close clinical supervision and monitoring.

2.2.3 Use of Systemic Antifungal Agents

The most widely used drug against leishmaniasis is amphotericin B (**2**); it is among the first line of drugs for treating leishmaniasis. It is used in a liposomal formulation (Tiuman *et al*., 2011; Nagle *et al*., 2020). Amphotericin B (**2**) binds with the membrane sterols and causes complete lysis of the cells (do Vale Morais *et al*., 2018). Its application, however, is met with high toxicity, which manifests in the form of nephrotoxicity and myocarditis (Croft and Yardley, 2002).

To avert the adverse side effects of amphotericin B, it is used in combination with other agents. Lower doses of tamoxifen (**9**) and amphotericin B (**2**) showed enhanced activity against human cutaneous leishmaniasis. Tamoxifen (**9**) was found to inhibit lipid peroxidation and thus reducing the harmful secondary effects of amphotericin B (Jawed and Majumdar, 2018).

9
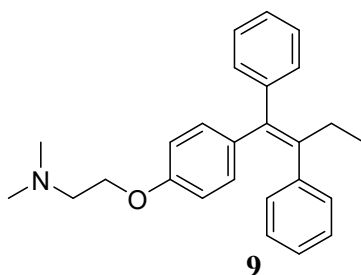
2.2.4 Combination Therapy

Monotherapy has succumbed to drug-resistant strains of *Leishmania* pathogen. As a remedy to this, scientists are leveraging the synergistic potency of the therapeutic agents through combination therapy. Combination therapies have also gained popularity in the treatment of leishmaniasis due to their tendency to avert the toxicity of chemotherapeutic agents. A combination of miltefosine (**4**) with liposomal amphotericin B (**2**) or paromomycin (**5**) has been reported to be less toxic than amphotericin B in monotherapy (de Menezes *et al*., 2015). Melaku *et al*., (2007) reported the use of paromomycin (**5**) in combination with sodium stibogluconate (**3**) to treat visceral leishmaniasis in Sudan.

2.3   Emerging Trends in Leishmaniasis Therapy

2.3.1   Immunization

Multiple approaches including the use of whole killed parasites, live-attenuated parasites and recombinant surface antigens and ligands have been considered in the search for the vaccine. Despite the efforts, no success has been registered so far (Jawed and Majumdar, 2018).

2.3.2 Immunotherapy

An immunotherapeutic approach against leishmaniasis is under consideration for combating the disease (Jawed and Majumdar, 2018). It involves alteration of the immune system to enhance the immunity of the body against the *Leishmania* parasite; this is achieved through activation of receptors, induction of cytokines and elevation of antimicrobial molecules to give the host ability to either directly kill the parasite or assist in increasing the efficacy of the antileishmanial drugs (Rasolzadeh *et al*., 2015; Jawed and Majumdar, 2018). In a study conducted in Peru, Arevalo *et al*. (2001) used Imiquimod (**10**), an immune response modifier to cure 90% of the patients of antimony-resistant cutaneous leishmaniasis (Arevalo *et al*., 2001). Imiquimod works by prompting the immune system to release cytokines like INF-α and TNF plus several interleukins (Testerman *et al*., 1995). Another immunoregulator, tucaresol (**11**), was reported to show *in vivo* activity against *L. donovani* instigated infection; it works by enhancing TH-1 response and stimulating the production of IL-6 and IFN-ɣ (Smith *et al*., 2000; Monzote, 2009).
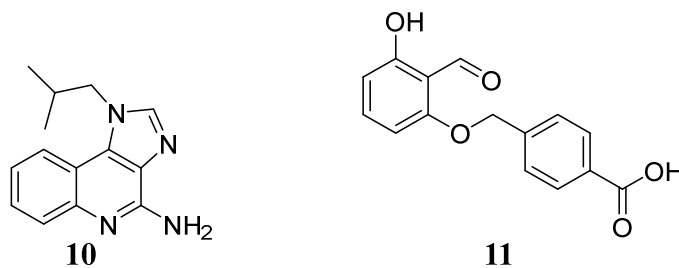
2.3.4 Nanotechnology

Nanotechnology is being leveraged to offer solutions to persistent challenges in drug discovery especially averting toxicity and aiding drug delivery. The application of nanotechnology to drug discovery is based on two cardinal approaches; the use of nanoparticles in drug delivery and nanoparticle formulations of therapeutic agents (Sundar and Singh, 2018). This technology has been employed in amphotericin B-based therapy where a liposomal solution of amphotericin B is used instead of sodium stibogluconate;

the results indicated a marked reduction in toxicity and an enhanced antileishmanial activity (Hamidi *et al*., 2008; Shio *et al*., 2014; de Menezes *et al*., 2015). In a certain study, silver nanoparticles were shown to inhibit *Leishmania infantum* trypanothione reductase (Baiocco *et al*., 2011).

2.4 Natural Products as Leads for Leishmaniasis Treatment

Nature, through its diversity, has offered millions of molecular templates that have guided drug development over time. In the contemporary world, the likelihood of using natural products to boost the efficacy of antibiotics or synthetic drugs through combination therapies is under consideration (Tiuman *et al*., 2011). Previous researchers have reported phytochemicals from various classes to exhibit antileishmanial activities against various strains of *Leishmania*. In the following subsections, the natural products that were reported to show antileishmanial activity are discussed.

2.4.1 Alkaloids

Reports have indicated that several subclasses of alkaloids have antileishmanial activity. Examples of alkaloids with antileishmanial activity are given in Table 2.2 and Figure 2.4. The mechanism for antileishmanial activity of some of the alkaloids such as harmaline (**16**) entails interactions with the parasite's DNA (Di Giorgio *et al*., 2004). Indole alkaloids interfere with the respiratory chain of the parasite (Mishra *et al*., 2009).

12

Table 2.2: Alkaloids with antileishmanial activity

Compound	IC$_{50}$ (µM)	Plant source	Reference
Berberine (**12**)	29.73	*Berberis aristate* (Berberidace*a*e)	Mishra *et al*., 2009
Isoguattouregidine (**13**)	292.9	*Guatteria foliosa* (Annonaceae)	Mishra *et al*., 2009
Anonaine (**14**)	376.9	*Annona spinescens* (Annonaceae)	Vila-Nova *et al*., 2011
Liriodenine (**15**)	26.16	*Annona spinescens* (Annonaceae)	del Rayo Camacho *et al*., 2000
Harmaline (**16**)	116.80	*Peganum harmala* (Nitrariaceae)	Di Giorgio *et al*., 2004
Sarachine (**17**)	25.08	*Saracha punctate* (Solanaceae)	Manuel & Luis, 2001
Klugine (**18**)	0.85	*Psychotria klugii* (Rubiacae)	Mishra *et al.* 2009
Cephaeline (**19**)	0.06	*Psychotria klugii* (Rubiacae)	Mishra *et al.* 2009
2-*n*-Propylquinoline (**20**)	291.0	*Galipea longiflora* (Rutaceae)	(Singh *et al*., 2014)
Isocephaeline (**21**)	0.83	*Psychotria klugii* (Rubiacae)	Mishra *et al.* 2009
Emetine (**22**)	0.06	*Psychotria klugii* (Rubiacae)	Mishra *et al.* 2009
Chimanine-D (**23**)	35.0	*Galipea longiflora* (Rutaceae)	Singh *et al*., 2014
Chimanine-B (**24**)	147.7	*Galipea longiflora* (Rutaceae)	Singh *et al*., 2014
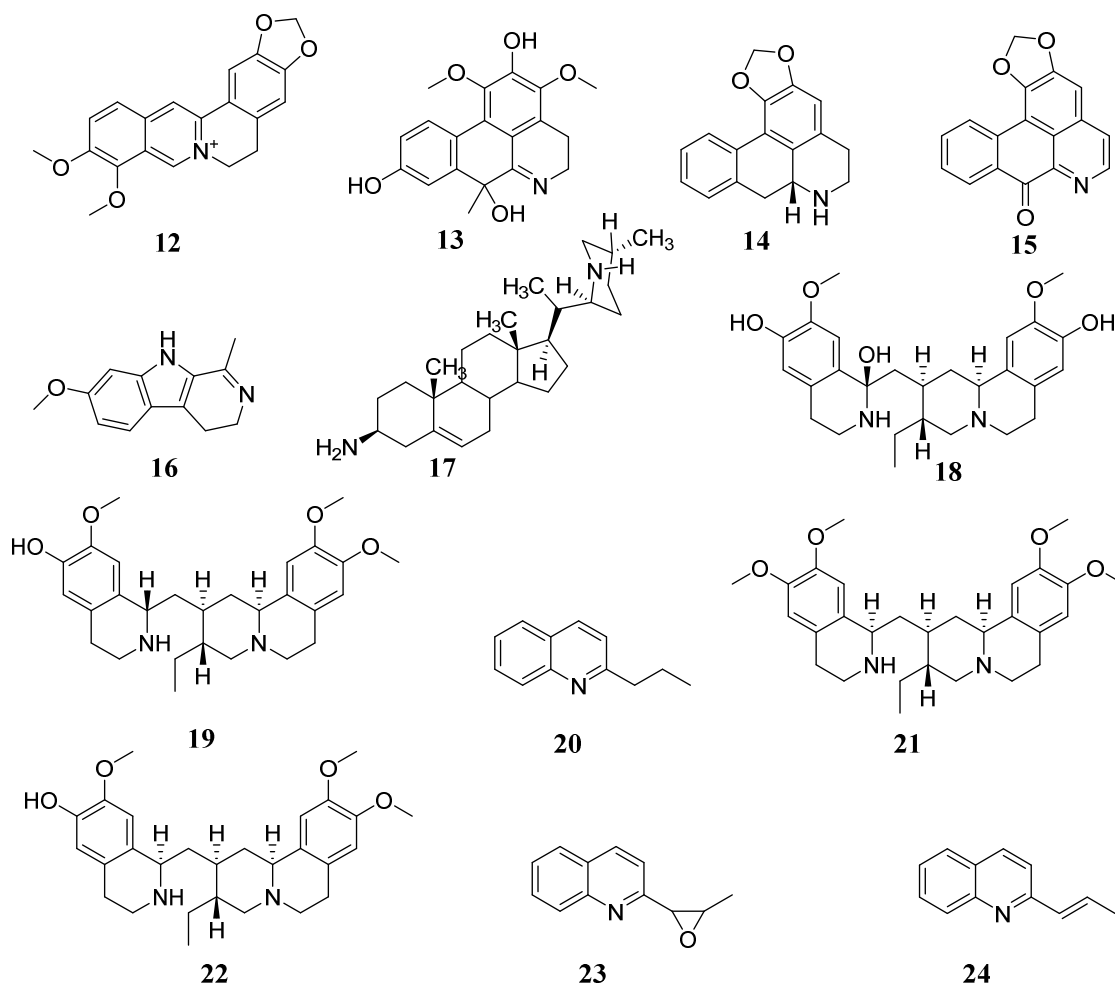
Figure 2.1: Alkaloids with antileishmanial activity

2.4.2 Terpenoids

Some terpenoids have shown significant antileishmanial activities, and some examples are shown in Table 2.3 and Figure 2.5. The antileishmanial mechanism of action of terpenoids was reported to involve an attack on the cell membrane of the parasite (Camargos *et al*., 2014). Studies also indicated that terpenoids cause fragmentation of pathogens' DNA strands and inhibit oxidative pathways (Sakyi *et al*., 2021).

Table 2.3: Terpenoids with antileishmanial activity

Compound	IC$_{50}$ (µM)	Plant source	Reference
Espintanol (**25**)	-	*Oxandra espintana* (Annonaceae)	Manuel & Luis, 2001
Grifolin (**26**)	304.0	*Peperomia galoides* (Piperaceae)	Manuel & Luis, 2001
Ursolic acid (**27**)	12.7	*Pentas lanceolata* (Rubiaceae)	Labib *et al.*, 2016
Piperogalin (**28**)	304.0	*Peperomia galoides* (Piperaceae)	Manuel & Luis, 2001
Chaparrinone (**29**)	-	*Hannoa chlorantha* (Simaroubaceae)	Rocha *et al.*, 2005
Betulin aldehyde (**30**)	26.16	*Doliocarpus dentatus* (Dilleniaceae)	Alakurtti *et al.*, 2010
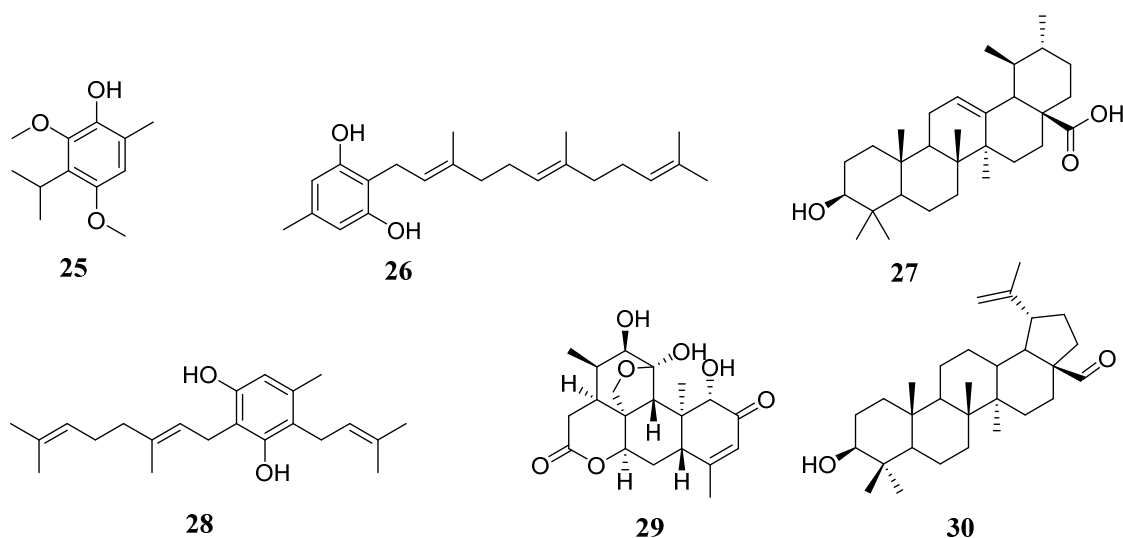
Figure 2.2: Terpenoids with antileishmanial activity

2.4.3   Flavonoids

Some flavonoids have shown significant antileishmanial activities and some examples are shown in Table **2.4** and Figure **2.6**. Some flavonoids trigger the generation of nitric oxide which is an antileishmanial agent (Sakyi *et al*., 2021). Quercetin (**33**) inhibited the growth of *L. amazonensis* by generating reactive oxygen species (ROS) ultimately causing mitochondria dysfunction (Fonseca-Silva *et al*., 2011).

Table 2.4: Flavonoids with antileishmanial activity

Compound	IC_{50} (µM)	Plant source	Reference
Strychnobiflavone (**31**)	5.4	*Strychnos pseudoquina* (Loganiaceae)	Lage *et al*., 2015
Quercetin-3-*O*-methyl ether (**32**)	-	*Strychnos pseudoquina* (Loganiaceae)	Lage *et al*., 2015
Quercetin (**33**)	31.4	*Kalanchoe pinnata* (Stonecrops)	Fonseca-Silva *et al*., 2011

Quercitrin (**34**)	18.0	*Kalanchoe pinnata* (Stonecrops)	Muzitano *et al*., 2006
8-Prenylmucronulatol (**35**)	6.9	*Smirnowia iranica* (Fabaceae)	Sairafianpour *et al*., 2002
Sakuranetin (**36**)	150.2 – 181.6	*Baccharis retusa* (Asteraceae)	Grecco *et al*., 2012
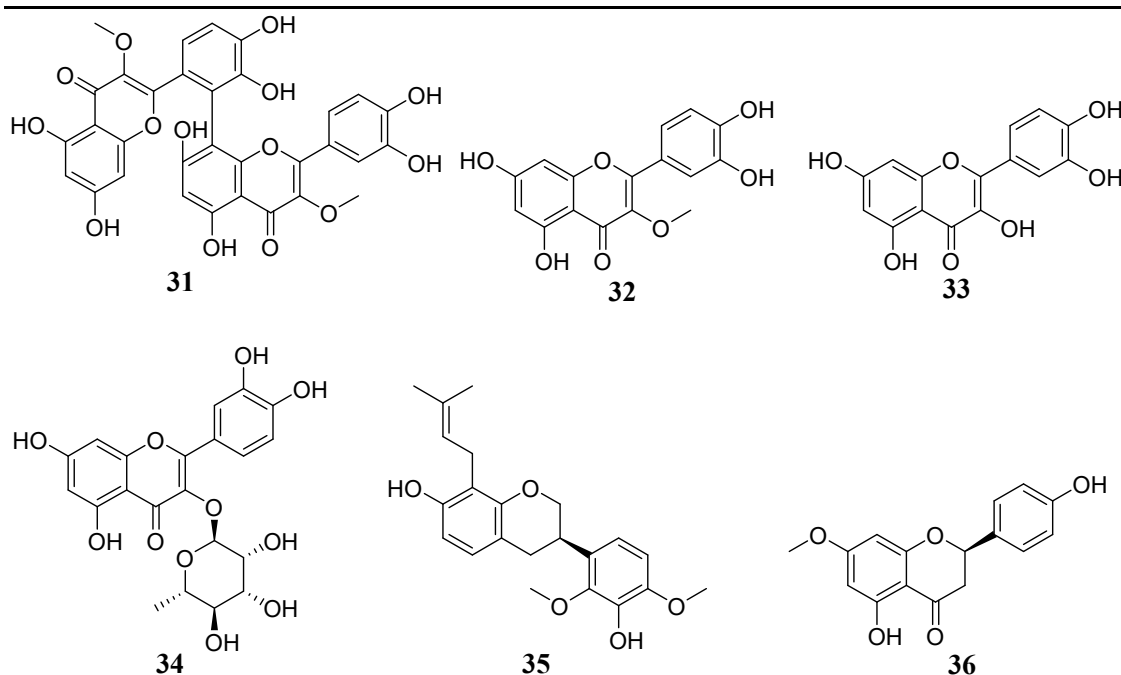
Figure 2.3: Flavonoids with antileishmanial activity

2.4.4 Quinones

Some quinones have shown significant antileishmanial activities and some examples are shown in Table 2.5 and Figure 2.7. The mode of action of naphthoquinone derivatives was reported to involve an attack on mitochondrial activity in *L. amazonensis* (Pisani *et al*., 1986). A certain study revealed the potential of naphthoquinone derivatives to inhibit manifold enzymes in *leishmania spp* particularly those involved in the metabolic pathway, lipids metabolism and electron transport chain (Peixoto *et al*., 2021). This makes quinones

and their derivatives attractive molecular templates for developing the next generation of antileishmanial drugs.

Table 2.5: Quinones with antileishmanial activity

Compound	IC$_{50}$ (µM)	Plant source	Reference
Diospyrin (**37**)	12.6	*Diospyros montana* (Ebenaceae)	Hazra *et al*., 2013
Plumbagin (**38**)	2.2	*Plumbago scandens* (Plumbaginaceae)	Croft *et al*., 1985
3,3′-Biplumbagin (**39**)	133.6	*Pera benensis* (Peraceae)	Manuel & Luis, 2001
8,8′-Biplumbagin (**40**)	5.0	*Pera benensis* (Peraceae)	Manuel & Luis, 2001
Lapachol (**41**)	79.84	*Tecoma spp* (Bignoniaceae	Araújo *et al*., 2019
Anthraquinone (**42**)	-	*Morinda lucida* (Rubiaceae)	Manuel & Luis, 2001
Anthraquinone (**43**)	-	*Morinda lucida* (Rubiaceae)	Manuel & Luis, 2001
Aloe-emodin (**44**)	90.0	*Stephania dinklagei* (Menispermaceae)	del Rayo Camacho *et al*., 2000
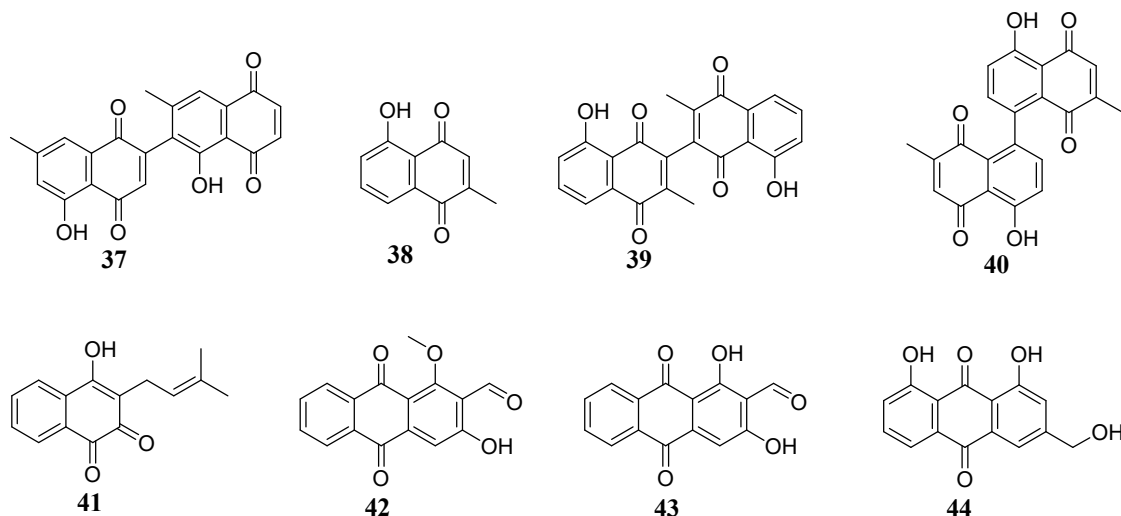
Figure 2.4: Quinones with antileishmanial activity

2.5   The Rubiaceae Family

The family Rubiaceae has close to 13,000 species in about 630 genera, primarily concentrated in the tropical and subtropical parts of the world. There are approximately 100 genera and 600 species of the Rubiaceae in East Africa (Bukuru, 2003). The Rubiaceous plants are employed around the world as ointments and food (Simplice *et al*., 2011). Several plants from the family have been investigated for biological activities, including antiplasmodial (Endale *et al*., 2012), antibacterial (Simplice *et al*., 2011), analgesic (Suman *et al*., 2014), antiperoxidative and protective (Adejo *et al*., 2014) activities. The Rubiaceae family is phytochemically rich in terpenoids (Simplice *et al*., 2011), iridoids (Inouye *et al*., 1988), anthraquinones (Wijnsma and Verpoorte, 1986) and indole alkaloids (Kisakuerek *et al*., 1983). The first highly efficacious cure for malaria, quinine (**45**), was isolated from a *Cinchona* species, belonging to family Rubiaceae. Quinine (**45**) has served as a scaffold for developing many synthetic analogues such as chloroquine (**46**). The Rubiaceae family is, therefore, a potential source of antiprotozoal agents.

45   **46**
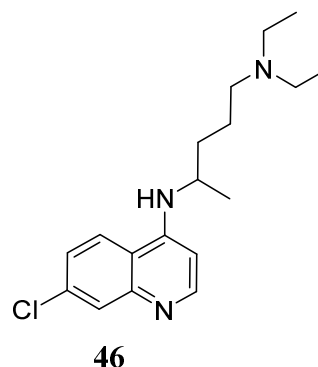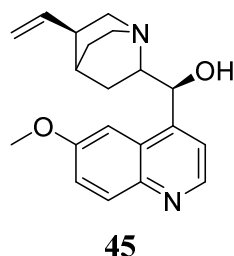
2.5.1 The Genus *Pentas*

The genus *Pentas* accommodates over 40 species that are extensively dispersed in tropical and southern Africa, Madagascar, the Arabian Peninsula and Comoros (Inouye *et al*., 1988, Verdcourt, 1976). The distribution of the genus *Pentas* in Kenya is summarised in the Table 2.6.

Table 2.6: Geographical distribution of *Pentas* species in East Africa

Species	Region
P. bussei	Coastal Province
P. decora	Mt. Elgon, Mumias, Cheranganyi, Aberdares, Kitale, Kisii
P. lanceolata	Mau, Loita, Aberdares, Mt. Kenya, Nyambene, Kitale, Mumias, Kisii, Kisumu, Baringo, Narok and Nairobi
P. longiflora	Mt. Elgon, Mumias, Cheranganyi, Aberdares, Narok, Kitake, Kisii, Baringo, Tinderet, Mau, Machakos, Kajiado
P. zanzibarica	Mt. Kenya, Mau, Loita, Aberdares, Nairobi, Nyambene, Kitale, Narok, Machakos, Kajiado.
P. parvifolia	Mumias, Embu, Kisii, Nanyuki, Baringo, Narok, Machakos, Kajiado and Nairobi

Note: Extracted from Endale (2012)

2.5.2 Application of the Genus *Pentas* in Ethnomedicine

Plants from the genus *Pentas* are used by various societies in Africa to treat a myriad of ailments some of which are listed in Table 2.7.

20

Table 2.7: Ethnomedical applications of plants from the genus *Pentas*

Species	Use	Reference
P. micrantha	Roots are soaked in water, boiled and drunk to relieve cough	Kokwaro, 2009
P. zanzibarica	Leaves soaked in water and the resultant liquid is taken as a laxative. Roots are boiled in water and the formulation used in the treatment of gonorrhoea and syphilis	Kokwaro, 2009
P. decora	Roots are used in combination with ghee to cure pimples. Leaf extract is used as a remedy for ringworms in Western Uganda.	Kokwaro, 2009, Ahumuza & Kirimuhuzya, 2011
P. lanceolata	Fresh roots are crushed and mixed with water and taken in case of a snake bite in cattle	Bekalo *et al*., 2009
P. bussei	Roots are used in Southern Kenya (Digo land) to treat syphilis and dysentery.	Kokwaro, 2009
P. longiflora	The roots are used as a relief for tapeworm. Roots are boiled in water and used against malaria. Powdered roots are mixed with butter to relieve skin infections like scabies and pityriasis versicolor in Rwanda.	Bukuru 2003, Kokwaro, 1976, Van Puyyelde *et. al*., 1985
P. purpurea	In Tanzania, a decoction is made from roots, mixed with sugar and orally administered to initiate menstruation.	Bukuru, 2003
P. hindsioides	Pounded roots are soaked in a water bath to heal scabies.	Bukuru, 2003
P. schimperi	Leaves are mixed with the bark of *Maesa lanceolate* and the concoction is drunk to alleviate hepatitis B liver infections. In Ethiopia, an aqueous suspension of the bark powder is taken to mitigate epilepsy and the root bark powder suspension in water is orally administered as a remedy for mental illness.	Focho *et al*., 2009

2.5.3 Phytochemistry of the Genus *Pentas*

The phytochemical composition of the following nine *Pentas* species has been studied (Table 2.8).

Table 2.8: Previously studied *Pentas* species

SN.	*Pentas* species	Reference
1.	*P. longiflora*	Endale, 2012
2.	*P. lanceolata*	Endale, 2012
3.	*P. decora*	Endale, 2012
4.	*P. zanzibarica*	Kusamba *et al.*, 1993
5.	*P. zanzibarica*	Kusamba *et al.*, 1993
6.	*P. bussei*	Bukuru, 2003 ; Endale, 2012
7.	*P. micrantha*	Endale *et al.*, 2012
8.	*P. parvifolia*	Endale, 2012
9.	*P. schimperi*	Donfack *et al.*, 2014

Previous studies showed that the genus *Pentas* is a rich source of anthraquinones, naphthol derivatives (Endale, 2012) and iridoids (Schripsema *et al.*, 2007). According to Effendi (2004), naturally occurring quinones (predominantly occurring as anthraquinone derivatives) have been found to occur in lichens, fungi, mosses, sea animals, algae and higher plants. Natural anthraquinones possess antioxidant, antitumor, antimutagenic, purgative, antioxidant, immunosuppressive and anti-inflammatory activities (Effendi, 2004). The naphthoquinones, anthraquinones and their biogenetic derivatives that occur in the genus *Pentas* are discussed in the subsequent sections.
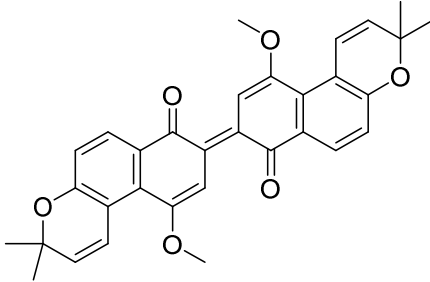
2.5.3.1　　　Chemical Composition of *Pentas bussei*

Pentas bussei is mainly rich in naphthol derivatives, anthraquinone glycosides and terpenoids (Table 2.9).

Table 2.9: Phytochemistry of *Pentas bussei*.

Name	Structure	Reference
Methyl-8-hydroxy-1,4,6,7-tetramethoxy-2-naphthoate (**47**)		Bukuru, 2003
Busseihydroquinone A (**7**)		Endale, 2012
Methyl-1,5-dihydroxy-4-methoxy-2-methyl-2'-(4'-methyl-3-pentenyl)-27/-benzo(/)-chromene-2-carboxylate (**48**)		Bukuru, 2003; Endale, 2012
9-Methoxy-2,2-dimethyl-2H-benzo[h]chromene-7,10-diol (**49)**		Bukuru, 2003
β-Stigmasterol (**50**)		Bukuru, 2003

23
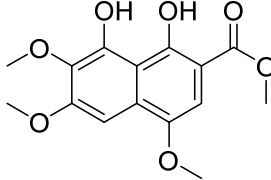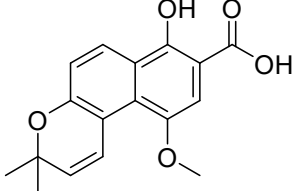
Name	Structure	Reference
Busseihydroquinone B (**51**)		Endale *et al.*, 2012
Busseihydroquinone C, (**52**)		Endale *et al.*, 2012
Busseihydroquinone D, (**53**)		Endale *et al.*, 2012
Rubiadin-1-methylether-3-*O*- β-primeveroside (**54**)		Bukuru, 2003
Damnacanthol-3-*O*-β-primeveroside (**55**)		Bukuru, 2003
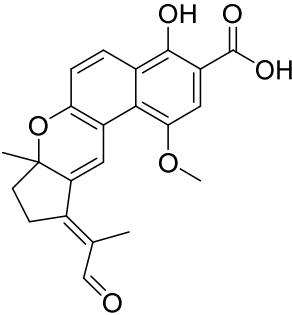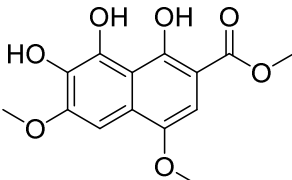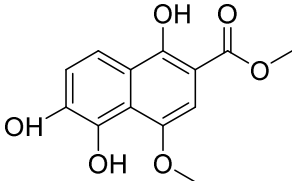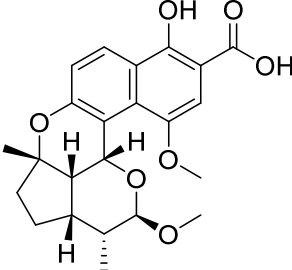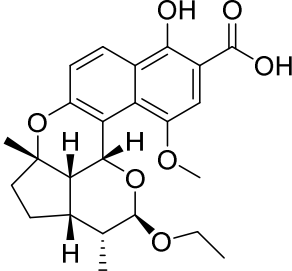
Name	Structure	Reference
Busseihydroquinone F (**56**)		Abdissa *et al*., 2016
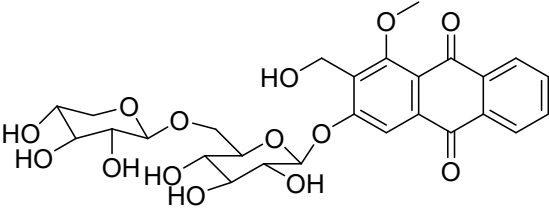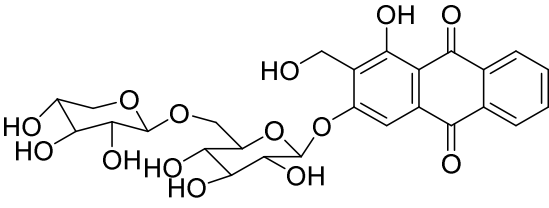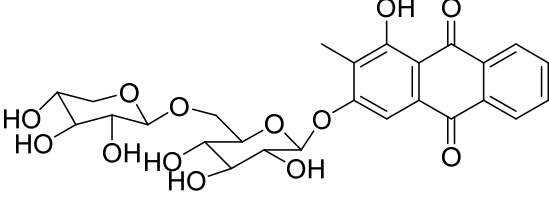
2.5.3.2 Chemical Composition of *Pentas parvifolia*

Pentas parvifolia produces naphthoquinones, anthraquinone glycosides and terpenoids (Table 2.10).

Table 2.10: Phytochemistry of *Pentas parvifolia*.

Name	Structure	Reference
Busseihydroquinone A (**7**)		Endale, 2012
Busseihydroquinone B (**51**)		Endale, 2012

Name	Structure	Reference
Busseihydroquinone D (**53**)		Endale, 2012
Parvinaphthol A (**57**)		Abdissa *et al.*, 2016
Parvinaphthol B (**58**)		Abdissa *et al.*, 2016
Parvinaphthol C (**59**)		Abdissa *et al.*, 2016
Parvinaphthol D (**60**)		Abdissa *et al.*, 2016

Name	Structure	Reference
Damnacanthol-3-*O*-β-primeveroside (**55**)		Bukuru, 2003
Lucidin-3-*O*-β-primeveroside (**61**)		Bukuru, 2003
Rubiadin-3-*O*-β-primeveroside (**62**)		Bukuru, 2003

2.5.3.3   Anthraquinones of *Pentas zanzibarica*

Bukuru (2003) has reported anthraquinones and anthraquinone glycosides from *Pentas zanzibarica* and these are listed in Table 2.11.
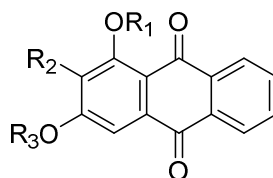
Table 2.11: Phytochemistry of *Pentas zanzibarica*

No.	R_3	R_2	R_1
54	Prim	CH_3	CH_3
55	Prim	CH_2OH	CH_3
63	H	CHO	CH_3
64	H	CH_3	H
65	H	CH_3	CH_3
62	Prim	CH_3	H
61	Prim	CH_2OH	H
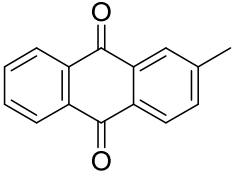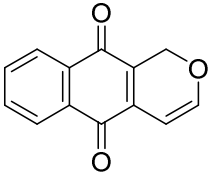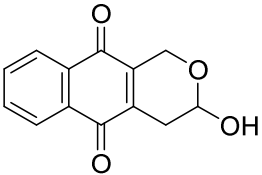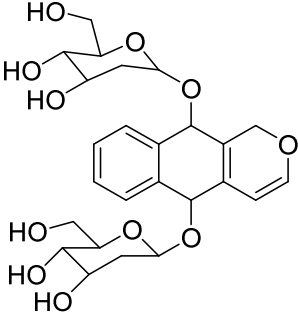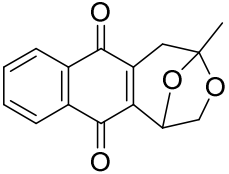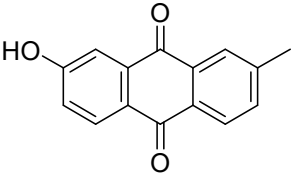
2.5.3.4   Chemical Composition of *Pentas longiflora*
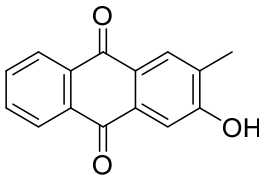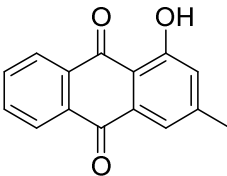
Pentas longiflora produces naphthol derivatives, anthraquinones and naphthoquinones (Table 2.12).

Table 2.12: Phytochemistry of *Pentas longiflora*

Name	Structure	Reference
Mollugin (**66**)		Endale, 2012

Name	Structure	Reference
3-Hydroxymollugin (**67**)		Endale, 2012
3-Methoxymollugin (**68**)		Endale, 2012
3,4,6-Trihydroxy-2,2-dimethyl-3,4-dihydro-2H-benzo[h]chromene-5-carboxylic acid methyl ester (**69**)		Bukuru, 2003
3,4,6-Trihydroxy-2,2-dimethyl-3,4-dihydro-2H-benzo[h]chromene-5-carboxylic acid methyl ester (**70**)		Bukuru, 2003
3-Hydroxy-1-methyl anthraquinone (**71**)		Bukuru, 2003
2-Methoxy-3-methylanthraquinone (**72**)		Bukuru, 2003

Name	Structure	Reference
Tectoquinone (**73**)		Endale, *et al*., 2012
Pentalongin (**74**)		Endale, *et al*., 2012
Psychorubrin (**75**)		Bukuru, 2003
Pentalonginhydroquinone diglycoside (**76**)		Harouna *et al*., 1995
Isagarin (**77**)		Bukuru, 2003
2-Hydroxy-7-methyl-anthraquinone (**78**)		Bukuru, 2003

Name	Structure	Reference
2-Hydroxy-3-methylanthraquinone (**79**)		Bukuru, 2003
Pachybasin (**80**)		Bukuru, 2003

2.5.3.5   Chemical Composition of *Pentas lanceolata*

Pentas lanceolata produced anthraquinones; damnacanthol (**81**), rubiadin (**64**), rubiadin-1-methyl ether (**65**), damnacanthol-3-*O*-methyl ether (**82**), lucid-ω-methyl ether (**83**) and an anthraquinone glycoside, Rubiadin-1-methylether-3-*O*-β-primeveroside (**54**) (Endale, 2012). Also, iridoids such as tudoside (**84**) and 13R-*epi*-gaertneroside (**85**) were also reported from *Pentas lanceolata* (Schripsema *et al*., 2007), Figure 2.9.

82

83

84

85
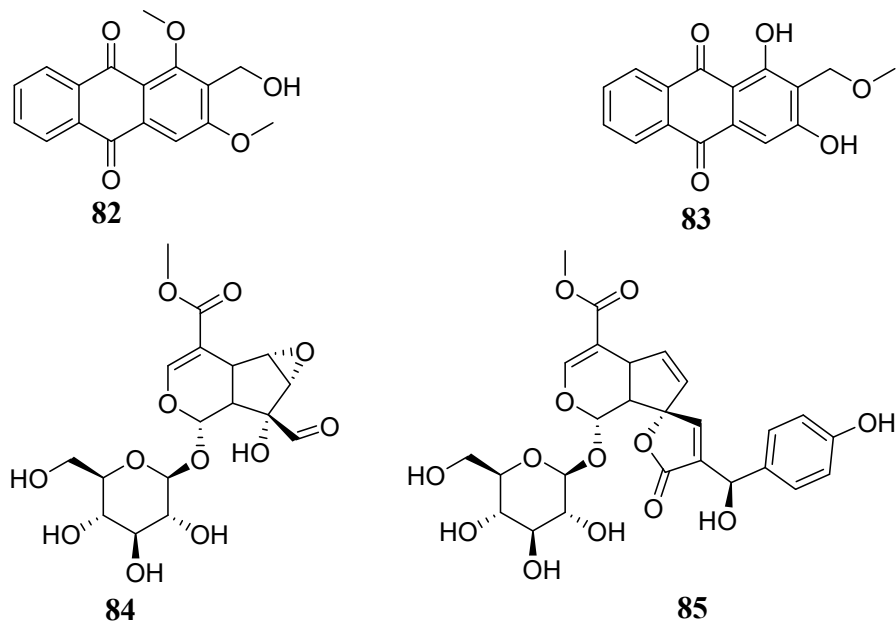
Figure 2.5: Phytochemicals from *Pentas lanceolata*

2.5.3.6   Anthraquinones of *Pentas micrantha*

Pentas micrantha mainly produces anthraquinones; some of these are shown in Figure 2.10 (Endale *et al*., 2012).

64

65

86

87

88

89
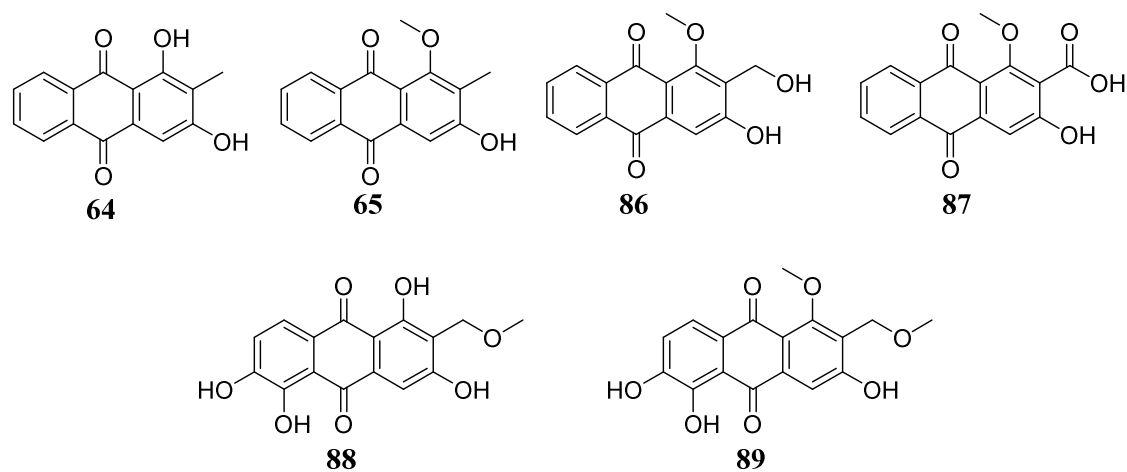
Figure 2.6: Phytochemicals from *Pentas micrantha*

2.5.3.7　　　Chemical Composition of *Pentas schimperi*

Pentas schimperi produced 2-hydroxymethylanthraquinone (**90**), cleomiscosin A (**91**), schimperiquinone A (**92**) and schimperiquinone B (**93**) (Donfack *et al*., 2014).

90　　　　**91**

92　　　　**93**
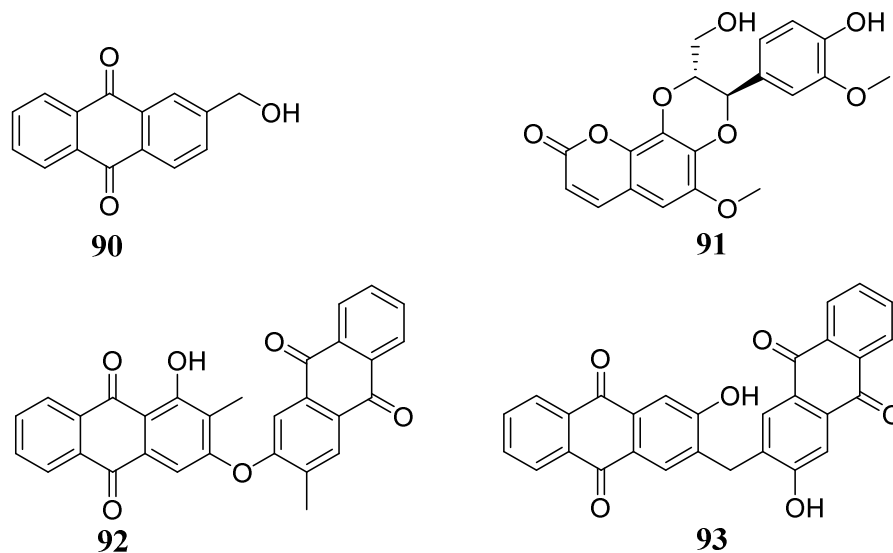
Figure 2.7: Phytochemicals from *Pentas schimperi*

2.6　　Biosynthesis of Phytochemicals in the Genus *Pentas*

Chorismate/*O*-succinyl benzoic acid and polyketide biogenetic pathways are the two principal pathways for the biosynthesis of anthraquinones in higher plants (Han *et al*., 2001). In the Rubiaceae family, the Chorismate/*O*-succinylbenzoic acid pathway takes place. The biosynthetic pathway of naphthoquinones and anthraquinones in the genus *Pentas* is illustrated in Scheme 2.1 (Han *et al*., 2001), and Scheme 2.2 (Endale, 2012).
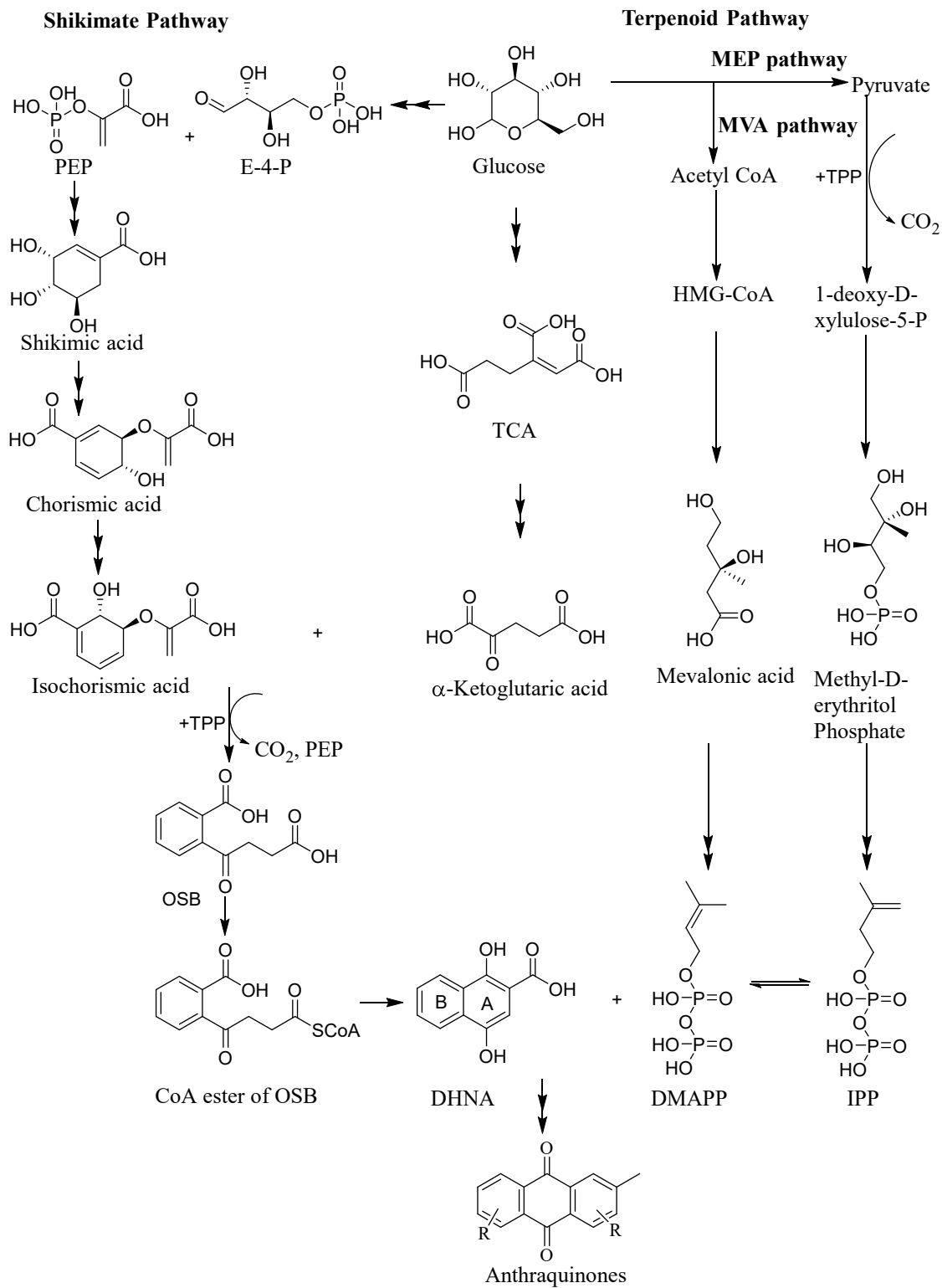
Scheme 2.1: Biosynthesis of naphthoquinones in the genus *Pentas* (Han *et al., 2001*)
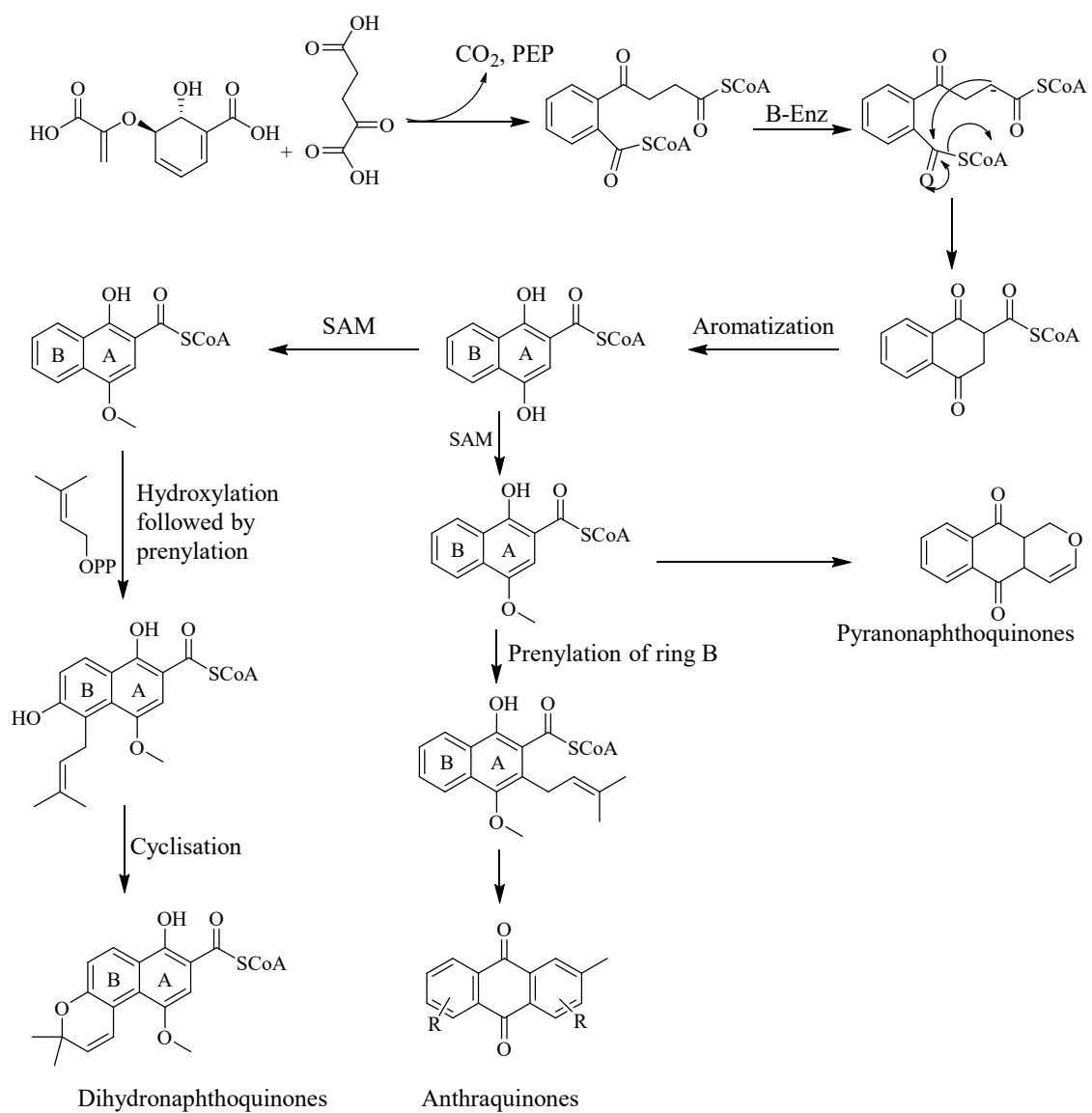
Scheme 2.2: Biosynthesis of quinones in the genus *Pentas* (Endale, 2012)

Note:

CoA	Coenzyme A
DHNA	1,4-dihydroxy-2-naphthoic acid
DMAP	Dimethylallyl diphosphate
E-4-P	D-Erythrose 4-phosphate
IPP	Isopentenyl diphosphate
MEP	Methyl-D-erythritol Phosphate
MVA	Mevalonic acid
OSB	*o*-Succinyl benzoic acid
PEP	Phosphoenolpyruvate
TCA	Tricarboxylic acid
SAM	S-Adenosyl methionine
TPP	Thiamine pyrophosphate

Isochorismic acid condenses with α-ketoglutaric acid in the presence of *O*-succinyl benzoate synthase enzyme to form *o*-succinyl benzoic acid (OSB), which on cyclisation forms 1,4-dihydroxy-2-naphthoic acid (DHNA), bearing ring A and ring B of naphthoquinones. The DHNA then reacts with Isopentenyl diphosphate (IPP) to form ring C of anthraquinones. These basic skeletons are then modified to give rise to the various naphthoquinone derivatives and anthraquinones in the genus *Pentas*, some of which have been discussed in Section 2.5.3.

2.7   Biological Activities of Compounds Isolated from *Pentas* Species

Previous studies show that the genus *Pentas* has an extensive spectrum of biological activities and these are mainly attributed to the inherent anthraquinones (Teuscher & Lindequist, 1994). The reported biological activities include; antiplasmodial (Endale *et al.*, 2012), antimicrobial (Sweelam *et al*., 2018) and analgesic (Suman *et al.*, 2014).

Compounds isolated from *Pentas* species are potential templates for synthesis of safe pharmacologically active molecules; for example, pentalongin (**74**), from the root bark of *P. longiflora* has been employed as a "lead" to aid the synthesis of highly efficacious antibiotics (Claessens *et al.*, 2007).

74
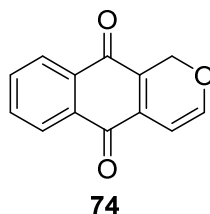
2.8 Application of CADD in the Development of Antileishmanial Drugs

By targeting specific enzymes involved in critical metabolic pathways of the pathogen, compounds with the potential to bind to such targets can be predicted using software to simulate the ligand-receptor interactions that occur in a typical biological system. The computational approaches employed are broadly categorised into two: Structure-based approach, which entails molecular docking and the Ligand-based approach, which uses methods like pharmacophore modelling and 3D-QSAR models (Njogu *et al*., 2016). Molecular docking studies are instrumental in screening large databases of molecules to establish their binding affinities with key receptors (enzyme targets) in the pathogen. The binding affinity of the ligand (in kcal/mol) with the receptor is scored using a scoring function. Based on the score, various ligand molecules can be ranked from the best to the worst binder. Consequently, potent ligand molecules are identified and can then be subjected to subsequent studies.

In the case of *Leishmania*, several protein targets (Table 2.13) have been reported, which are instrumental in guiding the development of antileishmanial drugs. In this study, the structure-based approach was undertaken to study the inhibitory potency of the phytochemicals from the genus *Pentas* for *Leishmania infantum* trypanothione reductase (*Li*TR).

Table 2.13: A sample of reported targets in *Leishmania* parasite.

Pathogen	Receptor	PDB ID	Resolution (Å)	Reference
L. infantum	14-alpha demethylase (CYP51)	3L4D	2.75	Hargrove *et al.* 2011
	Nicotinamidase	3R2J	2.68	Gazanion *et al.*, 2011
	Thiol-dependent reductase I	4AGS	2.30	Fyfe, Westrop, Silva, *et al.*, 2012
	Glyoxalase II	2P1E	1.90	Sousa Silva *et al.*, 2008
L. donovani	Trypanothione reductase	4ADW	3.61	Baiocco *et al.*, 2013
	N-Myristoyl transferase	2WUU	1.42	Brannigan *et al.*, 2010
	Tarentolae proteasome	6tcz	3.40	Nagle *et al.*, 2020
	Cyclophilin A	2HAQ	1.97	Venugopal *et al.*, 2007
	Ornithine decarboxylase	2OO0	1.90	Dufe *et al.*, 2007
	Cysteine synthase	4AIR	1.80	Fyfe, Westrop, Ramos, *et al.*, 2012
	Leishmanolysin - GP63	1LML	1.86	Schlagenhauf *et al.*, 1998
L. major	Methionyl-tRNA synthetase	3KFL	2.00	Larson *et al.*, 2011
	Nucleoside hydrolase	1EZR	2.50	Shi *et al.*, 1999
	Oligopeptidase B	2XE4	1.65	McLuskey *et al.*, 2010
	Phosphodiesterase 1	2R8Q	1.50	Wang *et al.*, 2007
	Glyceraldehyde-3-phosphate	1A7K	2.80	Kim & Hol, 1998
	Phosphomannomutase	2I54	2.10	Kedzierski *et al.*, 2006
L. mexicana	Phosphoglucose isomerase	1Q50	2.60	Cordeiro *et al.*, 2004
	Pyruvate kinase	1PKL	2.35	Rigden *et al.*, 1999
	Glycerol-3-phosphate	1EVZ	2.80	Suresh *et al.*, 2000
	Triosephosphate isomerase	2VXN	0.82	Alahuhta & Wierenga, 2010

2.8.1 *Leishmania Infantum* Trypanothione Reductase (*Li*TR)

Trypanothione reductase belongs to a family of FAD-dependent NAD(P)H oxidoreductases. It is unique to Trypanosomatidae parasites where it takes part in the metabolism of trypanothione, **94**, (Baiocco *et al*., 2013), Scheme 2.3. Trypanothione (**94**) guards the pathogen against oxidative and chemical stress. When trypanothione reductase is inhibited, the levels of trypanothione (**94**) in cells decrease; this exposes the parasite to the toxic free radicals from the host (Sharma & Anand, 1997). Since this pathway is absent in mammals, it is a desirable target for the development of antileishmanial drugs (Krauth-Siegel *et al*., 2003).

Quinone derivatives have been reported to bind effectively with *Leishmania infantum* trypanothione reductase at the FAD binding cavity (Venkatesan *et al*., 2010). In this study, the potential of naturally occurring quinones from the genus *Pentas* to inhibit trypanothione reductase was explored by docking at the active site of the receptor. The active site for *Leishmania infantum* trypanothione reductase is along Cys52, Cys57, and His461 (Baiocco *et al*., 2011).

94
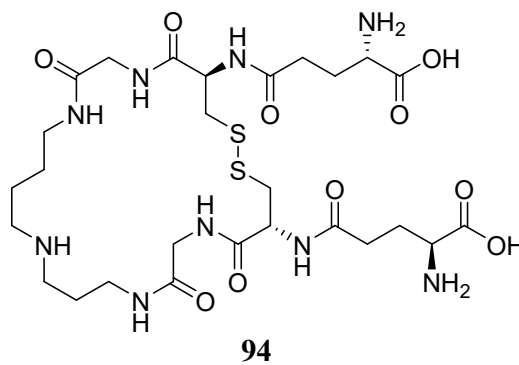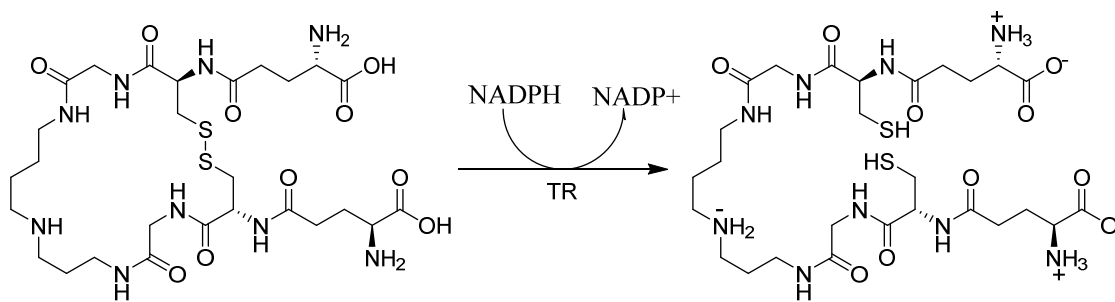
Scheme 2.3: Trypanothione reductase-catalysed reduction of trypanothione

CHAPTER THREE

MATERIALS AND METHODS

3.1   Materials

3.1.1   Plant Materials

The aerial parts of *Pentas bussei* and *Pentas micrantha* were collected in June 2013 from Coastal Region (Kenya), and specimens were deposited at the Herbarium, Department of Biology, the University of Nairobi; voucher numbers AYT-2013-048 and AYT-2013-049 respectively. The stem bark of *Pentas zanzibarica* was collected in June 2018 from Machakos, and its specimen was deposited at the Herbarium, Department of Biology, University of Nairobi (voucher number: AYT-2018-055). The roots of *Pentas parvifolia* were collected in April 2015 from Elgeyo-Marakwet, Kenya. *Pentas longiflora* roots were collected from Nandi Hills (Nandi East district, Kenya), and a specimen under voucher number MEA 2009/001 was deposited at the Herbarium, Department of Biology, University of Nairobi (Endale, *et. al.*, 2012). The roots of *Pentas longiflora* was collected from the Gusii region, Kenya, in December 2020.

3.1.2: Solvents and Reagents

The solvents used included ethanol, hexane, ethyl acetate, acetone, dichloromethane and acetonitrile. The solvents for chromatography were glass distilled to improve their percentage purity. Silver nitrate was used together with sodium hydroxide to prepare silver(I) oxide.

3.2   Methods

3.2.1: General Methods

The ^1H and ^{13}C NMR of the phytochemicals were done on a Bruker Avance 500 MHz Spectrometer; Tetramethyl silane and, in some cases, residual solvent signals served as the reference. H-H-COSY, HSQC and HMBC spectra were processed using MestReNova 14.1 (Mestrelab Research SL). The LC-ESIMS experiments were performed on a Micromass GC-TOF micromass spectrometer (Micromass, Wythenshawe, Waters, Inc. UK), with 70 eV ionization voltage.

Portions of the plant materials were extracted using dichloromethane-methanol, 1:1 (*ca*. 4 x 4 L) at room temperature to obtain crude extracts, which were concentrated with the aid of a rotary evaporator. The concentrated extracts were fractionated and purified by column chromatography to yield pure phytochemicals. The silica gel (stationary phase) used was impregnated with oxalic acid, where silica gel (2 kg) was soaked in a 3% aqueous solution of oxalic acid, left to stand, decanted and dried in an oven for 3 h.

3.2.2   General Extraction Method

The ground plant materials from the *Pentas* species (*P. parvifolia, P. bussei P. zanzibarica and P. micrantha*) were separately soaked in dichloromethane-methanol, 1:1 (*ca*. 4 L) for 24 hours at room temperature. The crude extracts were concentrated using a rotary evaporator (Type R-II) under low pressure at an average temperature range of 40-60 ^0C. The resultant crude extracts were then fractionated over oxalic acid impregnated silica gel as the stationary phase eluted with *n*-hexane-ethyl acetate in increasing polarities. TLC analysis of the fractions was done using precoated silica gel 60 F_{254} plates. The fractions were combined based on their TLC profiles, followed by subsequent purification utilizing Sephadex LH-20, Chromatotron, Preparative Thin Layer Chromatography and crystallization.

3.2.3 Extraction and Isolation of Compounds from Roots of *Pentas parvifolia*

The ground roots (1.0 Kg) of *Pentas parvifolia* were extracted with acetone (*ca*. 4 x 3 L) at room temperature. The combined extract was concentrated using a rotary evaporator to yield 70 g of crude extract. The crude extract was adsorbed and loaded on a column packed with 500 g of silica gel eluted with *n*-hexane-ethyl acetate mixture in increasing polarity. A total of 211 fractions were obtained, which were combined based on their TLC profiles. Eluting at 6% ethyl acetate in *n*-hexane yielded a pale-yellow precipitate, which was filtered off and washed with pure *n*-hexane to yield a pale-yellow powder of busseihydroquinone B (**51**, 816 mg); this compound was found to have a blue UV-fluorescence at 254 nm.

3.2.3 Extraction and Isolation of Compounds from the Stem Bark of *Pentas parvifolia*

The stem bark of *Pentas parvifolia* (2.5 kg) was extracted using dichloromethane-methanol, 1:1 to obtain 60 g of the crude extract, which was partitioned first between water and *n*-hexane to give 10 g of *n*-hexane-extract. The water layer was further partitioned between water and ethyl acetate to give 21 g of an extract. The *n*-hexane layer was adsorbed on oxalic acid impregnated silica gel and loaded on a column of oxalic acid impregnated silica gel, and eluted with *n*-hexane containing increasing amounts of dichloromethane. Eluting at 3% dichloromethane in *n*-hexane yielded a white precipitate of β-stigmasterol (**50**, 8.0 mg). The extract from the ethyl acetate layer was also adsorbed on oxalic acid impregnated silica gel and loaded on a column packed with oxalic acid impregnated silica gel (600 g). Elution was done with *n*-hexane containing increasing amounts of ethyl acetate, Elution at 6% ethyl acetate provided a white powdery UV-inactive solid of β-amyrin (**95**, 7 mg).

3.2.4 Extraction and Isolation of Compounds from the Aerial Parts of *Pentas parvifolia*

The aerial parts of *Pentas parvifolia* (1.0 kg) was extracted with dichloromethane-methanol, 1:1 (*ca*. 4 x 3L) for 24 h at room temperature. The extract obtained was concentrated using a rotary evaporator and loaded on a column (55 x 5 cm) prepacked with 200 g of oxalic acid impregnated silica gel. The column was subjected to gradient elution with *n*-hexane-ethyl acetate. Fractions eluted at 1-4% ethyl acetate in *n*-hexane were combined based on their TLC profiles and subjected to further purification over Sephadex LH-20 (eluent; dichloromethane-methanol, 1:1); this yielded a white powdery solid of vanillic acid (**96**, 3 mg). The fraction eluted at 7% ethyl acetate was purified over Sephadex LH-20 (eluent; dichloromethane-methanol, 1:1) to give a white powdery solid of *p*-hydroxybenzoic acid (**97**, 1 mg). Elution at 8-10% ethyl acetate yielded a brown powdery solid of protocatechuic acid (**98,** 1 mg).

3.2.5 Extraction and Isolation of Compounds from the Aerial Parts of *Pentas bussei*

The aerial parts of *Pentas bussei* (1 kg) were soaked in dichloromethane-methanol, 1:1 (*ca*. 4 x 3 L) for 24 hours at room temperature, and the combined extract was concentrated on a rotary evaporator to yield 20 g of a crude extract. The extract was adsorbed on 30 g of oxalic acid impregnated silica gel and loaded on a column prepacked with oxalic acid impregnated silica gel (200 g) and eluted with *n*-hexane/ethyl acetate solvent gradient. The fraction eluted with 1% ethyl acetate in *n*-hexane was purified using PTLC (CH$_2$Cl$_2$/CH$_3$OH, 95:5) to provide methyl-1,5-dihydroxy-4-methoxy-2-methyl-2'-(4'-methyl-3-pentenyl)-27/-benzo(/)-chromene-2-carboxylate (**48**, 8 mg).

Elution at 3% ethyl acetate in *n*-hexane yielded a pale yellow amorphous solid of busseihydroquinone A (**7**, 110 mg) and an amorphous solid of busseihydroquinone C (**52**, 14 mg). Further elution at 3% ethyl acetate in *n*-hexane gave a white precipitate of β-stigmasterol (**50**, 5 mg). Elution at 10% ethyl acetate in *n*-hexane yielded an amorphous solid of methyl-8-hydroxy-1,4,6,7-tetramethoxy-2-naphthoate (**47**, 7 mg).

Elution at 15% ethyl acetate in *n*-hexane followed by purification by Sephadex LH-20 (eluent; dichloromethane-methanol, 1:1) yielded *p*-hydroxybenzoic acid (**97,** 1 mg). At 30% ethyl acetate in *n*-hexane, a brown powdery solid of protocatechuic acid (**98**, 4 mg) was obtained.

3.2.6 Extraction and Isolation of Compounds from the Aerial Parts of *Pentas micrantha*

The aerial parts (1 kg) of *Pentas micrantha* was extracted with dichloromethane-methanol, 1:1 (*ca*. 4 x 4 L) for 24 hours at room temperature. The extract was concentrated to yield 29 g of crude extract which was fractionated over oxalic acid impregnated silica gel; elution was done with dichloromethane/*n*-hexane and then with dichloromethane-ethyl acetate solvent system. In each case, the polarity of the mobile phase was gradually elevated by increasing the proportion of the more polar solvent. Elution at 100% of dichloromethane followed by purification by column chromatography over Sephadex LH-20 (eluent; dichloromethane-methanol, 1:1) yielded 2.2 mg of 2-methoxy-3-methylanthraquinone (**72**).

3.2.7 Extraction and Isolation of Compounds from the Stem Bark of *Pentas zanzibarica*

The stem of *Pentas zanzibarica* (1 kg) was extracted with dichloromethane-methanol, 1:1 (*ca*. 4 x 4 L) to yield 20 g of crude extract. The crude extract was adsorbed on 30 g of oxalic acid impregnated silica gel and subjected to column chromatography using oxalic acid impregnated silica gel (400 g) as the stationary phase. *n*-hexane-ethyl acetate was used for gradient elution. Elution at 4% ethyl acetate in *n*-hexane yielded a yellow precipitate which was crystallized in dichloromethane-methanol, 1:1 to form a yellow crystalline solid of rubiadin (**64**, 6 mg).

Further elution at 4% ethyl acetate in *n*-hexane followed by purification by PTLC (dichloromethane-ethyl acetate, 95:5) yielded rubiadin-1-methyl ether (**65**, 5 mg).

3.2.8 Extraction and isolation of Pentalongin from the Roots of *Pentas longiflora*

The dried ground roots of *Pentas longiflora* (300 g) was extracted with dichloromethane-methanol, 1:1 (*ca*. 4 x 1.5 L). The extract was fractionated over oxalic acid impregnated silica gel. Elution was done with 8% dichloromethane in *n*-hexane and afforded pentalongin (**74,** 3 mg).

3.6 Derivatization

3.6.1 Synthesis of Compound 99

Busseihydroquinone A (**7**) (8 mg, 25.97 µmol) was dissolved in acetonitrile (1 mL), and silver (I) oxide (0.4 g) was added. The mixture was warmed to 40 ^{0}C over a water bath for about 10 minutes. The reaction was monitored using TLC. Distilled water (15 mL) was added to the resultant mixture; the mixture was then extracted with dichloromethane (10 x 5 mL). The dichloromethane layer was concentrated and further purified using Sephadex LH-20, eluting with CH_2Cl_2/CH_3OH, 1:1, to obtain a purple solid of 1-hydroxy-4,6-dimethoxy-7,8-dioxo-7,8-dihydro-naphthalene-2-carboxylic acid methyl ester (**99**, 0.8 mg, 2.74 µmol, 11% yield).

3.7 Antileishmanial Activity

The antileishmanial activity of phytochemicals from the genus *Pentas* was explored through *in silico* and *in vivo* experiments which are discussed in the following sections.

3.7.1 Computational Modelling

The binding affinities of the phytochemicals from *Pentas* species were predicted with the aid of UCSF Chimera 1.15 (Pettersen *et al*., 2004), which was used in combination with Avogadro (Hanwell *et al*., 2012) and Biovia Discovery Studio (Dassault systems, 2016).

3.7.2 Ligand Identification

Phytochemicals previously reported in the genus *Pentas* were docked with *Leishmania infantum* trypanothione reductase. The genus *Pentas* is a rich source of anthraquinones and naphthols, some of which were reported to show significant antiprotozoal activity against strains of *Plasmodia* (Endale *et al.*, 2012). These phytochemicals mainly were from *Pentas parvifolia*, *Pentas bussei*, *Pentas micrantha*, *Pentas longiflora, Pentas schimperi* and *Pentas lanceolata*.

3.7.3 Ligand Preparation and Optimisation

The molecular structures of the phytochemicals were downloaded from PubChem (https://pubchem.ncbi.nlm.nih.gov/). In some cases, the structures were drawn using ChemDraw Ultra 16.0 (PerkinElmer Informatics Inc.). The ligand molecules were then imported into Avogadro software and the energy of the 3D molecules was minimized using the Hamiltonian MMFF94s force field.

3.7.4 Receptor Preparation

The crystal structure of the receptor protein (PDB ID: 4adw) was downloaded from RCSB Protein Databank (https://www.rcsb.org/) and imported into Chimera. Hydrogens were added to the receptor, and all the non-standard residues (cofactors, water) were removed (Venkatesan *et al.*, 2010). For each ligand, ten binding modes were conducted, and the mode that gave the lowest binding energy was considered for further studies.

3.7.5 Docking of the Compound Library

The compounds were docked with the receptor binding site using the default USCF Chimera parameters. The binding affinities of the compounds were ranked based on the S-score; the more negative the S-score, the greater the binding affinity of the ligand for the binding site of the receptor. The ligand-receptor interactions were observed with the aid of Biovia Discovery Studio (Dassault systems, 2016).

3.8 *In vitro* Antileishmanial Assay

Strains of *Leishmania donovani* were obtained from the Indian Institute of Chemical Biology and maintained in BALB/c mice at West Bengal State University's animal facility. Pentalongin (**74**) was evaluated for antileishmanial activity against peritoneal macrophages and two strains of *L. donovani*: antimony sensitive strain (MHOM/IN/83/AG83) and antimony resistant strain (MHOM/IN/89/GE1). Intracellular amastigotes of infected spleen of BALB/c mice were transformed into promastigotes in M119 medium. The M119 medium was enriched with 1% penicillin-streptomycin and 10% FBS at 22 – 24 ^{0}C. MTT micro method was used to estimate the percentage inhibition (Schuchter *et al*., 1991; Sultana *et al*., 2018). The cultures of promastigotes with an accumulative concentration of pentalongin (**74**) were incubated for 48 h in a complete M119 medium (96-well plate, 296 µL per well, BD Falcon). Identical wells were incubated with increasing concentrations of miltefosine, and this served as a positive control experiment. Furthermore, identical well plates without test compounds were also treated similarly, and this served as the negative control experiment. Equal volumes of DMSO were added to the control experiment. MTT (5 mg/mL, 20 1 per well) was then added to each well and incubated for an extra 4 h at 37 ^{0}C. Acidified isopropanol was added to halt the reaction. The absorbance was then measured at 595 nm in a microplate reader (Bio-Rad, USA). The plots of per cent inhibition against concentration were used to determine the 50% inhibition concentration. Griess reagent was used to assay nitric oxide (NO) generation from RAW 264.7 cells (Dey *et al*., 2020).

Supernatants were collected and distributed (100 µL per well plate) in 96-well plates, and an equal volume of Griess reagent was added to each well. The wells were incubated for 15 minutes at 37 ^{0}C. Absorbance was taken at 540 nm utilizing a microplate reader (Bio-Rad, USA).

CHAPTER FOUR

RESULTS AND DISCUSSION

4.1   Introduction

The crude extracts from the five *Pentas* species were analysed using analytical Thin Layer Chromatography. This revealed the presence of phytochemicals as visualised under Ultraviolet light (254 and 366 nm) and with the aid of iodine vapour. The phytochemical constituents of the extracts were isolated using a combination of chromatographic techniques such as column chromatography and Preparative Thin Layer Chromatography. A combination of spectroscopic techniques were used to analyse the pure compounds, and the results obtained are discussed in the sections that follow.

4.2   Characterisation of Compounds Isolated from the Roots of *Pentas parvifolia*

Busseihydroquinone B (51)

Busseihydroquinone B was isolated as a yellow powder with a blue fluorescence on TLC under Ultra violate light (254 nm). ESI-MS showed a protonated molecular $[M+H]^+$ ion peak at *m/z* 301.2, corresponding to the molecular formula $C_{17}H_{16}O_5$ which was supported by the ^{13}C NMR data. The NMR spectra (Table 4.1) showed that the compound is a naphthalene derivative with 2,2-dimethyl chromene, carboxylic acid, methoxy and hydroxy substituents. The ^{13}C NMR spectrum revealed a total of seventeen signals. In the ^1H NMR spectrum, two protons resonating at δ_H 8.27 (1H, *d*, *J* = 10.0 Hz) and 7.11 (1H, *d*, *J* =10.0 Hz) exhibited *ortho*-coupling, which implied that ring B of the naphthol skeleton is di-substituted with a 2,2-dimethylchromene ring at C-5/C-6 with the oxygen being at C-6, which was apparent from the ^1H NMR spectrum that showed singlet at 1.49 (δ_C 27.7) integrating for 6 protons; hence two methyl groups shifted downfield. The two methine protons resonated at δ_H 5.62 (*d*, *J* = 10.3 Hz) and δ_H 7.72 (*d*, *J* = 10.3 Hz), Table 4.1. The signal at δ_H 8.27 showed an HMBC correlation with C-1; hence it was assigned to H-8 while the singlet at δ_H 7.11 was assigned to H-7. Ring A showed a singlet at δ_H 7.09; thus, it is tri-substituted with hydroxy, methoxy and carboxylic acid (Table 4.1).

The signal at δ_C 174.7 is consistent with the presence of an oxycarbonyl group which was placed at C-2 based on HMBC correlation of H-3 to the carbonyl carbon.

In the HMBC spectrum, a cross peak between methoxy protons and C-4 guided the placement of this group at C-4. The signal at δ_H 11.26 revealed intramolecular hydrogen bonded hydroxy group which was placed at C-1. Hence, based on the 1D and 2D NMR data (Table 4.1), the compound was characterised as 5,6-(2',2'-dimethylpyrano)-1-hydroxy-4-methoxy-2-naphthoic acid.

51
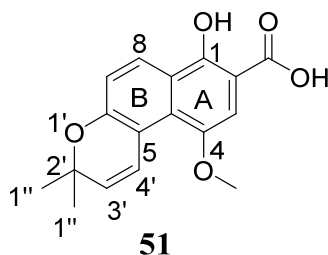
Table 4.1: ^{1}H (500 MHz) and ^{13}C (125 MHz) NMR data for busseihydroquinone B in CDCl$_3$

Position	δ_C in ppm	δ_H in ppm, m, (J in Hz)	HMBC
1	157.2	-	-
2	104.5	-	
3	103	7.09 (s)	C-1, C-2, C-4a, C-4, -COOH
4	149.6	-	-
4a	115.2	-	-
5	127.7	-	-
6	155.7	-	-
7	118.8	7.11 (d, J=9.3)	C-4a, C-5, C-8a
8	125.9	8.27 (d, J=9.0)	C-1, C-4a, C-5, C-6
8a	121.5	-	-
2'	75.6	-	-
3'	127.9	5.62 (d, J =10.3)	C-1", C-2', C-4a
4'	122.9	7.72 (J=10.2)	C-2', C-4a, C-5, C-6
1"	27.7	1.49 (s)	C-1", C-2', 3'
1-OH		11.26 (s)	C-1, C-2, C-8a
2-COOH	174.7	-	-
2-COOH	-	9.7, (s)	-
4-OCH$_3$	55.9	3.93 (s)	C-4

51

4.3 Characterisation of Compounds Isolated from the Stem of *Pentas parvifolia*

β-Stigmasterol (50)

Compound **50** was isolated as a white amorphous solid invisible on TLC under UV-light (354 nm and 366 nm). The ^{13}C NMR spectral data presented a total of twenty-nine signals, in agreement with a steroid skeleton. Of these signals, four occurred at δ_C 141.0, 121.9, 138.5 and 129.5, which were assigned to olefinic carbon atoms; this indicated the presence of a pair of olefinic functional groups. Signals due to methyl carbon atoms resonated at δ_C 12.1, 12.3, 19.2, 19.6, 20.0 and 21.3.

A characteristic signal at δ_C 71.9 typical to an oxy-methine carbon atom was observed; this is typical of C-3 on a steroid skeleton (Kiganda, 2012). In agreement with this, the ^{1}H NMR spectrum showed a multiplet at δ_H 3.51 belonging to an oxymethine proton at C-3. In addition, a signal at δ_H 5.01 (*dd, J* = 15.0, 5.0 Hz)) was ascribed to a vinyl proton that couples with another vinyl proton at δ_H 5.15 (*dd, J* =15.0, 5.0 Hz) which suggested presence of a *trans* double bond. A broad doublet was observed at δ_H 5.35, and it belongs to an olefinic proton at C-6. This assignment was supported by HMBC correlations between H-6 and C-1. The spectral data is consistent with that of β-stigmasterol (Kiganda, 2018).
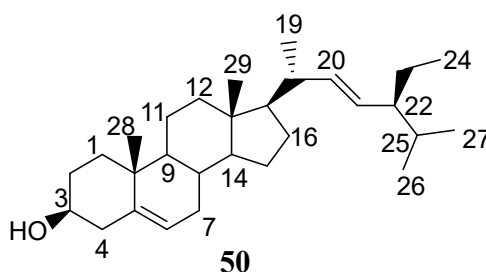
Table 4.2: ^{1}H (500 MHz) and ^{13}C (125 MHz) NMR data for β-stigmasterol in CDCl$_3$

Position	δ_H in ppm, *m*, *J* in Hz	δ_C Experimental	δ_C Literature (Kiganda, 2018)
1		37.5	37.8
2		32.0	32.2
3	3.51 (*m*)	71.9	72.2
4		42.6	42.9
5		141.0	141.5
6	5.35 (*J*=5.0)	121.9	122.0
7		31.9	32.5

Position	δ_H in ppm, *m*, *J* in Hz	δ_C Experimental	δ_C Literature (Kiganda, 2018)
8		32.2	32.5
9		50.4	50.7
10		36.7	36.7
11		21.4	21.6
12		40.0	40.3
13		42.5	41.1
14		57.1	57.4
15		24.5	24.8
16		29.5	29.5
17		56.3	56.6
18		40.6	40.4
19		21.3	21.6
20	5.15 (*dd*, *J*=15.0, *J*=5.0)	138.5	139.0
21	5.01 (*dd*, *J*=15.0, *J*=5.0)	129.5	129.8
22		46.1	46.1
23		25.6	26.0
24		12.1	12.2
25		29.1	29.7
26		20.0	20.1
27		19.6	19.7
28		19.2	19.1
29		12.3	12.3

β-Amyrin (95)

Compound **95** was obtained as a white powdery solid which was invisible on TLC under UV-light (354 and 366 nm) but visible with iodine vapour. The ^{13}C spectrum showed 30 signals, characteristic of a triterpene skeleton. The signals at δ_C 143.6 and δ_C 122.9 ppm were assigned to sp^2 hybridized carbon atoms. The presence of an oxymethine carbon atom was shown by a downfield shifted signal at δ_C 79.3, corresponding to C-3 of a triterpenol. An olefinic proton signal appeared at δ_H 5.29 (δ_C 122.9) while that of an oxymethine proton appeared as a doublet of a doublet (J = 15, J = 5 Hz) at δ_H 3.22 (δ_C 79.3). By comparison (Table 4.3) of the ^{13}C NMR spectral data with literature, the compound was identified as β-amyrin (Knight, 1974).

95
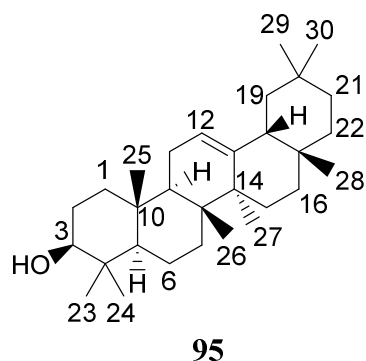
Table 4.3: ^{1}H (500 MHz) and ^{13}C (125 MHz) NMR data for β-amyrin in CDCl$_3$

Position	δ$_H$ in ppm, m, *J* in Hz	δ$_C$ in ppm	Literature (Knight, 1974)
1		39.0	38.7
2		28.3	27.3
3	3.22, (*dd*, *J*=15, *J*=5)	79.3	79.0
4		39.5	39.0
5		55.5	55.3
6		17.3	18.5
7		33.2	32.8
8		41.3	38.8
9		47.9	47.7
10		37.3	37.0
11		23.6	23.6
12	5.29 (*m*)	122.9	121.2
13		143.6	145.1
14		41.9	41.8
15		27.9	26.2
16		27.4	27.0
17		32.9	32.5
18		46.7	47.4
19		46.0	46.9
20		32.6	31.1
21		34.0	34.8
22		38.7	37.2
23		23.3	28.2
24		18.5	15.5
25		15.5	15.6
26		15.7	16.9
27		26.1	26.0
28		23.8	28.4
29		30.8	33.3

Position	δH in ppm, m, *J* in Hz	δC in ppm	Literature (Knight, 1974)
30		23.8	23.7

4.4 Characterisation of Compounds Isolated from the Aerial Parts of *Pentas parvifolia*

Vanillic acid (96)

Compound **96** was isolated as a white solid. ESI-MS gave a protonated molecular ion peak at *m/z* 169.4 $[M+H]^+$, which along with ^{13}C NMR data (Table 4.4) fits the molecular formula $C_8H_8O_4$. The ^1H NMR spectrum revealed a pair of *ortho*-coupled protons (δ_H 7.54 and 6.88, *J* = 8.22, 2.09). Due to higher-order coupling, the proton resonating at δ_H 7.54 also showed *meta*-coupling with the broad singlet at δ_H 7.52. The ^1H NMR further showed evidence of methoxy protons resonating at δ_H 3.89; which suggests that the compound has a tri-substituted benzene ring. From ^{13}C NMR, a signal at δ_c 167.5 was assigned to a carbonyl carbon of a carboxylic acid. The signal at δ_c 151.7 was assigned to an oxygenated carbon bearing a hydroxy group. Based on HSQC, COSY and HMBC correlations, the compound was identified as 4-hydroxy-3-methoxybenzoic acid.

96
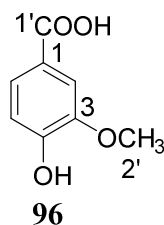
Table 4.4: ^1H (500 MHz) and ^{13}C (125 MHz) NMR data for vanillic acid in CDCl₃

Position	δc in ppm	δH in ppm, *m, J* in Hz	HMBC
1	122.7	-	
2	113.4	7.52 (*s*)	C-1', C-3, C-4, C-6,
3	147.9	-	-
4	151.7	-	-
5	115.4	6.88, (*d, J* = 8.15	C-1, C-3, C-4
6	125.0	7.54 (*dd, J* = 8.22, 2.09	C-2, C-4, C-1'
1-COOH	167.5	-	-
3-OCH₃	56.7	3.89 (*s*)	C-3
5-OH	-	-	-

_p_-Hydroxybenzoic acid (97)

Compound **97** was isolated as a white powder. ESI-MS showed a protonated molecular ion peak at _m/z_ 139.3 [M+H]$^+$, which along with ^{13}C NMR data (Table 4.5) fits the molecular formula $C_7H_6O_3$. From the ^{13}C NMR spectral data, a signal at δ_C 167.4 was assigned to the carbonyl carbon of a carboxylic acid, while δ_C 162.3 was assigned to an oxygenated carbon. In the ^{1}H NMR spectrum, the presence of an AA′XX′ spin system at 7.87 (2H, H-2/6) and 6.86 (2H, H-3/5) for aromatic protons is consistent with a 1,4-disubstituted benzene ring (with carboxylic acid and hydroxy groups) and was supported by HMBC correlations of H-2/H-6 with C-1′, C-2, C-5 and C-6, as well as correlation of H-3/H-5 with C-1, C-4, C-5. Therefore, the compound was identified as _p_-hydroxybenzoic acid.

97
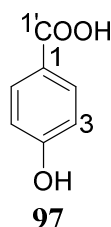
Table 4.5: ^{1}H (500 MHz) and ^{13}C (125 MHz) NMR data for _p_-hydroxybenzoic acid in CD$_3$CN

Position	δ_C in ppm	δ_H in ppm, _m_, _J_ in Hz	HMBC
1	122.5	-	-
2/6	132.9	7.87 (2H) AA′	C-1′, C-2, C-5, C-6
3/5	116.0	6.86, (2H) XX′	C-1, C-4, C-5
4	162.3	-	-
1-COOH	167.4	-	-
4-OH	-	-	-

Protocatechuic acid (98)

Compound **98** was isolated as a brown powder. ESI-MS of compound **98** gave a protonated molecular ion peak at _m/z_ 155.2 [M+H]$^+$, which along with ^{13}C NMR (Table 4.6) matches the molecular formula $C_7H_6O_4$. The ^{1}H NMR data shows three aromatic protons with an ABX spin system at δ_H 7.42 (_d_, _J_ = 2.0 Hz) (δ_C 115.8), 7.44 (_dd_, _J_ = 8.2, 2.0 Hz) (δ_C 145.0) and 6.87 (_d_, _J_ = 8.2 Hz) (δ_C 117.3). This pattern suggests the presence of a tri-substituted

(two hydroxy groups and carboxylic acid) benzene ring. In the ^{13}C spectrum, a chemical shift value of 167.2 ppm was consistent with a carbonyl carbon of a carboxylic acid.

The positioning of hydroxy substituents was fixed at C-3 and C-4 based on the HMBC correlations of H-2 and H-4 with C-3 (δ_C 150.4) and C-4 (δ_C 145.0), typical of oxygenated aromatic carbon atoms. The cross peak between H-5 and C-3 in the HMBC spectrum guided the assignment of δ_C 150.4 to C-4. Based on the spectroscopic data presented in Table 4.6, the compound was identified as 3,4-dihydroxybenzoic acid, also known as protocatechuic acid.

98
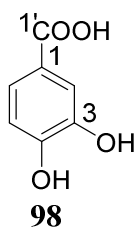
Table 4.6: ^1H (500 MHz) and ^{13}C (125 MHz) NMR data for Protocatechuic acid in DMSO-d$_6$

Position	δ_C in ppm	δ_H in ppm, *m*, *J* in Hz	HMBC
1	122.9	-	-
2	115.8	7.42(1H, *d*, *J* = 2.0)	C-3, C-4, C-6, COOH
3	145.0	-	-
4	150.4	-	-
5	117.3	6.87 (1H, *d*, *J* = 8.2)	C-1, C-3, C-4, C-6,
6	124.0	7.44 (1H, *dd*, *J* = 8.2, 2.0)	C-2, C-4, C-6, COOH
1-COOH	167.2	-	-
3-OH	-	-	-
4-OH	-	-	-

4.5   Characterisation of Compounds Isolated from the Aerial Parts of *Pentas bussei*

Busseihydroquinone A (7)

Compound **7** was isolated as a pale-yellow powder. ESI-MS of compound **7** gave a protonated molecular ion peak at *m/z* 309.3 [M+H]$^+$ corresponding to molecular formula

$C_{15}H_{16}O_7$. The observed fragmentation is most likely due to loss of the methoxy through α-cleavage of a methyl ester moiety (Scheme 4.1).
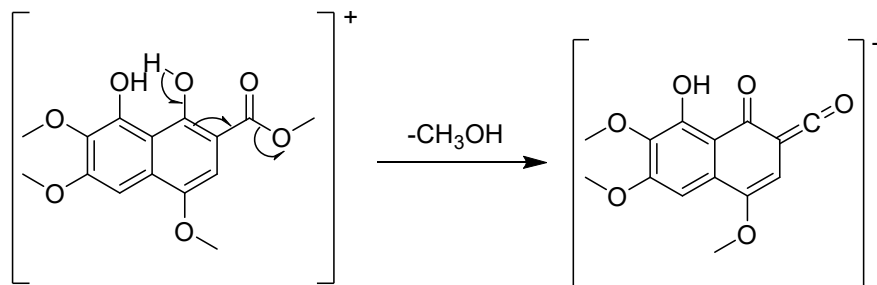
Scheme 4.1: Proposed fragmentation pattern of busseihydroquinone A

The ^1H NMR spectrum (Table 4.7) showed resonances for three methoxy groups (δ_H 3.83, 3.95 and 3.96) and two hydrogen-bonded hydroxy groups (δ_H 13.0 and 9.7) on a naphthalene skeleton. There were also two aromatic singlets at δ_H 6.96 (H-3) and 7.14 (H-5) consistent with substituents at C-1, C-2, C-4, C-6 and C-8 on a naphthalene skeleton. The C-7 methoxy carbon appears downfield (at δ_C 60.6) because of the non-coplanarity of this methoxy group with the aromatic ring since it is sandwiched between two heavy groups, which affects the resonance position (Agrawal, 2013).

Based on the 1D, 2D NMR and MS data, compound **7** was characterised as methyl 1,8-dihydroxy-4,6,7-trimethoxy-2-naphthalenecarboxylate.
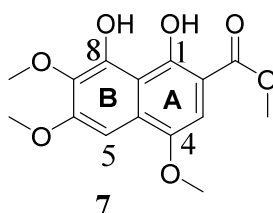
Table 4.7: ^1H (500 MHz) and ^{13}C (125 MHz) NMR data for busseihydroquinone A in acetone-d_6

Position	δ_C in ppm	δ_H in ppm, *m*, *J* in Hz	HMBC
1	156.6	-	-
2	103.0	-	-
3	100.9	6.96 (*s*)	C-1, C-1' C-2, C-4, C-4a, C-5
4	148.4	-	-
4a	128.9	-	-
5	94.9	7.14 (*s*)	C-4, C-4a, C-6, C-7, C-8a
6	157.5	-	-
7	136.5	-	-

Position	δ_C in ppm	δ_H in ppm, m, J in Hz	HMBC
8	157.5	-	-
8a	111.4	-	-
1-OH		13.06 (s)	-
2-COOCH₃	53.2	4.01 (s)	C-1′
2-COOCH₃	172.6	-	-
4-CH₃	56.3	3.95 (s)	C-3, C-4
6-OCH₃	56.3	3.96, (s)	C-6, C-5
7-OCH₃	60.6	3.83 (s)	C-7
8-OH		9.58 (s)	-

Compound 48

Compound **48** was isolated as a red paste. The ESI-MS of compound **48** gave a protonated molecular ion [M+H]⁺ peak at *m/z* 399.2, which together with NMR data (Table 4.8) was consistent with the molecular formula $C_{23}H_{26}O_6$. This compound is also a naphthalene derivative as shown from NMR data (Table 4.8). The ¹H NMR data also revealed the presence of only two singlets in the aromatic region of the naphthalene skeleton suggesting that both rings are tri-substituted. ¹H NMR data further showed the presence of a cyclised geranyl substituent as evidenced by the presence of signals for three methyl-groups, (δ_H 1.66, 1.47 and 1.57); this is further supported by the presence of signals corresponding to olefinic protons at δ_H 5.1, *t* (δ_C 124.0), 8.02, *d*, *J* = 10.4 Hz (δ_C 123.5) and δ_H 5.67, *d*, *J* = 10.4 Hz (δ_C 128.0). The magnitude of the coupling constant (*J* = 10.4 Hz) is consistent with mutually coupled cis-oriented olefinic protons belonging to a chromene moiety. The NOESY correlation between H-5 and 4-OCH₃ guided the placement of the chromene moiety at C-7/C-8; this was further confirmed by NOESY correlation between 1-OH and H-1'. The HMBC spectrum indicated correlations of H-3 with C-1, C-2, C-3, C-4a, C-5 and COOCH₃ which ascertained the placement of the hydroxy, methyl ester and methoxy on ring A.

Basing on the COSY, HSQC and HMBC, compound **48** was characterised as methyl 1,5-dihydroxy-4-methoxy-2-methyl-2'-(4'-methyl-3-pentenyl)-27/-benzo(/)-chromene-2-carboxylate. The compound has already been reported in the literature (Endale, 2012; Bukuru, 2002).

48
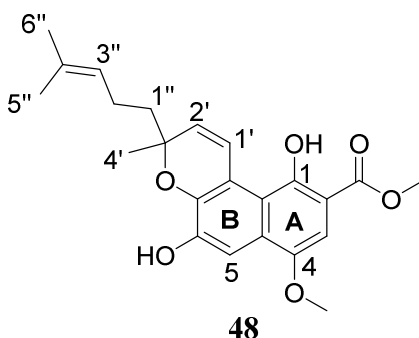
Table 4.8: ^{1}H (500 MHz) and ^{13}C (125 MHz) NMR data for compound **48** in CDCl$_3$

Position	δ$_C$ in ppm	δ$_H$ in ppm, *m*, *J* in Hz	HMBC
1	157.7	-	-
2	103.7	-	-
3	99.7	6.92 (*s*)	C-1, C-2, C-3, C-4a, C-5, COOCH$_3$
4	147.4	-	-
4a	127.3	-	-
5	105.5	7.61 (*s*)	C-1, C-4a, C-4, C-6, C-7, C-8a
6	147.0	-	-
7	141.1	-	-
8	117.5	-	-
8a	116.1	-	-
1′	123.5	8.02 (*d*, *J* = 10.4)	C-3′, C-6, C-7, C-8, C-8a
2′	128.0	5.67 (*d*, *J* = 10.4)	C-1″, C-3′, C-4′, C-7, C-8
3′	79.0	-	-
4′	25.7	1.47 (*s*)	C-1″, C-2′, C-3′
1″	40.5	1.77-1.82, (*m*)	C-2′, C-2″, C-3′, C-3″, C-4′
2″	22.9	2.11-2.18 (*m*)	C-1″, C-3″
3″	124.0	5.1 (1H, *t*)	C-1″, C-2″, C-5″, C-6″
4″	132.1	-	-
5″	17.8	1.57 (*s*)	C-3″, C-6″
6″	25.8	1.66 (*s*)	C-3″, C-4″, C-5″
1-OH	-	12.27 (*s*)	C-1, C-2, C-4a, C-8a, COOCH$_3$
2-COOCH$_3$	52.3	3.97 (*s*)	COOCH$_3$
2-COOCH$_3$	172.1	-	-
4-OCH$_3$	56.0	3.92 (*s*)	C-4
6-OH	-	6.06 (*s*)	C-4a, C-5, C-6, C-7
1-OH	-	12.27 (*s*)	C-1, C-2, C-8a

Busseihydroquinone C (52)

Compound **52** was isolated as a yellow powder. ESI-MS of compound **52** gave a protonated molecular ion [M+H]$^+$ peak at *m/z* 369.1 which together with NMR data (Table 4.9) dictated the molecular formula $C_{22}H_{24}O_5$. The NMR data further suggested the presence of a naphthalene moiety with ring A tri-substituted at C-1, C-2 and C-4; the substituents being hydroxy (δ_H 11.24, at C-1), carboxyl (δ_C 173.4, at C-2) and methoxy (δ_H 3.89, δ_C 56.39, at C-4). The singlet at δ_H 7.15 showed HMBC cross-peaks with C-1, C-2, C-4a and the carbonyl carbon, confirming the substitution pattern in ring A.

A pair of *ortho*-coupled protons at δ_H 7.05, *d*, *J* = 9.0 Hz (δ_C 116.0) and δ_H 8.18, *d*, *J* = 9.0 Hz (δ_C 126.0) suggested a di-substituted ring B of the naphthol skeleton.

The NMR data indicated that the substituent is a cyclized geranyl group forming a chromene ring at C-5/C-6. The placement of the chromene substituent was based on the HMBC correlation of H-6 with the oxygenated aromatic carbon at δ_C 156.7 (C-1). The HMBC correlations further confirmed the placement of the functional groups, and the compound was characterized as 7,8-(2'-methyIpyrano-2,-(4"-methyl-3,-pentenyI)-l-hydroxy-4-methoxy-2-naphthoic acid; it is a known natural product previously isolated from the roots of *Pentas parvifolia* and *Pentas bussei* (Endale, 2012).

52
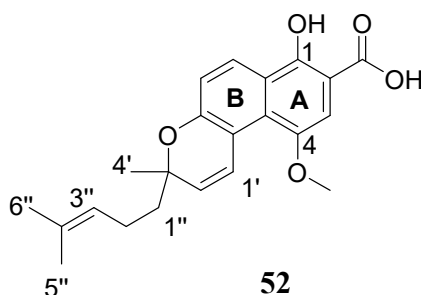
Table 4.9: ^{1}H (500 MHz) and ^{1}H (125 MHz) NMR data for Busseihydroquinone C in CDCl$_3$

Position	δ_C in ppm	δ_H in ppm, *m*, *J* in Hz	HMBC
1	156.7	-	-
2	104.2	-	-
3	105.7	7.15 (*s*)	C-1, C-2, C-4a, C-4, COOH
4	149.8	-	-
4a	115.7	-	-
5	122.3	-	-

Position	δC in ppm	δH in ppm, *m*, *J* in Hz	HMBC
6	155.8	-	-
7	119.5	7.05 (*d*, *J* = 9)	C-5, C-6
8	126.0	8.18 (*d*, *J* = 9)	C-1, C-4, C-4a, C-6, C-8a
8a	127.4	-	
1′	123.8	7.78, (*d*, *J* = 10.3)	C-4a, C-6, C-3′
2′	128.2	5.67, (*d*, *J* = 10.4)	C-1″, C-3′, C-4a, C-4′
3′	78.5	-	-
4′	25.7	1.41 (*s*)	C-1″, C-2′, C-3′
1″	41.0	1.72-1.83 (*m*)	C-2′, C-2″, C-3′, C-3″, C-4′
2″	23.4	2.12-2.18 (*m*)	C-1″, C-3′, C-3″, C-4″
3″	125.0	5.11 (*t*)	C-2″, C-5″, C-6″
4″	132.5	-	-
5″	25.8	1.64 (*s*)	C-3″, C-4″, C-6″
6″	17.6	1.55 (*s*)	C-3″, C-4″, C-5″
1-OH	-	11.24 (*s*)	-
2-COOH	173.4	-	-
4-OCH₃	56.4	3.89 (*s*)	C-4

Methyl 8-hydroxy-1,4,6,7-tetramethoxy-2-naphthoate (47)

ESI-MS of compound **47** gave a protonated molecular ion [M+H]$^+$ peak at *m/z* 323.3 which together with NMR data (Table 4.10) is consistent with molecular formula $C_{16}H_{18}O_7$. The NMR data further suggested the compound is a naphthalene derivative which is tri-substitution in both ring A and ring B. The NMR data also revealed the presence of four methoxy groups [δH 4.01 (δC 64.6), δH 4.00 (δC 56.0), δH 4.00 (δC 56.1) and δH 3.96 (δC 60.9)], methyl ester (δH 3.98 and δC 52.5 for methyl group and δC 166.2 for C=O) and a hydroxy group (δH 9.83). The signal at δH 7.11 (s), was assigned to H-3 based on its HMBC correlations with C-1, C-4a, C-5, C-8a and -COOCH₃, which confirmed the substitution pattern in ring A. The HMBC correlation between methyl protons resonating at δH 3.98 and the carbonyl carbon (δC 166.2) confirmed the presence of the methyl ester group. Comparing with a similar structure (busseihydroquinone A (**7**), Table 4.7), the ester carbonyl carbon in compound **47** is up-field shifted (δC 166.2) than the ester carbonyl busseihydroquinone A (**7**) (δC 172.6) where the carbonyl is involved in intramolecular hydrogen bonding with the hydroxy group at C-1.

The up-field shifted (δC 166.2) chemical shift value of the ester carbonyl carbon in

compound **47** indicates the absence of intramolecular hydrogen bonding and hence C-1 is substituted with a methoxy rather than a hydroxy group of compound **47**. The placement of -COOCH$_3$ at C-2 was guided by HMBC correlation of the methyl ester protons (δ_H 3.98) with C-2 (δ_C 114.0); additionally, H-3 showed an HMBC correlation with the ester carbonyl. The signal at δ_H 7.14 (*s*) was assigned to H-5; this was supported by HMBC correlations of this proton with C-1, C-4, C-6, C-7 and C-8a. The placement of a hydroxy substituent at C-8 was guided by HMBC correlations of the signal at δ_H 9.83 with C-7 and C-8. HMBC correlations were further used to establish the structure, and based on this data, compound **47** was characterised as methyl 8-hydroxy-1,4,6,7-tetramethoxy-2-naphthoate, which appears to be a new compound.

47
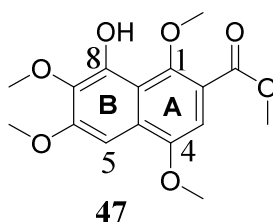
Table 4.10: ^{1}H (500 MHz) and ^{13}C (125 MHz) NMR data for compound **47** in CDCl$_3$

Position	δ_C in ppm	δ_H in ppm, *m*, *J* in Hz	HMBC	δ_C in ppm (Busseihydroquinone A, 7)
1	152.5	-	-	156.6
2	126.7	-	-	103.0
3	103.8	7.11 (*s*)	C-1, C-4a, C-5, C-8a, -COOCH$_3$	100.9
4	150.8	-	-	148.4
4a	115.1	-	-	128.9
5	93.6	7.14 (*s*)	C-1, C-4, C-6, C-7, C-8a	94.9
6	155.4	-	-	157.5
7	135.9	-	-	136.5
8	148.1	-	-	157.5
8a	115.1	-	-	111.4
1-OCH$_3$	64.6	4.01 (*s*)	C-1	-
2-COOCH$_3$	52.5	3.98 (*s*)	C-2, -COOCH$_3$	53.2
2-COOCH$_3$	166.2	-	-	172.6
4-OCH$_3$	56.0	4.00 (*s*)	C-3, C-4	56.3
6-OCH$_3$	56.1	4.00 (*s*)	C-6	56.3
7-OCH$_3$	60.9	3.96 (*s*)	C-7	60.6

Position	δ_C in ppm	δ_H in ppm, m, J in Hz	HMBC	δ_C in ppm (Busseihydroquinone A, 7)
8-OH	-	9.83, (*s*)	C-7, C-8	-

Protocatechuic acid (98)

Protocatechuic acid (**98**) was isolated as a brown powder. The ^{1}H NMR data for compound **98** showed the presence of three mutually coupled aromatic protons in an AMX spin system (Table 4.11); this suggests the presence of a tri-substituted benzene ring with the substituents being carboxyl group (δ_C 167.3) and two hydroxy groups located at C-3 (δ_C 145.0) and C-4 (δ_C 150.0). The identity of the compound was confirmed from the HMBC spectral data (Table 4.11); the compound was therefore identified as 3,4-dihydroxybenzoic acid. The same compound was also isolated from the aerial parts of *Pentas parvifolia*.

98
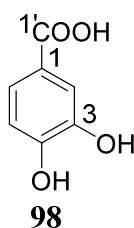
Table 4.11: [1]H (500 MHz) and ^{13}C (125 MHz) NMR data for protocatechuic acid in DMSO-d$_6$

Position	δ_C in ppm	δ_H, in ppm, m, J in Hz	HMBC
1	121.7	-	-
2	115.2	7.33 (*d*, $J = 2.0$)	C-1, C-3, C-4, C-6, COOH
3	150.0	-	-
4	144.9		
5	116.6	6.78 (*d*, $J = 8.2$)	C-1, C-2, C-3, C-4, C-6, COOH
6	121.9	7.28 (*dd*, $J = 8.3, 2.0$)	C-4, C-5, COOH
1-COOH	167.3	-	-
3-OH	-	-	-
4-OH	-	-	-

4.6   Characterisation of Compounds Isolated from the Aerial Parts of *Pentas micrantha*

2-Methoxy-3-methyl-anthracene-9,10-dione (72)

Compound **72** was isolated as a yellow powder. The ^{1}H NMR together with ^{13}C NMR, for which there are 14 sp^2 hybridised carbon atoms, two of which are carbonyl (Table 4.12) suggested an anthraquinone skeleton. The ^{1}H NMR data showed six signals in the aromatic region of which the signals at δ_H 7.6 (s) and 7.35 are due to *para*-oriented protons (H-1 and H-4) of ring A, which is disubstituted at C-2 and C-3 with methyl (δ_H 2.25) and methoxy (δ_H 3.89), respectively. The ^{1}H NMR chemical shift values at δ_H 8.23 (*brd*, *J* = 7.2 Hz), 7.82, (*ddd*, *J* = 7.5, 7.43, 1.4 Hz), 7.88 (*ddd*, *J* = 7.6, 7.52, 1.5 Hz) and 8.1 (*dd*, *J* = 7.64, 1.4 Hz) confirmed the presence of an unsubstituted ring C of anthraquinone. The ^{13}C-NMR chemical shift values of carbonyl carbons at δ_C 183.6 and 181.3 are typical of ring B of the anthraquinone skeleton. In the HMBC spectrum, correlation of δ_H 7.35 with C-2 and C-10 allowed assignment of the signal at δ_H 7.34 to H-4. Furthermore, HMBC correlations of the signal at δ_H 7.60 with C-1a and C-9 is consistent with the signal δ_H 7.60 being due to H-1. Hence, based on the 1D and 2D NMR data (Table 4.12), the compound was characterised as 2-methoxy-3-methyl-anthracene-9,10-dione.

72
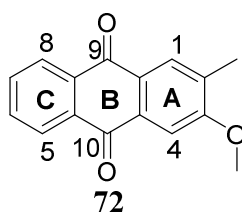
Table 4.12: ^{1}H (500 MHz) and ^{13}C (125 MHz) NMR data for compound **72** in acetone-d$_6$

Position	δc in ppm	δH in ppm, *m, J* in Hz	HMBC
1	110.0	7.60 (1H, *s*)	C-1a, C-9
1a	119.8	-	-
2	127.4	-	-
3	162.2	-	-
4	129.2	7.35 (1H, *s*)	C-2, C-10
4a	108.2	-	-
5a	133.6	-	
5	127.7	8.23 (1H, *d, J* = 7.2)	C-10
6	134.0	7.82 (1 H, *td, J* = 7.5, 7.43, 1.4)	C-5, C-5a, C-8
7	135.2	7.88 (1H, *td, J* = 7.6, 7.5, 1.5)	C-5, C-8a, C-8,
8	127.0	8.16 (1 H, dd, *J* = 7.64, 1.4)	C-9
8a	136.0	-	-
9	183.6	-	-
10	181.3	-	-
2-CH$_3$	9.3	2.25 (3H, *s*)	C-1a, C-2, C-3
3-OCH$_3$	61.3	3.89 (3H, *s*)	C-3

4.7   Characterisation of Compounds Isolated from the Stem Bark of *Pentas*

zanzibarica

Rubiadin-1-methyl ether (65)

Compound **65** was isolated as a yellow powder. ESI-MS of compound **65** indicated a protonated molecular ion peak at *m/z* 269.3 [M+H]$^{+}$, which together with NMR data (Table 4.13) suggested the molecular formula C$_{16}$H$_{12}$O$_4$. The ^{13}C NMR spectrum further revealed the presence of two carbonyl groups resonating at δ$_C$ 182.6 and δ$_C$ 180.2, typical of ring B of an anthraquinone skeleton. The ^{1}H NMR data showed four sets of mutually coupled signals [at δ$_H$ 8.10 (1H, *dd*. 7.6, 1.4 Hz), 7.83 (*ddd, J* = 7.4, 7.4, 1.4 Hz) and δ$_H$ 7.89 (*ddd, J* = 7.7, 7.6, 1.5Hz)] for unsubstituted ring C, while in ring A, the singlet aromatic signal at δ$_H$ 7.51 implies that ring A is tri-substituted with hydroxy (δ$_H$ 11.12), methyl (δ$_H$ 2.16) and methoxy (δ$_H$ 3.79) groups. The placement of the substituents was guided by HMBC correlations. The signal at δ$_H$ 7.51 showed a cross peak with the methyl carbon, C-1a, C-2, C-4a, C-3, C-9 and C-10; which allowed the assignment of this proton to H-4. Based on the above spectroscopic data, the compound was characterized as 3-hydroxy-1-methoxy-2-methylanthraquinone.

66

65
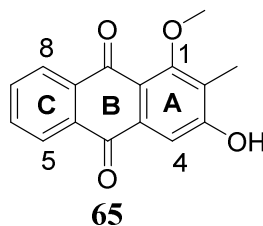
Table 4.13: ^{1}H (500 MHz) and ^{13}C (125 MHz) NMR data for rubiadin-1-methyl ether
(**65**) in DMSO-d$_6$

Position	δ_C in ppm	δ_H in ppm, m, J in Hz	HMBC
1	160.6	-	-
1a	133.7	-	-
2	126.1	-	-
3	161.6	-	-
4	109.0	7.51 (s)	C-1a, C-2, C-3, C-4a, C-9, C-10, 2-CH$_3$
4a	119.0	-	-
5a	132.0	-	-
5	126.0	8.10 (dd, 7.6, 1.4)	C-7, C-8a, C-10
6	133.4	7.83 (ddd, J = 7.44, 7.4, 1.4)	C-5a, C-5, C-7, C-8,
7	134.5	7.89 (ddd, J = 7.7, 7.6, 1.5)	C-8a, C-8
8	126.6	8.15 (dd, J = 7.8, 1.4)	C-5a, C-6, C-9
8a	134.5	-	-
9	180.2	-	-
10	182.6	-	-
1-OCH$_3$	60.6	3.79 (s)	-
2-CH$_3$	9.0	2.16 (s)	C-1a, C-1, C-2, C-3, C-4, C-4a
3-OH	-	11.12 (s)	C-2, C-3, C-4

Rubiadin (64)

Compound **64** was isolated as a yellow powder. ESI-MS of compound **64** revealed a molecular ion peak at m/z 253.8 [M-H]$^-$ which together with the NMR data (Table 4.14) was consistent with the molecular formula $C_{15}H_{10}O_4$. The ^{1}H NMR data shows signals due to a methyl group (δ_H 2.15), two hydroxy groups (δ_H 13.1, 8.02) and five aromatic protons (δ_H 7.36, 8.21, 8.28 and 7.87-7.93) showing the same substitution pattern as in compound **65**. The substituent here being, methyl, and two hydroxy groups (Table 4.14).

The ^{13}C NMR spectrum showed 15 signals, including signals of two carbonyl carbon atoms at δ_C 187.4 and 182.6, typical of 9,10-anthraquinones. The carbon resonating at δ_C 187.4 is significantly more de-shielded than its counterpart at δ_C 182.6; this can be attributed to

intramolecular hydrogen bonding involving the hydroxy group OH-1 (δ_H 13.10). Based on HSQC and HMBC correlations, compound **64** was characterized as 1,3-dihydroxy-2-methyl-9,10-anthraquinone; previously isolated from *Pentas micrantha* and *Pentas suswaensis* (Endale, 2012).

64
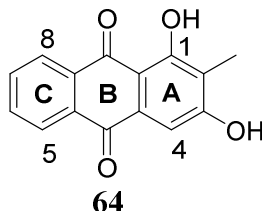
Table 4.14: ^{1}H (500 MHz) and ^{13}C (125 MHz) NMR data for Rubiadin in acetode-d_6

Position	δ_C in ppm	δ_H in ppm, m, J in Hz	HMBC
1	163.8	-	-
1a	132.9	-	-
2	118.5	-	-
3	163.4	-	-
4	107.9	7.36 (*s*)	C-1a, C-2, C-3, C-4a, C-9, C-10
4a	110.1	-	-
5a	134.1	-	-
5	127.3	8.21 (*dd*, *J* = 7.3, 1.8)	C-2, C-10
6	134.8	7.89, (*m*)	C-5, C-5a
7	134.9	7.91 (*m*)	C-5, C-8a
8	127.0	8.28 (*dd*, *J* = 7.3, 1.8)	C-8a, 9
8a	134.0	-	-
9	187.4	-	-
10	182.6	-	-
1-OH	-	-	C-3, C-4a
2-CH$_3$	7.9	2.15 (*s*)	C-1, C-1a, C-2, C-3, C-4
3-OH	-	-	-

4.8   Characterisation of Compounds Isolated from the Roots of *Pentas longiflora*

Pentalongin (74)

Compound **74** was isolated as a brown crystalline solid. The ^{1}H NMR data of compound **74** showed overlapping signals due to aromatic protons (δ_H 8.44, 8.07, 7.72), indicating the presence of an unsubstituted aromatic ring. Methylene protons resonating at δ_H 5.16 reveal attachment to an oxygen atom. Two mutual coupled protons resonating at δ_H 6.96 and δ_H 6.01 revealed the presence of olefinic functionality. The ^{13}C NMR spectrum revealed 13

carbon atoms, including two carbonyl carbon atoms (δ_C 182.4 and 180.6). This spectral data agrees with that reported by Endale (2012) for pentalongin (**74**. The compound was confirmed to be 1*H*-benzo[g]isochromene-5,10-dione.

74
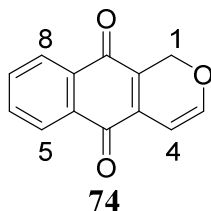
Table 4.15: ^{1}H (500 MHz) and ^{13}C (125 MHz) NMR data for Pentalongin in CDCl$_3$

Position	δ_C in ppm	δ_H in ppm, *m*, *J* in Hz
1	62.3	5.16, (*s*)
1a	136.8	-
3	154.9	6.96
4	97.5	6.01
4a	124.5	-
5	133.6	-
5a	132.6	-
6	126.2	7.61 (*m*)
7	126.7	7.72 (*m*)
8	133.6	8.07 (*m*)
8a	131.9	-
9	182.4	-
10	180.8	-

4.9   Characterization of Compound 99

Compound **99** was obtained as a purple amorphous solid by oxidizing busseihydroquinone A (**7**) using silver (I) oxide (Scheme 4.2).
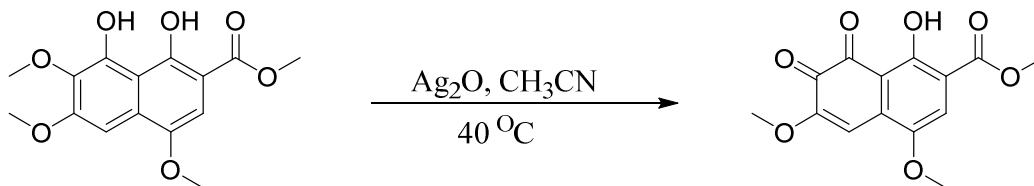
Scheme 4.2: Oxidation of busseihydroquinone A (**7**) using silver (I) oxide

ESI-MS of compound **99** gave [M-H]⁻ ion peak at *m/z* 291.6 which together with NMR data (Table 4.16) is consistent with the molecular formula $C_{14}H_{12}O_7$. The observed fragmentation was attributed to loss of the methoxy as illustrated in Scheme 4.3.
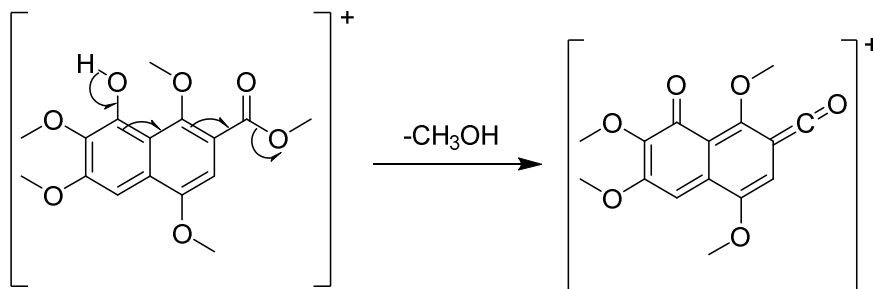
Scheme 4.3: Proposed fragmentation pattern of compound 99

The NMR data suggests a naphthoquinone skeleton substituted at C-1, C-2 and C-4 (with hydroxy, δ_H 12.57), methyl ester (δ_H 3.97, δ_C 52.9 for methyl group and δ_C 165.6 for C=O) and methoxy (δ_H 3.95, δ_C 56.9) respectively as in the starting material (Table 4.16). The placement of the substituents in ring A was confirmed by HMBC correlations of H-3 (δ_H 7.78) with C-1, C-2, C-4, C-4a, C-5, C-8a and COOCH₃. In ring B, the NMR spectral data showed the presence of a methoxy group (δ_H 3.88, δ_C 56.1) at C-6. The data also indicates that C-7 and C-8 were oxidized into carbonyl groups at δ_C 175.8 and δ_C 180.7, respectively. A singlet at δ_H 6.93 was assigned to H-5, the only aromatic proton in ring B. The nature of the ring was confirmed using the HMBC spectrum which showed correlations of H-5 with C-4, C-4a, C-6 and C-7.

The ¹³C NMR spectral data revealed signals due to three carbonyl carbon atoms resonating at δ_C 165.6, 175.8 and 180.7; these were placed at 2-COOCH₃, C-7 and C-8, respectively. The structure was confirmed based on HMBC correlations (Table 4.16) and compound **99** was characterised as 1-hydroxy-4,6-dimethoxy-7,8-dioxo-7,8-dihydro-naphthalene-2-carboxylic acid methyl ester.

99
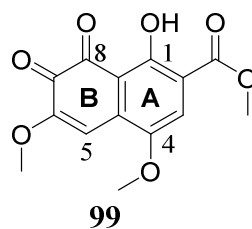
Table 4.16: ^{1}H (500 MHz) and ^{13}C (125 MHz) NMR data for compound **99** in CDCl$_3$

Position	δ$_C$ in ppm	δ$_H$ in ppm, *m*, *J* in Hz	HMBC
1	160.7	-	-
2	127.3	-	-
3	125.5	7.78 (*s*)	C-1, C-2, C-4a, C-4, C-5, C-8a, 2-COOCH$_3$
4	148.5	-	-
4a	114.2	-	-
5	107.8	6.93 (*s*)	C-4a, C-4, C-6, C-7
6	152.2	-	-
7	175.8	-	-
8	180.7	-	-
8a	119.2	-	-
1-OH	-	12.57 (*s*)	-
2-COOCH$_3$	52.9	3.97 (*s*)	COOCH$_3$
2-COOCH$_3$	165.6	-	-
4-OCH$_3$	56.9	3.95 (*s*)	C-4
6-OCH$_3$	56.1	3.88 (*s*)	C-6

71

4.10 Computational Modelling

The binding affinities of the selected phytochemicals from the genus *Pentas* with *Leishmania infantum* trypanothione reductase, Figure 4.2, (Baiocco *et al*., 2013) were predicted using UCSF Chimera 1.15 tool.
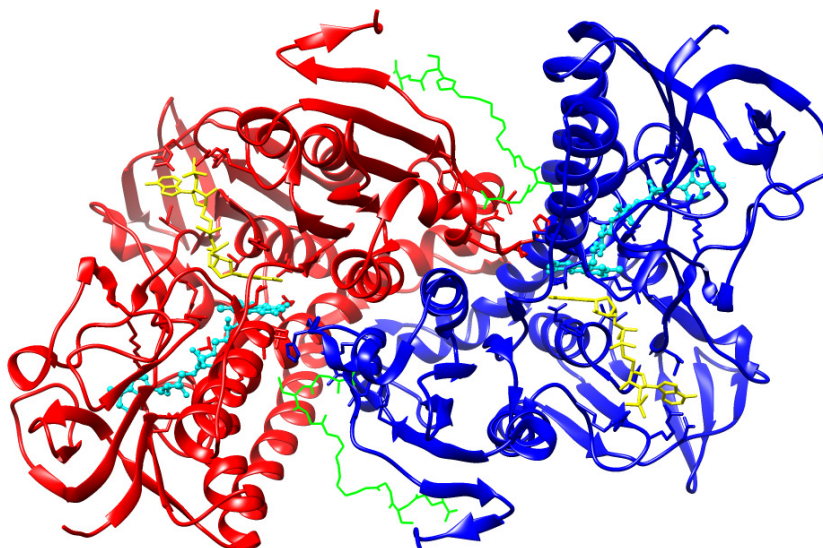
Figure 4.1: Crystal Structure of *Leishmania infantum* trypanothione reductase

Note: The cyan balls and sticks represent FAD, the yellow sticks represent NADPH, and the green wires represent GCG.

4.10.1 Docking Protocol Validation

The native ligand (FAD, **100**) was redocked into the binding site of *Leishmania infantum* trypanothione reductase. The most favourable pose gave a binding energy of -9.8 kcal/mol. FAD (**100**) formed hydrogen bonds with Lys60, Glu202, Ala365, Ser162, Thr335, Thr51 and Asp327 in addition to Van der Waal's interactions with several amino acid residues as demonstrated in Figure 4.2.

100
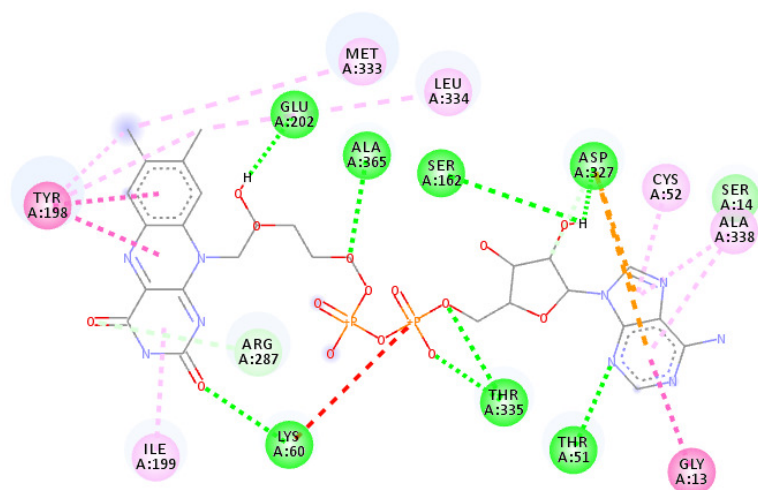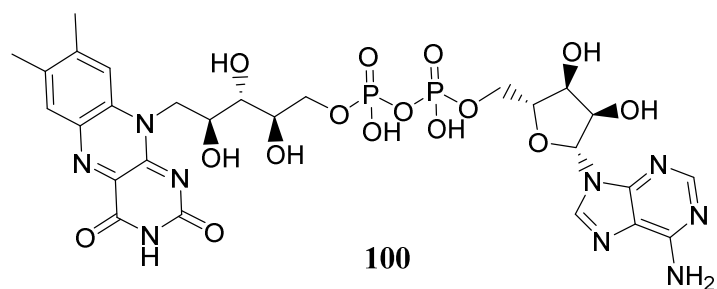
Figure 4.2: Ligand interactions for FAD (**100**)

Key to Interactions

■ Conventional hydrogen bond

□ Carbon hydrogen bond

■ Pi-Sulphur interaction

□ Pi-Alkyl interaction

4.10.2 Docking of the Compound Library

The compound library was docked with *Leishmania infantum* trypanothione reductase (*Li*TR) and their binding energies were predicted using Chimera autodock vina. The corresponding inhibition constants were also computed (Table 4.17).

Table 4.17: Binding energies for phytochemicals from the genus *Pentas*.

SN.	Ligand (Compound)	Compound Class	Binding energy (kcal/mol)	Inhibition constant, K_i (μM)
1	Schimperiquinone A (**92**)	Anthraquinone	-10.9	0.010
2	Rubiadin-3-*O*-β-primeveroside (**62**)	Anthraquinone glycoside	-10.7	0.014
3	Schimperiquinone B (**93**)	Anthraquinone	-10.4	0.024
4	Lucidin-3-*O*-β-primeveroside (61)	Anthraquinone glycoside	-10.2	0.033
5	Rubiadin-1-methylether-3-*O*- β-primeveroside (**54**)	Anthraquinone glycoside	-10.0	0.046
6	13R-*epi*-gaertneroside (**85**)	Iridoid	-9.8	0.065
7	Damnacanthol-3-*O*-β-primeveroside (55)	Anthraquinone glycoside	-9.5	0.108
8	Cleomiscosin A (**91**)	Coumarino-lignoid	-8.9	0.297
9	Isagarin (**77**)	Naphthol	-8.7	0.416
10	Damnacanthal (**63**)	Anthraquinone	-8.6	0.493
11	Lucid-ω-methyl ether (**83**)	Anthraquinone	-8.5	0.583
12	Rubiadin (**64**)	Anthraquinone	-8.5	0.583
13	Nordamnacanthal (**102**)	Anthraquinone	-8.5	0.583
14	Rubiadin-1-methyl ether (**65**)	Anthraquinone	-8.5	0.583
15	3-Hydroxy-1-methylanthraquinone (**71**)	Anthraquinone	-8.4	0.691
16	Damnacanthol (**81**)	Anthraquinone	-8.3	0.818
17	Damnacanthol-3-*O*-methyl ether (**82**),	Anthraquinone	8.2	0.968
18	Tectoquinone (**73**)	Anthraquinone	-8.2	0.968
19	2-Methoxy-3-methylanthraquinone (**72**)	Anthraquinone	-8.2	0.968
20	Busseihydroquinone C (**52**)	Naphthol	-8.2	0.968
21	Methyl 1,5-dihydroxy-4-methoxy-2,-methyl-2'-(4'-methyl-3,-pentenyl)-27/-benzo(/)-chromene-2-carboxylate (**55**)	Naphthol	-8.2	0.968
22	Pentalonginhydroquinone diglycoside (**76**)	Naphthol glycoside	-8.1	1.146
23	Busseihydroquinone D (**53**)	Naphthol	-8.1	1.146
24	Parvinaphthol C (**59**)	Naphthol	-8.1	1.146
25	3,4,6-Trihydroxy-2,2-dimethyl-3,4-dihydro-2H-benzo[h]chromene-5-carboxylic acid methyl ester (**69**)	Naphthol	-8.1	1.146

SN.	Ligand (Compound)	Compound Class	Binding energy (kcal/mol)	Inhibition constant, K_i (μM)
26	2-Hydroxy-3-methyl-anthraquinone (**79**)	Anthraquinone	-8.1	1.146
27	Pachybasin (**80**)	Anthraquinone	-8.1	1.146
28	Busseihydroquinone F (**56**)	Naphthol	-8.0	1.357
29	Mollugin (**66**)	Naphthol	-8.0	1.357
30	3-Hydroxymollugin (**67**)	Naphthol	-8.0	1.357
31	2-Hydroxymethylanthraquinone (**90**)	Anthraquinone	-7.9	1.607
32	Tudoside (**84**)	Iridoid	-7.9	1.607
33	5,6-Dihydroxydamnacanthol (**89**)	Anthraquinone	-7.8	1.903
34	5,6-Dihydroxylucid-ω-methyl ether (**88**)	Anthraquinone	-7.8	1.903
35	Parvinaphthol D (**60**)	Naphthol	-7.8	1.903
36	Psychorubrin (**75**)	Naphthol	-7.8	1.903
37	3,4,6-Trihydroxy-2,2-dimethyl-3,4-dihydro-2H-benzo[h]chromene-5-carboxylic acid methyl ester (**79**)	Naphthol	-7.8	1.903
38	2-Hydroxy-7-methyl-anthraquinone (**78**)	Anthraquinone	-7.8	1.903
39	3-Methoxymollugin (**68**)	Naphthol	-7.7	2.253
40	Pentalongin (**74**)	Naphthol	-7.5	3.158
41	Busseihydroquinone B (**51**)	Naphthol	-7.4	3.739
42	Compound **99**	Naphthol	-6.9	8.698
43	Busseihydroquinone A (**7**)	Naphthol	-6.9	8.698
44	Parvinaphthol A (**57**)	Naphthol	-6.6	14.437
45	Parvinaphthol B (**58**)	Naphthol	-6.6	14.437
46	Methyl 8-hydroxy-1,4,6,7-tetramethoxy-2-naphthoate (47)	Naphthol	-6.3	23.960
47	Protocatechuic acid (**98**)	Benzoic acid derivative	-6.1	33.587
48	Vanillic acid (**96**)	Benzoic acid derivative	-6.1	33.587
49	*p*-Hydroxybenzoic acid (**97**)	Benzoic acid derivative	-5.6	78.141
	Average		**-7.79**	**5.329**

4.10.2.1 Structure-Activity Relationships

The benzoic acid derivatives, which were isolated from the aerial parts of *Pentas parvifolia* and *Pentas bussei*, exhibited the lowest binding affinities for the catalytic site of *Li*TR. The binding affinities of the naphthols ranged from low to moderate; anthraquinones had moderate binding affinity while anthraquinone glycosides had the highest binding affinity for the catalytic site, (Table 4.18). Generally, the binding affinities of the compound classes increased in the order;

Benzoic acid derivatives < Naphthols < Anthraquinones < Iridoids < Anthraquinone glycosides (Table 4.18).

Table 4.18: Comparison of binding affinities for the compound classes

Binding energy range (kcal/mol)	Compound Class and Compound Number				
	Benzoic acid derivatives	Naphthols	Anthraquinones	Iridoids	Anthraquinone glycoside
-5.5 – -6.4	94, 95, 96	53			
-6.5 – -7.4		54, 60, 66, 67, 97			
-7.5 – -8.4		55, 61, 62, 65, 68, 75, 76, 77, 78, 79, 83, 8	80, 82, 86, 88, 89, 91, 92, 103 107	104	
-8.5 – -9.4		85	72, 73, 74, 101, 102		
-9.5 – -10.4			99	105	63, 64, 70
-10.5 – -11.4			98		71

A previous study indicated that molecular flexibility enhances the binding affinity of a ligand (Forrey *et al*., 2012). Therefore, the high binding affinity of the anthraquinone glycosides can be attributed to their structural flexibility rendered by the bridging -*O*-functionality. In addition, the glycoside moiety enables more extensive ligand interactions in the FAD binding cavity (Figure 4.3). For instance, rubiadin-3-*O*-β-primeveroside (**71**) (binding energy: -10.7 kcal/mol) showed a higher affinity for the catalytic site of the

enzyme than its non-glycosidic analogue, rubiadin, (**64**) (binding energy: -8.5 kcal/mol), because it is more flexible and it forms additional hydrogen bonds with Asp327 and Thr51 (Figures 4.3) which is not the case with rubiadin (**64**) (Figure 4.4).
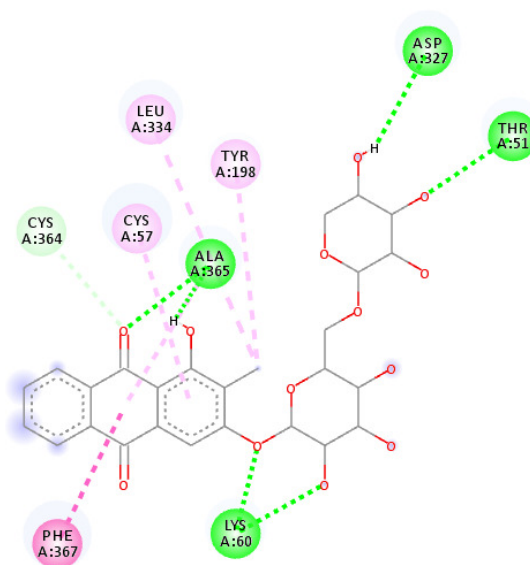
Figure 4.3: Ligand interactions for rubiadin-3-*O*-β-primeveroside (**62**)
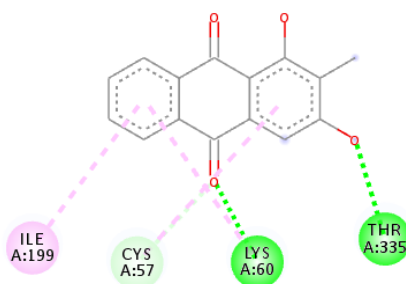
Figure 4.4: Ligand interactions for rubiadin (**64**)

The dimeric anthraquinones exhibited greater binding affinities for the binding site than their monomeric analogues. Due to their structural flexibility, the schimperiquinones A (**92**) (binding energy: -10.9 kcal/mol) and B (**93**) (binding energy: -10.4 kcal/mol) showed superior inhibitory potency than their monomeric analogues (Figures 4.5 and 4.6). The flexibility of the dimers is attributed to their bridging functionalities, *-O-* for schimperiquinone A (**92**) and -CH$_2$- for schimperiquinone B (**93**). In contrast, a naphthol

dimer, busseihydroquinone F (**56**) showed a moderate binding affinity (binding energy: -8.0 kcal/mol) which can be attributed to the rigid -C=C- bridge. Amongst the naphthols, isagarin (**77**) (binding energy: -8.7 kcal/mol) showed the highest affinity for the catalytic site of *Li*TR followed by busseihydroquinone C (**52**) (binding energy: -8.2 kcal/mol), figure 4.7.
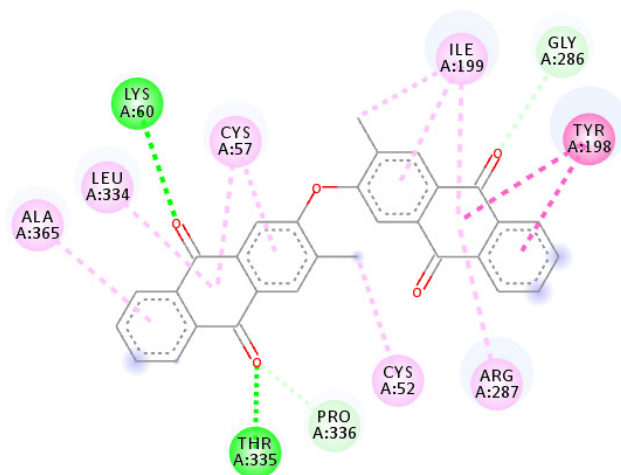
Figure 4.5: Ligand interactions for schimperiquinone A (**92**)
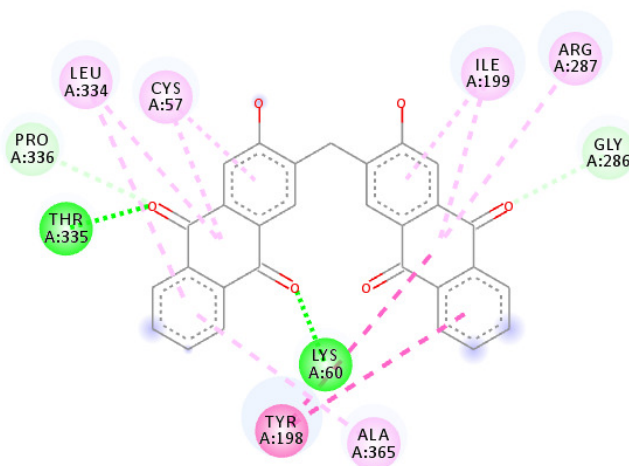
Figure 4.6: Ligand interactions for schimperiquinone B (**93**)
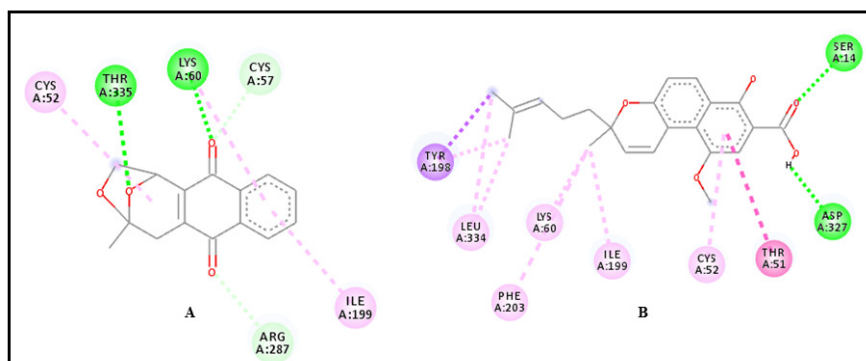
Figure 4.7: Ligand interactions for isagarin (**77**, **A**) and busseihydroquinone C (**52**, **B**)

4.10.2.2 Ligand Interactions for Busseihydroquinone A and its Synthetic Derivative

Both busseihydroquinone A (**7**) and its synthetic derivative, 1-hydroxy-4,6-dimethoxy-7,8-dioxo-7,8-dihydro-naphthalene-2-carboxylic acid methyl ester (**99**) showed similar affinities for the binding site. These ligands formed hydrogen bonds with Thr335, Cys52 and Lys60 in addition to pi-alkyl interactions with Cys57 (Figure 4.8). These amino acid residues orient FAD towards the catalytic site of *Li*TR to enable the enzyme to catalyse the reduction of trypanothione (Venkatesan *et al*., 2010). Therefore, busseihydroquinone A (**7**) and its synthetic derivative (**99**) are potential scaffolds for developing inhibitors for trypanothione reductase.
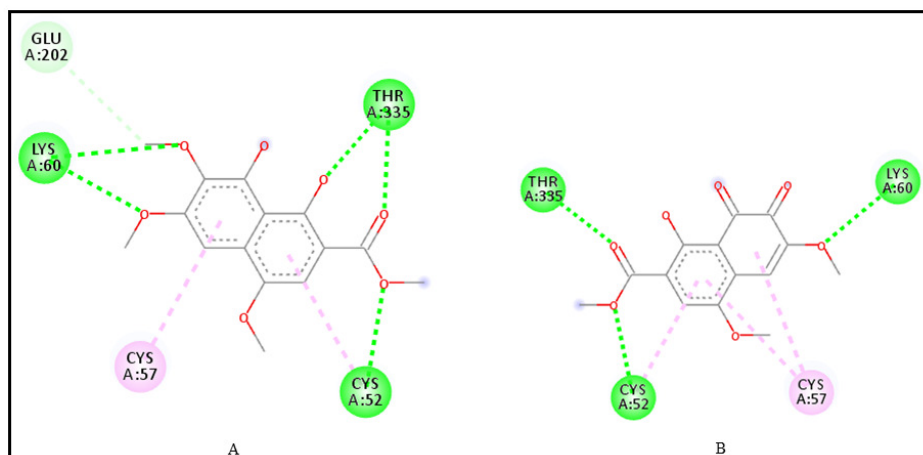
Figure 4.8: Ligand interactions for busseihydroquinone A (**7**) and compound **99**

4.11   Predictive Pharmacokinetic Analysis

The pharmacokinetic properties (Table 4.19) of the ligands were predicted using SWISS-ADME tool (Daina *et al*., 2017). Canonical SMILES for the ligand molecules were imported into the SWISS-ADME interface and their pharmacokinetic and physiochemical data were computed. Despite forming hydrogen bonds with numerous amino acids in the FAD binding domain, busseihydroquinone A (**7**) showed a less desirable logP value of 2.78 (Table 4.19). According to Bhal (2007), for oral and intestinal absorption, the ideal logP value should range from 1.35 to 1.8   (Bhal, 2007). This requirement was met through synthetic modification; the synthetic derivative of busseihydroquinone A (**7**). SWISS ADME computations showed that the synthetic derivative (**99**) has a more favourable logP value of 1.69, making it more suited for oral and intestinal absorption.

The modification had no significant effect on the ligand interactions with amino acid residues at the FAD binding cavity. In fact, busseihydroquinone A (**7**) and its synthetic analogue had equal binding energies (-6.9 kcal/mol).

Table 4.19: Predictive pharmacokinetic analysis

Ligand	XLog P3	Water Solubility (ESOL Class)	BBB permeant	Lipinski #violations	Bioavailability Score	Lead-likeness #violations
Schimperiquinone A (**92**)	6.07	Poorly soluble	No	0	0.55	2
Rubiadin-3-*O*-β-primeveroside (**62**)	-0.81	Soluble	No	3	0.17	1
Schimperiquinone B (**93**)	5.02	Poorly soluble	No	0	0.55	2
Lucidin-3-*O*-β-primeveroside (**61**)	-2.06	Very soluble	No	3	0.17	1
Rubiadin-1-methylether-3-*O*- β-primeveroside (54)	-1.03	Soluble	No	3	0.17	1
13R-epi-gaertneroside (**85**)	-0.26	Soluble	No	3	0.11	1
Damnacanthol-3-*O*-β-primeveroside (55)	-2.29	Very soluble	No	3	0.17	1
Cleomiscosin A (**91**)	2.12	Soluble	No	0	0.55	1
Isagarin (**77**)	1.16	Soluble	Yes	0	0.55	0
Damnacanthal (**63**)	2.5	Soluble	No	0	0.55	0
Lucid-ω-methyl ether (**83**)	2.36	Soluble	No	0	0.55	0
Rubiadin (**64**)	3.07	Soluble	Yes	0	0.55	0
Nordamnacanthal (**101**)	2.72	Soluble	No	0	0.55	0
Rubiadin-1-methyl ether (**65**)	2.85	Soluble	Yes	0	0.55	0
3-Hydroxy-1-methylanthraquinone (**71**)	2.88	Soluble	Yes	0	0.55	1
Damnacanthol (**81**)	2.15	Soluble	No	0	0.55	0
damnacanthol-3-*O*-methyl ether (**82**)	1.92	Soluble	Yes	0	0.55	0
Tectoquinone (**73**)	3.94	Moderately soluble	Yes	0	0.55	2
2-Methoxy-3-methylanthraquinone (**72**)	3.2	Soluble	Yes	0	0.55	0

Ligand	XLogP3	Water Solubility (ESOL Class)	BBB permeant	Lipinski #violations	Bioavailability Score	Lead-likeness #violations
Busseihydroquinone C (**52**)	5.74	Moderately soluble	No	0	0.56	2
Pentalonginhydroquinone diglycoside (**76**)	-3.26	Very soluble	No	3	0.17	1
Busseihydroquinone D (**53**)	4.55	Moderately soluble	No	0	0.56	2
Parvinaphthol C (**59**)	4.13	Moderately soluble	No	0	0.56	2
3,4,6-Trihydroxy-2,2-dimethyl-3,4-dihydro-2H-benzo[h]chromene-5-carboxylic acid methyl ester (**69**)	2.11	Soluble	No	0	0.55	0
2-Hydroxy-3-methyl-anthraquinone (**79**)	2.88	Soluble	Yes	0	0.55	1
Pachybasin (**80**)	3.88	Moderately soluble	Yes	0	0.55	2
Busseihydroquinone F (**56**)	5.6	Poorly soluble	No	1	0.55	2
Mollugin (**75**)	2.61	Soluble	Yes	0	0.85	0
3-Hydroxymollugin (**67**)	2.06	Soluble	Yes	0	0.56	0
2-Hydroxymethylanthraquinone (**90**)	2.69	Soluble	Yes	0	0.55	1
Tudoside (**84**)	-3.46	Highly soluble	No	1	0.11	1
Methyl 1,5-dihydroxy-4-methoxy-2-methyl-2'-(4'-methyl-3-pentenyl)-27/-benzo(/)-chromene-2-carboxylate (**48**)	4.55	Moderately soluble	No	0	0.55	2

Ligand	XLogP3	Water Solubility (ESOL Class)	BBB permeant	Lipinski #violations	Bioavailability Score	Lead-likeness #violations
5,6-Dihydroxydamnacanthol (**89**)	1.99	Soluble	No	0	0.55	0
5,6-Dihydroxylucid-ω-methyl ether (**88**)	2.2	Soluble	No	0	0.55	0
Parvinaphthol D (**60**)	4.5	Moderately soluble	No	0	0.56	2
Psychorubrin (**75**)	0.63	Very soluble	Yes	0	0.55	1
3,4,6-Trihydroxy-2,2-dimethyl-3,4-dihydro-2H-benzo[h]chromene-5-carboxylic acid methyl ester (**70**)	2.11	Soluble	No	0	0.55	0
2-Hydroxy-7-methyl-anthraquinone (**78**)	2.88	Soluble	Yes	0	0.55	1
3-Methoxymollugin (**68**)	3.83	Moderately soluble	Yes	0	0.55	1
Pentalongin (**74**)	1.51	Soluble	Yes	0	0.55	1
Bussei hydroquinone B (**60**)	3.79	Moderately soluble	Yes	0	0.56	1
1-Hydroxy-4,6-dimethoxy-7,8-dioxo-7,8-dihydro-naphthalene-2-carboxylic acid methyl ester (**99**)	1.69	Soluble	No	0	0.55	0
Bussei hydroquinone A (54)	2.78	Soluble	No	0	0.55	0
Parvinaphthol A (**57**)	2.45	Soluble	No	0	0.55	0
Parvinaphthol B (**58**)	2.48	Soluble	No	0	0.55	0
Compound **47**	2.55	Soluble	No	0	0.55	0
Protocatechuic acid (**98**)	1.15	Very soluble	No	0	0.56	1
Vanillic acid (**96**)	1.43	Soluble	No	0	0.85	1

Ligand	XLog P3	Water Solubility (ESOL Class)	BBB permeant	Lipinski #violations	Bioavailability Score	Lead-likeness #violations
p-Hydroxybenzoic acid (**97**)	1.58	Soluble	Yes	0	0.85	1

4.12 Antileishmanial Activity

Pentalongin (**74**) showed antileishmanial activity against the antimony sensitive strain of *L. donovani* (IC_{50} 11 μM). Relative to the positive control (miltefosine (**4**)), pentalongin (**74**) gave a high concentration of nitric oxide (Table 4.20) which is a known antileishmanial agent. Despite the promising antileishmanial activity of pentalongin (**74**), it has been reported by Endale (2012) to have high toxicity ($LD_{50} < 1 \, \mu gmL^{-1}$); this hinders its direct application for the treatment of leishmaniasis.

Table 4.20: Antileishmanial activity of pentalongin against *Leishmania donovani*.

Compound	IC_{50} (μM)			Nitric Oxide generation
	MHOM/IN/83/AG83	MHOM/IN/89/GE1	Peritoneal macrophages	
Pentalongin (**74**)	11	>50	51.35	1.08
Miltefosine (**4**)	5.5	6.75	19.85	1.11

4.13 Mechanism of Action of Pentalongin

Pentalongin (**74**) was docked with *Li*TR at the catalytic site of the receptor and the ligand-receptor complex was analysed with Biovia Discovery Studio. Pentalongin (**74**) interacted with amino acid residues in the FAD binding cavity through conventional hydrogen bonding with Lys60, carbon hydrogen bonding with Cys57, Arg287, Asp327 and pi-alkyl interactions with Ile199; accounting for a binding energy of -7.5 kcal/mol (Figure 4.9).

Therefore, in addition to inducing the generation of nitric oxide, pentalongin is likely to combat *Leishmania* by inhibiting trypanothione reductase. Inhibiting trypanothione reductase exposes the parasite to oxidative and chemical stress (Sharma & Anand, 1997).
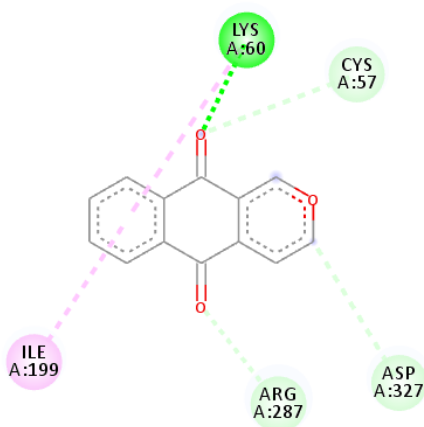

Figure 4.9: Ligand interaction for pentalongin (**74**)

CHAPTER FIVE

CONCLUSIONS AND RECOMMENDATIONS

5.1   CONCLUSIONS

Six compounds were isolated from the roots of *Pentas parvifolia*: busseihydroquinone B (**51**) was isolated from the roots, β-stigmasterol (**50**) and β-amyrin (**95**) were isolated from the stem, while vanillic acid (**96**), *p*-hydroxybenzoic acid (**97**) and protocatechuic acid (**98**) were isolated from the aerial parts. Seven compounds were isolated from the aerial parts of *Pentas bussei*: Busseihydroquinone A (**7**), busseihydroquinone B (**51**), busseihydroquinone C (**52**), methyl 5,10-dihydroxy-7-methoxy-3-methyl-3-(4-methyl-3-pentenyl)-3H-benzo[f]chromene9-carboxylate (**48**), methyl 8-hydroxy-1,4,6,7-tetramethoxy-2-naphthoate (**47**), *p*-hydroxybenzoic acid (**97**), protocatechuic acid (**98**) and β-stigmasterol (**50**). Two anthraquinones were isolated from the stem bark of *Pentas zanzibarica*: rubiadin-1-methyl ether (**65**), and rubiadin (**64**). 2-Methoxy-3-methyl anthraquinone (**72**), was isolated from the aerial parts of *Penta micrantha*. Pentalongin (**74**) was isolated from the roots of *Pentas longiflora*.

Pentalongin (**74**) showed antileishmanial activity (IC_{50} = 11 µM) against antimony sensitive strains of *Leishmania donovani* in amastigote form. A substantial amount of toxic nitric oxide was produced in the amastigotes when treated with pentalongin (**74**). Hence, pentalongin (**74**) combats the pathogen through inducing the production of nitric oxide.

Through computational modelling, it was observed that the anthraquinones and naphthol derivatives from the genus *Pentas* have a substantial affinity for the FAD binding domain of *Leishmania infantum* trypanothione reductase. Therefore, they are worth considering as templates to guide the development of antileishmanial therapeutic agents. Synthetic modification of busseihydroquinone A (**7**) yielded 1-hydroxy-4,6-dimethoxy-7,8-dioxo-7,8-dihydro-naphthalene-2-carboxylic acid methyl ester (**99**).

5.2 RECOMMENDATIONS

1. Pentalongin should be structurally modified to minimise toxicity and enable its direct application in the treatment of leishmaniasis.

2. Compounds with promising *in silico* activities should be further studied for *in vitro* and *in vivo* activity.

3. The inhibitory potential of phytochemicals in the genus *Pentas* for alternative pathways in the *Leishmania* parasite should be studied.

REFERENCES

Abdissa, N., Pan, F., Gruhonjic, A., Gräfenstein, J., Fitzpatrick, P. A., Landberg, G., Rissanen, K., Yenesew, A., & Erdélyi, M. (2016). Naphthalene Derivatives from the Roots of *Pentas parvifolia* and *Pentas bussei*. *Journal of Natural Products*, *79*(9), 2181–2187. https://doi.org/10.1021/acs.jnatprod.6b00178

Adejo, G. O., Atawodi, S., Ameh, D., & Ibrahim, S. (2014). Anti-Peroxidative, Protective and Ameliorative Properties of Methanol Extract of All Parts of Morinda Lucida Benth in CCl4-Induced Liver Injury. *Natural Products Chemistry & Research*. https://doi.org/10.4172/2329-6836.S1-003

Agrawal, P. K. (2013). *Carbon-13 NMR of flavonoids*. Elsevier.

Alahuhta, M., & Wierenga, R. K. (2010). Atomic resolution crystallography of a complex of triosephosphate isomerase with a reaction-intermediate analog: New insight in the proton transfer reaction mechanism: The 0.82-Å Structure of the TIM-PGH Complex. *Proteins: Structure, Function, and Bioinformatics*, *78*(8), 1878–1888. https://doi.org/10.1002/prot.22701

Alakurtti, S., Bergström, P., Sacerdoti-Sierra, N., Jaffe, C. L., & Yli-Kauhaluoma, J. (2010). Anti-leishmanial activity of betulin derivatives. *The Journal of Antibiotics*, *63*(3), 123–126.

Al-Salem, W., Herricks, J. R., & Hotez, P. J. (2016). A review of visceral leishmaniasis during the conflict in South Sudan and the consequences for East African countries. *Parasites & Vectors*, *9*(1), 1–11.

Alvar, J., Croft, S., & Olliaro, P. (2006). Chemotherapy in the treatment and control of leishmaniasis. *Advances in Parasitology*, *61*, 223–274.

Araújo, I. A. C., de Paula, R. C., Alves, C. L., Faria, K. F., de Oliveira, M. M., Mendes,

 G. G., Dias, E. M. F. A., Ribeiro, R. R., de Oliveira, A. B., & da Silva, S. M.

 (2019). Efficacy of lapachol on treatment of cutaneous and visceral leishmaniasis.

 Experimental Parasitology, *199*, 67–73.

Arevalo, I., Ward, B., Miller, R., Meng, T.-C., Najar, E., Alvarez, E., Matlashewski, G.,

 & Alejandro, L.-C. (2001). Successful treatment of drug-resistant cutaneous

 leishmaniasis in humans by use of imiquimod, an immunomodulator. *Clinical*

 Infectious Diseases, *33*(11), 1847–1851.

Baiocco, P., Ilari, A., Ceci, P., Orsini, S., Gramiccia, M., Di Muccio, T., & Colotti, G.

 (2011). Inhibitory effect of silver nanoparticles on trypanothione reductase

 activity and Leishmania infantum proliferation. *ACS Medicinal Chemistry Letters*,

 2(3), 230–233.

Baiocco, P., Poce, G., Alfonso, S., Cocozza, M., Porretta, G. C., Colotti, G., Biava, M.,

 Moraca, F., Botta, M., Yardley, V., Fiorillo, A., Lantella, A., Malatesta, F., &

 Ilari, A. (2013). Inhibition of *Leishmania infantum* Trypanothione Reductase by

 Azole-Based Compounds: A Comparative Analysis with Its Physiological

 Substrate by X-ray Crystallography. *ChemMedChem*, *8*(7), 1175–1183.

 https://doi.org/10.1002/cmdc.201300176

Bhal, S. K. (2007). LogP—Making sense of the value. *Advanced Chemistry*

 Development, Toronto, ON, Canada, 1–4.

Brannigan, J. A., Smith, B. A., Yu, Z., Brzozowski, A. M., Hodgkinson, M. R., Maroof,

 A., Price, H. P., Meier, F., Leatherbarrow, R. J., Tate, E. W., Smith, D. F., &

 Wilkinson, A. J. (2010). N-Myristoyltransferase from Leishmania donovani:

Structural and Functional Characterisation of a Potential Drug Target for Visceral Leishmaniasis. *Journal of Molecular Biology*, *396*(4), 985–999. https://doi.org/10.1016/j.jmb.2009.12.032

Bukuru, J. (2003). *Isolation and structural elucidation of natural products from Pentas bussei K. Krause, Pentas lanceolata (Forsk.) Deflers and Pentas parvifolia Hiern (Rubiaceae)* [PhD Thesis]. Ghent University.

Camargos, H. S., Moreira, R. A., Mendanha, S. A., Fernandes, K. S., Dorta, M. L., & Alonso, A. (2014). Terpenes increase the lipid dynamics in the Leishmania plasma membrane at concentrations similar to their IC50 values. *PLoS One*, *9*(8), e104429.

Chepkirui, C., Ochieng, P. J., Sarkar, B., Hussain, A., Pal, C., Yang, L. J., Coghi, P., Akala, H. M., Derese, S., & Ndakala, A. (2021). Antiplasmodial and antileishmanial flavonoids from Mundulea sericea. *Fitoterapia*, *149*, 104796.

Cordeiro, A. T., Michels, P. A. M., Delboni, L. F., & Thiemann, O. H. (2004). The crystal structure of glucose-6-phosphate isomerase from Leishmania mexicana reveals novel active site features: Leishmania PGI crystal structure. *European Journal of Biochemistry*, *271*(13), 2765–2772. https://doi.org/10.1111/j.1432-1033.2004.04205.x

Croft, S. L., Evans, A. T., & Neal, R. A. (1985). The activity of plumbagin and other electron carriers against Leishmania donovani and Leishmania mexicana amazonensis. *Annals of Tropical Medicine & Parasitology*, *79*(6), 651–653.

Croft, S. L., & Olliaro, P. (2011). Leishmaniasis chemotherapy—Challenges and opportunities. *Clinical Microbiology and Infection*, *17*(10), 1478–1483.

Croft, S. L., & Yardley, V. (2002). Chemotherapy of leishmaniasis. *Current Pharmaceutical Design*, *8*(4), 319–342.

Daina, A., Michielin, O., & Zoete, V. (2017). SwissADME: A free web tool to evaluate pharmacokinetics, drug-likeness and medicinal chemistry friendliness of small molecules. *Scientific Reports*, *7*(1), 1–13.

de Menezes, J. P. B., Guedes, C. E. S., Petersen, A. L. de O. A., Fraga, D. B. M., & Veras, P. S. T. (2015). Advances in Development of New Treatment for Leishmaniasis. *BioMed Research International*, *2015*, 1–11. https://doi.org/10.1155/2015/815023

del Rayo Camacho, M., Kirby, G. C., Warhurst, D. C., Croft, S. L., & Phillipson, J. D. (2000). Oxoaporphine alkaloids and quinones from Stephania dinklagei and evaluation of their antiprotozoal activities. *Planta Medica*, *66*(05), 478–480.

Dey, S., Mukherjee, D., Sultana, S. S., Mallick, S., Dutta, A., Ghosh, J., Hussain, A., Sarkar, B., Mandal, S., & Patra, P. (2020). Combination of Mycobacterium indicus pranii and heat-induced promastigotes cures drug-resistant Leishmania infection: Critical role of interleukin-6-producing classical dendritic cells. *Infection and Immunity*, *88*(6), e00222-19.

Di Giorgio, C., Delmas, F., Ollivier, E., Elias, R., Balansard, G., & Timon-David, P. (2004). In vitro activity of the β-carboline alkaloids harmane, harmine, and harmaline toward parasites of the species Leishmania infantum. *Experimental Parasitology*, *106*(3–4), 67–74.

do Vale Morais, A. R., Silva, A. L., Cojean, S., Balaraman, K., Bories, C., Pomel, S., Barratt, G., do Egito, E. S. T., & Loiseau, P. M. (2018). In-vitro and in-vivo

91

antileishmanial activity of inexpensive Amphotericin B formulations: Heated

Amphotericin B and Amphotericin B-loaded microemulsion. *Experimental*

Parasitology, *192*, 85–92.

Donfack, A. R. N., Tala, M. F., Wabo, H. K., Jerz, G., Zeng, G.-Z., Winterhalter, P., Tan,

N.-H., & Tane, P. (2014). Two new anthraquinone dimers from the stem bark of

Pentas schimperi (Rubiaceae). *Phytochemistry Letters*, *8*, 55–58.

Dufe, V. T., Ingner, D., Heby, O., Khomutov, A. R., Persson, L., & Al-Karadaghi, S.

(2007). A structural insight into the inhibition of human and Leishmania donovani

ornithine decarboxylases by 1-amino-oxy-3-aminopropane. *Biochemical Journal*,

405(2), 261–268. https://doi.org/10.1042/BJ20070188

Effendi, H. (2004). *Isolation and structure elucidation of bioactive secondary metabolites*

of sponge-derived fungi collected from the Mediterranean sea (Italy) and Bali sea

(Indonesia) [PhD Thesis]. Verlag nicht ermittelbar.

Endale, M. (2012). Phytochemical Analysis Of Six Pentas Species For Antiplasmodial

Principles. *PhD Thesis*.

Endale, M., Alao, J. P., Akala, H. M., Rono, N. K., Eyase, F. L., Derese, S., Ndakala, A.,

Mbugua, M., Walsh, D. S., & Sunnerhagen, P. (2012). Antiplasmodial Quinones

from Pentas longiflora and Pentas lanceolata. *Planta Medica*, *78*(01), 31–35.

Endale, M., Ekberg, A., Akala, H. M., Alao, J. P., Sunnerhagen, P., Yenesew, A., &

Erdélyi, M. (2012). Busseihydroquinones A–D from the Roots of Pentas bussei.

Journal of Natural Products, *75*(7), 1299–1304.

Endale, M., Ekberg, A., Alao, J., Akala, H., Ndakala, A., Sunnerhagen, P., Erdélyi, M., &
Yenesew, A. (2012). Anthraquinones of the Roots of Pentas micrantha.
Molecules, *18*(1), 311–321.

Fonseca-Silva, F., Inacio, J. D., Canto-Cavalheiro, M. M., & Almeida-Amaral, E. E.
(2011). Reactive oxygen species production and mitochondrial dysfunction
contribute to quercetin induced death in Leishmania amazonensis. *PloS One*, *6*(2),
e14666.

Forrey, C., Douglas, J. F., & Gilson, M. K. (2012). The fundamental role of flexibility on
the strength of molecular binding. *Soft Matter*, *8*(23), 6385–6392.

Fyfe, P. K., Westrop, G. D., Ramos, T., Müller, S., Coombs, G. H., & Hunter, W. N.
(2012). Structure of *Leishmania major* cysteine synthase. *Acta Crystallographica
Section F Structural Biology and Crystallization Communications*, *68*(7), 738–
743. https://doi.org/10.1107/S1744309112019124

Fyfe, P. K., Westrop, G. D., Silva, A. M., Coombs, G. H., & Hunter, W. N. (2012).
Leishmania TDR1 structure, a unique trimeric glutathione transferase capable of
deglutathionylation and antimonial prodrug activation. *Proceedings of the
National Academy of Sciences*, *109*(29), 11693–11698.
https://doi.org/10.1073/pnas.1202593109

Gazanion, E., Garcia, D., Silvestre, R., Gérard, C., Guichou, J. F., Labesse, G., Seveno,
M., Cordeiro-Da-Silva, A., Ouaissi, A., Sereno, D., & Vergnes, B. (2011). The
Leishmania nicotinamidase is essential for NAD+ production and parasite
proliferation: Leishmania NAD+ metabolism. *Molecular Microbiology*, *82*(1),
21–38. https://doi.org/10.1111/j.1365-2958.2011.07799.x

Hamidi, M., Azadi, A., & Rafiei, P. (2008). Hydrogel nanoparticles in drug delivery. *Advanced Drug Delivery Reviews*, *60*(15), 1638–1649.

Han, Y.-S., Van der Heijden, R., & Verpoorte, R. (2001). Biosynthesis of anthraquinones in cell cultures of the Rubiaceae. *Plant Cell, Tissue and Organ Culture*, *67*(3), 201–220.

Hanwell, M. D., Curtis, D. E., Lonie, D. C., Vandermeersch, T., Zurek, E., & Hutchison, G. R. (2012). Avogadro: An advanced semantic chemical editor, visualization, and analysis platform. *Journal of Cheminformatics*, *4*(1), 1–17.

Hargrove, T. Y., Wawrzak, Z., Liu, J., Nes, W. D., Waterman, M. R., & Lepesheva, G. I. (2011). Substrate Preferences and Catalytic Parameters Determined by Structural Characteristics of Sterol 14α-Demethylase (CYP51) from Leishmania infantum. *Journal of Biological Chemistry*, *286*(30), 26838–26848. https://doi.org/10.1074/jbc.M111.237099

Harouna, H., Faure, R., Elias, R., Debrauwer, L., Saadou, M., Balansard, G., & Boudon, G. (1995). Harounoside a pentalongin hydroquinone diglycoside from Mitracarpus scaber. *Phytochemistry*, *39*(6), 1483–1484.

Hazra, S., Ghosh, S., Sarma, M. D., Sharma, S., Das, M., Saudagar, P., Prajapati, V. K., Dubey, V. K., Sundar, S., & Hazra, B. (2013). Evaluation of a diospyrin derivative as antileishmanial agent and potential modulator of ornithine decarboxylase of Leishmania donovani. *Experimental Parasitology*, *135*(2), 407–413.

Hernández-Bojorge, S. E., Blass-Alfaro, G. G., Rickloff, M. A., Gómez-Guerrero, M. J.,

    & Izurieta, R. (2020). Epidemiology of cutaneous and mucocutaneous

    leishmaniasis in Nicaragua. *Parasite Epidemiology and Control*, *11*, e00192.

Inouye, H., Takeda, Y., Nishimura, H., Kanoni, A., Okuda, T., & Puff, C. (1988).

    Chemotaxonomic Studies of Rubiaceous Plants Containing Iridoid Glycosides.

Jawed, J. J., & Majumdar, S. (2018a). *Recent Trends in Leishmania Research: A*

    Therapeutic Perspective. *1*(3), 1–4.

Jawed, J. J., & Majumdar, S. (2018b). Recent Trends in Leishmania Research: A

    Therapeutic Perspective. *Journal of Infectiology*, *1*(3), 1–4.

Jones, C. M., & Welburn, S. C. (2021). Leishmaniasis Beyond East Africa. *Frontiers in*

    Veterinary Science, *8*.

Kapadia, N. S., Isarani, S. A., & Shah, M. B. (2005). A Simple Method for Isolation of

    Plumbagin from Roots of Plumbago rosea. *Pharmaceutical Biology*, *43*(6), 551–

    553.

Kaye, P. M., Cruz, I., Picado, A., Van Bocxlaer, K., & Croft, S. L. (2020). Leishmaniasis

    immunopathology—Impact on design and use of vaccines, diagnostics and drugs.

    Seminars in Immunopathology, *42*(3), 247–264.

Kedzierski, L., Malby, R. L., Smith, B. J., Perugini, M. A., Hodder, A. N., Ilg, T.,

    Colman, P. M., & Handman, E. (2006). *Structure of Leishmania mexicana*

    Phosphomannomutase Highlights Similarities with Human Isoforms. 13.

Kim, H., & Hol, W. G. J. (1998). Crystal structure of Leishmania mexicana glycosomal

    glyceraldehyde-3-phosphate dehydrogenase in a new crystal form confirms the

putative physiological active site structure. *Journal of Molecular Biology*, *278*(1), 5–11. https://doi.org/10.1006/jmbi.1998.1661

Kiprotich, W. T. (2006). *Situational Analysis of Leishmaniases Research in Kenya. 13*.

Kisakuerek, M. V., Leeuwenberg, A. J. M., & Hesse, M. (1983). *A Chemotaxonomic Investigation of the Plant Families of Apocyanaceae, Loganiaceae, and Rubiaceae by the Indole Alkaloid Content. In: Pelletier, S. W. (ed.)*. Wiley and Sons.

Krauth-Siegel, R. L., Meiering, S. K., & Schmidt, H. (2003). *The parasite-specific trypanothione metabolism of Trypanosoma and Leishmania*.

Labib, R. M., Ebada, S. S., Youssef, F. S., Ashour, M. L., & Ross, S. A. (2016). Ursolic acid, a natural pentacylcic triterpene from Ochrosia elliptica and its role in the management of certain neglected tropical diseases. *Pharmacognosy Magazine*, *12*(48), 319.

Lage, P. S., Chavez-Fumagalli, M. A., Mesquita, J. T., Mata, L. M., Fernandes, S. O. A., Cardoso, V. N., Soto, M., Tavares, C. A. P., Leite, J. P. V., Tempone, A. G., & Coelho, E. A. F. (2015). *Antileishmanial Activity and Evaluation of the Mechanism of Action of Strychnobiflavone flavonoid isolated from Strychnos pseudoquina Agaist Leishmania infantum*.

Larson, E. T., Kim, J. E., Zucker, F. H., Kelley, A., Mueller, N., Napuli, A. J., Verlinde, C. L. M. J., Fan, E., Buckner, F. S., Van Voorhis, W. C., Merritt, E. A., & Hol, W. G. J. (2011). Structure of Leishmania major methionyl-tRNA synthetase in complex with intermediate products methionyladenylate and pyrophosphate. *Biochimie*, *93*(3), 570–582. https://doi.org/10.1016/j.biochi.2010.11.015

Lévêque, M. F., Lachaud, L., Simon, L., Battery, E., Marty, P., & Pomares, C. (2020).

Place of serology in the diagnosis of zoonotic leishmaniases with a focus on

visceral leishmaniasis due to Leishmania infantum. *Frontiers in Cellular and*

Infection Microbiology, *10*, 67.

Manuel, J. C.-B., & Luis, M. P.-R. (2001). *Plant natural products with leishmanicidal*

activity. *18*. https://doi.org/10.1039/b100455g

Marlet, M. V. L., Sang, D. K., Ritmeijer, K., Muga, R. O., Onsongo, J., & Davidson, R.

N. (2003). Emergence or re-emergence of visceral leishmaniasis in areas of

Somalia, northeastern Kenya, and south-eastern Ethiopia in 2000–2001.

Transactions of the Royal Society of Tropical Medicine and Hygiene, *97*(5), 515–

518. https://doi.org/10.1016/S0035-9203(03)80012-3

McLuskey, K., Paterson, N. G., Bland, N. D., Isaacs, N. W., & Mottram, J. C. (2010).

Crystal Structure of Leishmania major Oligopeptidase B Gives Insight into the

Enzymatic Properties of a Trypanosomatid Virulence Factor. *Journal of*

Biological Chemistry, *285*(50), 39249–39259.

https://doi.org/10.1074/jbc.M110.156679

Melaku, Y., Collin, S. M., Keus, K., Gatluak, F., Ritmeijer, K., & Davidson, R. N.

(2007). Treatment of kala-azar in southern Sudan using a 17-day regimen of

sodium stibogluconate combined with paromomycin: A retrospective comparison

with 30-day sodium stibogluconate monotherapy. *The American Journal of*

Tropical Medicine and Hygiene, *77*(1), 89–94.

Miranda-Verastegui, C., Tulliano, G., Gyorkos, T. W., Calderon, W., Rahme, E., Ward,

B., Cruz, M., Llanos-Cuentas, A., & Matlashewski, G. (2009). First-line therapy

for human cutaneous leishmaniasis in Peru using the TLR7 agonist imiquimod in combination with pentavalent antimony. *PLoS Negl Trop Dis*, *3*(7), e491.

Mishra, B. B., Kale, R. R., Singh, R. K., & Tiwari, V. K. (2009). *Alkaloids: Futrue Prospective to Combat Leishmaniasis*.

Monzote, L. (2009). Current treatment of leishmaniasis: A review. *The Open Antimicrobial Agents Journal*, *1*(1).

Murray, H. W., Berman, J. D., Davies, C. R., & Saravia, N. G. (2005). Advances in leishmaniasis. *The Lancet*, *366*(9496), 1561–1577. https://doi.org/10.1016/S0140-6736(05)67629-5

Muzitano, M. F., Cruz, E. A., de Almeida, A. P., Da silva, silvia A. G., Kaiser, C. R., Guette, C., Rossi-Bergmann, B., & Costa, S. S. (2006). *Quercitrin: An Antileishmanial Flavonoid Glycoside from Kalanchoe pinnata*.

Nagle, A., Biggart, A., Be, C., Srinivas, H., Hein, A., Caridha, D., Sciotti, R. J., Pybus, B., Kreishman-Deitrick, M., & Bursulaya, B. (2020). Discovery and characterization of clinical candidate LXE408 as a kinetoplastid-selective proteasome inhibitor for the treatment of leishmaniases. *Journal of Medicinal Chemistry*, *63*(19), 10773–10781.

Neal, R. A. (1968). The effect of antibiotics of the neomycin group on experimental cutaneous leishmaniasis. *Annals of Tropical Medicine & Parasitology*, *62*(1), 54–62.

Njogu, P. M., Guantai, E. M., Pavadai, E., & Chibale, K. (2016). Computer-aided drug discovery approaches against the tropical infectious diseases malaria,

tuberculosis, trypanosomiasis, and leishmaniasis. *ACS Infectious Diseases*, *2*(1), 8–31.

Peixoto, J. F., Oliveira, A. da S., Monteiro, P. Q., Gonçalves-Oliveira, L. F., Andrade-Neto, V. V., Ferreira, V. F., Souza-Silva, F., & Alves, C. R. (2021). In Silico Insights into the Mechanism of Action of Epoxy-α-Lapachone and Epoxymethyl-Lawsone in Leishmania spp. *Molecules*, *26*(12), 3537.

Pettersen, E. F., Goddard, T. D., Huang, C. C., Couch, G. S., Greenblatt, D. M., Meng, E. C., & Ferrin, T. E. (2004). UCSF Chimera—A visualization system for exploratory research and analysis. *Journal of Computational Chemistry*, *25*(13), 1605–1612.

Pisani, D. E., Elliot, A. J., Hinman, D. R., Aaronson, L. M., & Pardini, R. S. (1986). Relationship between inhibition of mitochondrial respiration by naphthoquinones, their antitumor activity, and their redox potential. *Biochemical Pharmacology*, *35*(21), 3791–3798.

Rasolzadeh, S., Fatahaliha, M. H., Hosseini, M., Jafari, R., Miahipour, A., Sadreddini, S., Babalo, Z., Kafil, H. S., & Yousefi, M. (2015). Recombinant LPG3 stimulates IFN-Γ and TNF-A secretion by human NK cells. *Iranian Journal of Parasitology*, *10*(3), 457.

Reithinger, R., Dujardin, J.-C., Louzir, H., Pirmez, C., Alexander, B., & Brooker, S. (2007). Cutaneous leishmaniasis. *The Lancet Infectious Diseases*, *7*(9), 581–596.

Rigden, D. J., Phillips, S. E. V., Michels, P. A. M., & Fothergill-Gilmore, L. A. (1999). The structure of pyruvate kinase from Leishmania mexicana reveals details of the

allosteric transition and unusual effector specificity. *Journal of Molecular Biology*, *293*(3), 745–749. https://doi.org/10.1006/jmbi.1999.3170

Rocha, L. G., Almeida, J., Macedo, R. O., & Barbosa-Filho, J. M. (2005). A review of natural products with antileishmanial activity. *Phytomedicine*, *12*(6–7), 514–535.

Sakyi, P. O., Amewu, R. K., Devine, R. N., Ismaila, E., Miller, W. A., & Kwofie, S. K. (2021). The Search for Putative Hits in Combating Leishmaniasis: The Contributions of Natural Products Over the Last Decade. *Natural Products and Bioprospecting*, *11*(5), 489–544.

Scala, A., Piperno, A., Micale, N., Mineo, P. G., Abbadessa, A., Risoluti, R., Castelli, G., Bruno, F., Vitale, F., & Cascio, A. (2018). "Click" on PLGA-PEG and hyaluronic acid: Gaining access to anti-leishmanial pentamidine bioconjugates. *Journal of Biomedical Materials Research Part B: Applied Biomaterials*, *106*(8), 2778–2785.

Schlagenhauf, E., Etges, R., & Metcalf, P. (1998). The crystal structure of the Leishmania major surface proteinase leishmanolysin (gp63). *Structure*, *6*(8), 1035–1046. https://doi.org/10.1016/S0969-2126(98)00104-X

Schripsema, J., Caprini, G. P., van der Heijden, R., Bino, R., de Vos, R., & Dagnino, D. (2007). Iridoids from Pentas lanceolata. *Journal of Natural Products*, *70*(9), 1495–1498.

Schuchter, L. M., Esa, A. H., May, W. S., Laulis, M. K., Pettit, G. R., & Hess, A. D. (1991). Successful treatment of murine melanoma with bryostatin 1. *Cancer Research*, *51*(2), 682–687.

Sharma, S., & Anand, N. (1997). *Biochemical Trargets for Antiprotozoal Activity* (Vol. 25). Elsevier. https://doi.org/10.1016/S0165-7208(97)80035-9

Shi, W., Schramm, V. L., & Almo, S. C. (1999). Nucleoside Hydrolase from Leishmania major. *Journal of Biological Chemistry*, *274*(30), 21114–21120. https://doi.org/10.1074/jbc.274.30.21114

Simplice, D. K., Tchadjobo, T., Denise, P. llboudo, & Jacques, S. (2011). *Sub-Saharan Rubiaceae: A Review of Their Traditional Uses, Phytochemistry and Biological Activities*. *14(3)*. https://doi.org/10.8923/pjbs.2011.149.169

Singh, N., Kumar, M., & Singh, R. K. (2012). Leishmaniasis: Current status of available drugs and new potential drug targets. *Asian Pacific Journal of Tropical Medicine*, *5*(6), 485–497.

Singh, N., Mishra, B. B., Bajpai, S., Singh, R. K., & Tiwari, V. K. (2014). Natural product based leads to fight against leishmaniasis. *Bioorganic & Medicinal Chemistry*, *22*(1), 18–45.

Smith, A. C., Yardley, V., Rhodes, J., & Croft, S. L. (2000). Activity of the Novel Immunomodulatory Compound Tucaresol against Experimental Visceral Leishmaniasis. *Antimicrobial Agents and Chemotherapy*, *44*(6), 1494–1498. https://doi.org/10.1128/AAC.44.6.1494-1498.2000

Sousa Silva, M., Barata, L., Ferreira, A. E. N., Romão, S., Tomás, A. M., Ponces Freire, A., & Cordeiro, C. (2008). Catalysis and Structural Properties of *Leishmania infantum* Glyoxalase II: Trypanothione Specificity and Phylogeny [†,‡]. *Biochemistry*, *47*(1), 195–204. https://doi.org/10.1021/bi700989m

Sultana, S. S., Ghosh, J., Chakraborty, S., Mukherjee, D., Dey, S., Mallick, S., Dutta, A., Paloi, S., Khatua, S., & Dutta, T. (2018). Selective in vitro inhibition of Leishmania donovani by a semi-purified fraction of wild mushroom Grifola frondosa. *Experimental Parasitology*, *192*, 73–84.

Suman, D., Vishwanadham, Y., Kumaraswamy, T., Shirisha, P., & Hemalatha, K. (2014). Phytochemical Evaluation and Analgesic Activity of Pentas lanceolata Leaves. *Natural Products Chemistry & Research*, *2*(4). https://doi.org/10.4172/2329-6836.1000135

Sundar, S., & Singh, B. (2018). Emerging therapeutic targets for treatment of leishmaniasis. *Expert Opinion on Therapeutic Targets*, *22*(6), 467–486. https://doi.org/10.1080/14728222.2018.1472241

Suresh, S., Turley, S., Opperdoes, F. R., Michels, P. A., & Hol, W. G. (2000). A potential target enzyme for trypanocidal drugs revealed by the crystal structure of NAD-dependent glycerol-3-phosphate dehydrogenase from Leishmania mexicana. *Structure*, *8*(5), 541–552. https://doi.org/10.1016/S0969-2126(00)00135-0

Sweelam, H. M., Abd-Alla, H. I., Abdelwahab, A. B., Gabr, M. M., & Kirsch, G. (2018). Secondary metabolites and biological activity of Pentas species: A minireview. *Journal of Advanced Research*, *10*, 21–30. https://doi.org/10.1016/j.jare.2017.12.003

Testerman, T. L., Gerster, J. F., Imbertson, L. M., Reiter, M. J., Miller, R. L., Gibson, S. J., Wagner, T. L., & Tomai, M. A. (1995). Cytokine induction by the immunomodulators imiquimod and S-27609. *Journal of Leukocyte Biology*, *58*(3), 365–372.

Teuscher, E., & Lindequist, U. (1994). *Biogene Gifte*. Gustav Fischer Verlag.

Tiuman, T. S., Santos, A. O., Ueda-Nakamura, T., Filho, B. P. D., & Nakamura, C. V. (2011). Recent advances in leishmaniasis treatment. *International Journal of Infectious Diseases*, *15*(8), e525–e532. https://doi.org/10.1016/j.ijid.2011.03.021

Venkatesan, S. K., Shukla, A. K., & Dubey, V. K. (2010). Molecular docking studies of selected tricyclic and quinone derivatives on trypanothione reductase of Leishmania infantum. *Journal of Computational Chemistry*, *31*(13), 2463–2475.

Venugopal, V., Sen, B., Datta, A. K., & Banerjee, R. (2007). Structure of cyclophilin from *Leishmania donovani* at 1.97 Å resolution. *Acta Crystallographica Section F Structural Biology and Crystallization Communications*, *63*(2), 60–64. https://doi.org/10.1107/S1744309106056351

Verdcourt, B. (1976). *Rubiaceae (part 1)*. Crown Agents for Oversea Governments and Administrations.

Vila-Nova, N. S., Morais, S. M. de, Falcão, M. J. C., Machado, L. K. A., Beviláqua, C. M. L., Costa, I. R. S., Brasil, N. V. G. P. de S., & Andrade Júnior, H. F. de. (2011). Leishmanicidal activity and cytotoxicity of compounds from two Annonacea species cultivated in Northeastern Brazil. *Revista Da Sociedade Brasileira de Medicina Tropical*, *44*(5), 567–571.

Villa-Pulgarín, J. A., Gajate, C., Botet, J., Jimenez, A., Justies, N., Varela-M, R. E., Cuesta-Marbán, Á., Müller, I., Modolell, M., & Revuelta, J. L. (2017). Mitochondria and lipid raft-located FOF1-ATP synthase as major therapeutic targets in the antileishmanial and anticancer activities of ether lipid edelfosine. *PLoS Neglected Tropical Diseases*, *11*(8), e0005805.

Wang, H., Yan, Z., Geng, J., Kunz, S., Seebeck, T., & Ke, H. (2007). Crystal structure of the Leishmania major phosphodiesterase LmjPDEB1 and insight into the design of the parasite-selective inhibitors. *Molecular Microbiology*, *66*(4), 1029–1038. https://doi.org/10.1111/j.1365-2958.2007.05976.x

WHO. (2015). *Visceral leishmaniasis: Control strategies and epidemiological situation update in East Africa*. 42.

WHO. (2021). *Weekly Bulletin on Outbreaks and Other Emergencies*.

Wijnsma, R., & Verpoorte, R. (1986). *Anthraquinones in the Rubiaceae. In: Herz, W.; Grisebach, H.; Kirby, G. W.; and Tamm, Ch. (Eds.) Progress in the Chemistry of Organic Natural Products.* Wien, Springer-Verlag.

INTERNET REFERENCES

https://www.rcsb.org/ Link valid on 12th July 2021.

https://pubchem.ncbi.nlm.nih.gov/ Link valid on 12th July 2021.

https://www.who.int/news-room/fact-sheets/detail/leishmaniasis Link valid on 12th July 2021.

http://www.cgl.ucsf.edu/chimera Link valid on 12th July 202.

https://scifinder-n.cas.org/search/substance/60f97a8073ecf1605a8aeee2/1 (Link valid on 7th October, 2021.

http://www.swissadme.ch/ Link valid on 7th October, 2021.

https://www.who.int/leishmaniasis/resources/KENYA.pdf?ua=1 (Link valid on 11th October, 2021)

APPENDIX A: Physical and Spectroscopic Data

Physical and Spectroscopic Data of Compounds Isolated from the Roots of *Pentas parvifolia*

Busseihydroquinone B (51)

Pale yellow powder; ^{1}H NMR (500 MHz, CDCl$_3$) δ 11.26 (*s*, 1H, 1-OH), 8.27 (*d*, 1H, *J* = 9.0, H-8), 7.72 (*d*,1H, *J* = 10.2 H-4′), 7.11 (*d*, 1H, *J* = 9.3, H-7), 7.09 (*s*, 1H, C-3), 5.62 (*d*, 1H, *J* = 10.3, H-3′), 3.93 (*s*, 1H, 4-OCH_3), 1.49 (*s*, 6H, H-1″).

^{13}C NMR (126 MHz, CDCl$_3$) δ 174.70 (2 − $COOH$), 157.2 (C-1), 155.7 (C-6), 149.61 (C-4), 127.90 (C-3′), 127.7 C-5), 125.9 (C-8), 121.5 (C-8a), 118.8 (C-7), 115.2 (C-4a), 103.7 (C-3), 75.5 (C-2′), 55.9 (OCH_3), 27.65 (C-1″).

Physical and Spectroscopic Data of Compounds Isolated from the Stem Bark of *Pentas parvifolia*

β-Stigmasterol (50)

White amorphous solid; ^{1}H NMR (500 MHz, CDCl$_3$) δ 5.35 (*t*, 1H, *J* = 5.0, H-6), 5.15 (*dd*, 1H, *J*=15.0, J = 5.0, H-20), 5.01 (dd, 1H, *J* = 15.0, *J*=5.0, H-21), 3.51 (*m*,1H, H-3).
^{13}C NMR (125 MHz, CDCl$_3$) δ 141 (C-5), 138.5 (C-20), 129.5 (C-21), 121.9 (C-6), 71.9 (C-3), 57.1 (C-14), 56.3 (C-17), 50.4 (C-9), 46.1 (C-22), 42.6 (C-4), 42.5 (C-13), 40.6 (C-18), 40 (C-12), 37.5 (C-1), 36.7 (C-10), 32.2 (C-8), 32 (C-2), 31.9 (C-7), 29.5 (C-16), 29.1 (C-25), 25.6 (C-23), 24.5 (C-15), 21.4 (C-11), 21.3 (C-19), 20 (C-26), 19.6 (C-27), 19.2 (C-28), 12.3 (C-29), 12.1 (C-24).

β-Amyrin (95)

White amorphous solid; ^{1}H NMR (500 MHz, CDCl$_3$) δ 5.29 (*m*, 1H, H-12), 3.22 (*dd*, *J* = 15, 5 Hz, H-3)
^{13}C NMR (125 MHz, CDCl$_3$) δ 143.6 (C-13), 122.9 (C-12), 79.3 (C-3), 55.5 (C-5), 47.9 (C-9), 46.7 (C-18), 46.0 (C-19), 41.9 (C-14), 41.3 (C-8), 39.5 (C-4), 39 (C-1), 38.7 (C-22), 37.3 (C-10), 34 (C-21), 33.2 (C-7), 32.9 (C-17), 32.6 (C-20), 30.8 (C-29), 28.3 (C-2), 27.9 (C-15), 27.4 (C-16), 26.1 (C-27), 23.8 (C-28), 23.8 (C-30), 23.6 (C-11), 23.3 (C-23), 18.5 (C-24), 17.3 (C-6), 15.7 (C-26), 15.5 (C-25).

Physical and Spectroscopic Data of Compounds Isolated from the Aerial Parts of *Pentas parvifolia*

Vanillic acid (96)

White powdery solid; ^{1}H NMR (500 MHz, CD$_3$CN) δ 7.52 (*s*, 1H, H-2), 7.54 (*dd*, 1H, *J* = 8.2, 2.1), 6.88 (*d*, 1H, 6.88, *J* = 8.2, H-5), 3.89 (*s*, 1H, 3-OCH$_3$).

^{13}C NMR (125 MHz, CD$_3$CN) δ 167.5 (1-$COOH$), 151.7 (C-4), 147.9 (C-3), 125.0 (C-6), 122.7 (C-1), 115.4 (C-5), 113.4 (C-2), 56.7 (3-OCH$_3$).

p-hydroxybenzoic acid (97)

White powdery solid; ^{1}H NMR (500 MHz, CD$_3$CN) δ 7.87 (*d*, 1H, *J* = 8.7, H-2, H-6), 6.86 (*d*, 1H, *J* = 8.9, H-3, H-5).
^{13}C NMR (125 MHz, CD$_3$CN) δ 167.4 (1-COOH), 162.3 (C-4), 132.9 (C-2, C-6), 122.5 (C-1), 116.0 (C-3, C-5).

Protocatechuic acid (98)

Brown powdery solid; ^{1}H NMR (500 MHz, CD$_3$CN) δ 7.44 (*dd*, 1H, *J* = 8.3, 2.01 H-6) 7.42 (*d*, 1H, *J* = 2.0, H-2), 6.87 (*d*, 1H, *J* = 8.2).
^{13}C NMR (125 MHz, CD$_3$CN) δ 168.2 (1-*COOH*), 150.4 (C-3), 145.0 (124.0 (C-6), 122.9 (C-1), 117.3 (C-3), 115.8 (C-2).

Physical and Spectroscopic Data of Compounds Isolated from the Aerial Parts of *Pentas bussei*

Methyl-1,5-dihydroxy-4-methoxy-2-methyl-2'-(4'-methyl-3-pentenyl)-27/-benzo(/)-chromene-2-carboxylate (55)

Red paste; ^{1}H NMR (500 MHz, CDCl$_3$) δ 12.27 (*s*, 1H, 1-OH), 8.02 (d, *J* = 10.4 Hz, 1H, H-1'), 7.61 (*s*, 1H, H-5), 6.92 (s, 1H, H-3), 6.06 (*s*, 1H, 6- OH), 5.67 (*d*, *J* = 10.4 Hz, 1H, C-2'), 5.10 (1H, H-3''), 3.97 (*s*, 3H, 2-COOCH$_3$), 3.92 (*s*, 3H, 4-OCH$_3$), 2.11-2.18 (*m*, 2H, H-2''), 1.77-1.82 (*m*, 2H, H-1''), 1.66 (s, 3H, H-6''), 1.57 (*s*, 3H, H-5''), 1.47 (*s*, 3H, H-4').

^{13}C NMR (125 MHz, CDCl$_3$) δ 172.1 (2-COOCH$_3$), 157.7 (C-1), 147.4 (C-4), 147.1 (C-6), 141.1 (C-7), 132.1 (C-4''), 128.0 (C-2'), 127.3 (C-4a), 124.0 (C-3''), 123.5 (C-1'), 117.5 (C-8), 116.1 (C-8a), 105.5, (C-5), 103.7 (C-2), 100.0 (C-3), 79.0 (C-3'), 56.0 (4-*OCH$_3$*), 52.3 (COOCH$_3$), 40.5 (C-1''), 25.8 (C-6''), 25.7 (C-4'), 22.9 (C-2''), 17.8 (C-5'').

Busseihydroquinone A (7) Pale yellow powder; ^{1}H NMR (500 MHz, Acetone-d6) δ 13.05 (*s*, 1H, 1-OH), 9.6 (*s*, 1H, 8-OH), 7.14 (*s*, 1H, H-3), 6.96 (*s*, 1H, H-5), 4.01, (*s*, 3H, 2-*COOCH$_3$*), 3.96 (*s*, 3H, 6-*OCH$_3$*), 3.95 (*s*, 3H, 4-*OCH$_3$*), 3.83, (s, 3H, 7-*OCH$_3$*).

^{13}C NMR (125 MHz, Acetone-d6) δ 172.6 (2-*COOCH$_3$*), 157.5 (C-6), 148.4 (C-4), 136.5 (C-7), 128.9 (C-4a), 111.1 (C-8a), 103.0 (C-2), 100.9 (C-3), 94.9 (C-5), 60.6 ((7-*OCH$_3$*), 56.3 (6-*OCH$_3$*), 56.3 (4-*OCH$_3$*), 53.2 (2-*COOCH$_3$)*.

Busseihydroquinone C (52) Pale yellow powder; ^{1}H NMR (500 MHz, CD$_3$CN) δ 8.18 (*d*, *J* = 9.0 Hz, 1H, H-8), 7.78 (*d*, *J* = 10.3 Hz, 1H, H-1'), 7.15 (*s*, 1H, H-3), 7.05 (*d*, *J* = 9.0 Hz, 1H, H-7), 5.67 (*d*, *J* = 10.4 Hz, 1H, H-2'), 5.14 – 5.09 (*m*, 1H, H-3''), 3.89 (*s*, 3H, 4-*OCH$_3$*), 2.17 – 2.07 (*m*, 3H, H-2''), 1.78 – 1.69 (*m*, 2H, H-1''), 1.64 (*s*, 3H, H-5''), 1.55 (*s*, 3H, H-6''), 1.41 (*s*, 3H, H-4').

^{13}C NMR (125 MHz, CD$_3$CN) δ 173.4 (2-C*OOH*), 156.7 (C-1), 155.8 (C-6), 149.8 (C-4), 132.5 (C-4''), 128.2 (C-2'), 127.4 (C-8a), 126.1 (C-8), 125.0 (C-3''), 123.8 (C-1'), 122.3 (C-5), 119.2 (C-7), 115.7 (C-4a), 105.7 (C-3), 104.2 (C-2), 78.5 (C-3'), 56.4 (4-*OCH$_3$*), 41.0 (C-1''), 25.8 (C-5''), 25.7 (C-4'), 23.4 (C-2''), 17.6 (C-6'').

Methyl-8-hydroxy-1,4,6,7-tetramethoxy-2-naphthoate (47)

^{1}H NMR (500 MHz, CDCl$_3$) δ 9.83(s, 1H, 8-OH, 7.14 (s, 1H, H-5), 7.11 (s, 1H, H-3), 4.01 (s, 3H, 1- OCH$_3$), 4.00 (s, 3H, 4-OCH$_3$), 4.00 (s, 3H, 6- OCH$_3$), 3.98 (2-COOCH$_3$), 3.96 (s, 3H, 7-OCH$_3$).

^{13}C NMR (125 MHz, CDCl$_3$) δ 166.2 (2-COOCH$_3$), 155.4 (C-8), 152.5 (C-1), 150.8 (C-6), 148.1 (C-4), 135.9 (C-7), 115.27 (C-8a), 114.0 (C-2), 103.8 (C-3), 64.7 (1-OCH$_3$), 60.9 (7-OCH$_3$), 56.1 (4-OCH$_3$), 55.95 (6-CH$_3$), 52.5 (2-COOCH$_3$).

Physical and Spectroscopic Data of Compounds Isolated from the Aerial Parts of *Pentas micrantha*

2-Methoxy-3-methylanthraquinone (2-methoxy-3-methyl-anthracene-9,10-dione, 72)

Yellow powder; ^{1}H NMR (500 MHz, Acetone-d$_6$) δ 8.23 (*dd*, 1H, *J* = 7.15, 1.3 Hz, H-5), 8.16 (*dd*, 1H, *J* = 7.64, 1.4 Hz), 7.88 (*ddd*, 1H, *J* =7.6, 7.52, 1.5 Hz, H-7), 7.82 (*ddd*, 1H, *J* = 7.5, 7.4, 1.4 Hz, H-6), 7,35 (*s*, 1H, H-4), 3.89 (*s*, 3H, 3-*OCH$_3$*), 2.25 (*s*, 3H, 2-CH$_3$).

^{13}C NMR (125 MHz, Acetone) δ 183.6 (C-9), 181.3 (C-10), 162.2 (C-3), 136.0 (C-8a), 135.2 (C-7), 134.0 (C-6), 133.6 (C-5a),129.2 (C-4), 127.7 (C-5), 127.0 (C-8), 119.8 (C-1a), 110.0 (C-1), 61.3 (3- *OCH$_3$*), 9.3 (2-CH$_3$).

Physical and Spectroscopic Data of Compounds Isolated from the Stem Bark of *Pentas zanzibarica*

Rubiadin-1-methyl ether (65)

Yellow powder; ^{1}H NMR (500 MHz, DMSO-d$_6$) δ 11.12 (*s*, 1H, $3 - OH$), 8.15 (*dd*, *J* = 7.75, 1.37 Hz, 1H, H-8), 8.10 (*dd*, *J* = 7.6, 1.4 Hz, 1H, H-5), 7.89 (*ddd*, *J* = 7.7, 7.6, 1.5 Hz, 1H, H-7), 7.83 (*ddd*, *J* = 7.4, 7.4, 1.4 Hz, 1H, H-6), 7.51 (*s*, 1H, H-4), 3.79 (*s*, 3H, 1-OCH$_3$), 2.16 (*s*, 3H, 2-CH$_3$).

^{13}C NMR (125 MHz, DMSO-d$_6$) δ 182.6 (C-10), 180.2 (C-9), 161.6 (C-3), 160.6 (C-1), 134.5 (C-8a), 134.5 (C-7), 133.73 (C-1a), 133.4 (C-6), 132.0 (C-5a), 126.6 (C-8), 126.14 (C-2), 126.0 (C-5), 118.0 (C-4a), 108.99 (C-4), 60.6 ($1-OCH_3$), 9.01 ($2 - CH_3$).

Rubiadin (64)

Yellow powder; ^{1}H NMR (500 MHz, Acetone-d6) δ 8.28 (*dd*, 1H, *J* = 7.28, 1.75 Hz, H-8), 8.21 (*dd*, 1H, *J* = 7.28, 1.82 Hz, H-5), 7.91 (*m*, 1H, H-7), 7.89 (*m*, 1H, H-6), 7.36 (*s*, 1H, H-4), 2.15 (*s*, 3H, $2-CH_3$)

^{13}C NMR (125 MHz, Acetone-d6) δ 187.44 (C-9), 182.55 (C-10), 163.81 (C-1), 163.49 (C-3), 134.88 (C-7), 134.80 (C-6), 134.13 (C-5a), 134.05 (C-8a), 132.90 (C-1a), 127.33 (C-5), 127.04 (C-8), 118.51 (C-2), 110.14 (C-4a), 107.91 (C-4), 7.92 ($2-CH_3$).

Physical and Spectroscopic Data of Compounds Isolated from the Roots of *Pentas longiflora*

Pentalongin

Brown crystals; ^{1}H NMR (500 MHz, CDCl$_3$) δ 8.07 (m, 1H, H-8), 7.72 (*m*, 1H, H-7), 7.61 (*m*, 1H, H-6), 6.96 (*d*, *J* = 5.53, 1H, H-3), 6.01 (*d*, *J* = 5.56, 1H, H-4).
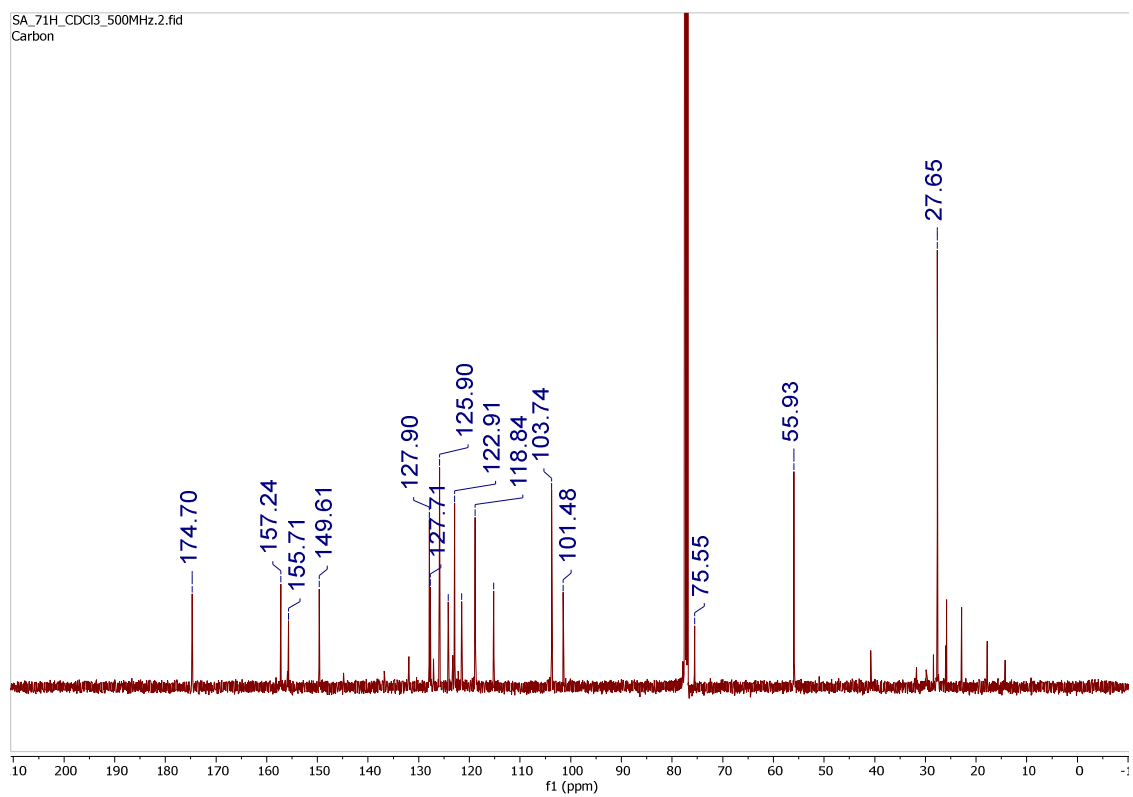
^{13}C NMR (125 MHz, CDCl$_3$) δ 182.4 (C-9), 180.8 (C-10), 154.9 (C-3), 136.8 (C-1a), 133.6 (C-5), 133.6 (C-8), 132.6 (C-5a),131.9 (C-8a), 126.7 (C-7), 126.2 (C-6), 124.5 (C-4a), 97.5 (C-4), 62.3 (C-1)

KVBA-38F4_CDCl3_PROTON_01

Busseihydroquinone B

f1 (ppm)

1

APPENDIX 1.1: ^{13}C NMR Spectrum of Busseihydroquinone B (CD$_3$CN, 500 MHz)

174.70
157.24
155.71
149.61
127.90
127.71
125.90
122.91
118.84
103.74
101.48
75.55
55.93
27.65

f1 (ppm)

APPENDIX 1.2: ESI-MS Spectrum for Busseihydroquinone A

KVBA-BHB
KVBA-BHB 235 (4.737)   1: Scan ES+
                                                                    8.76e5
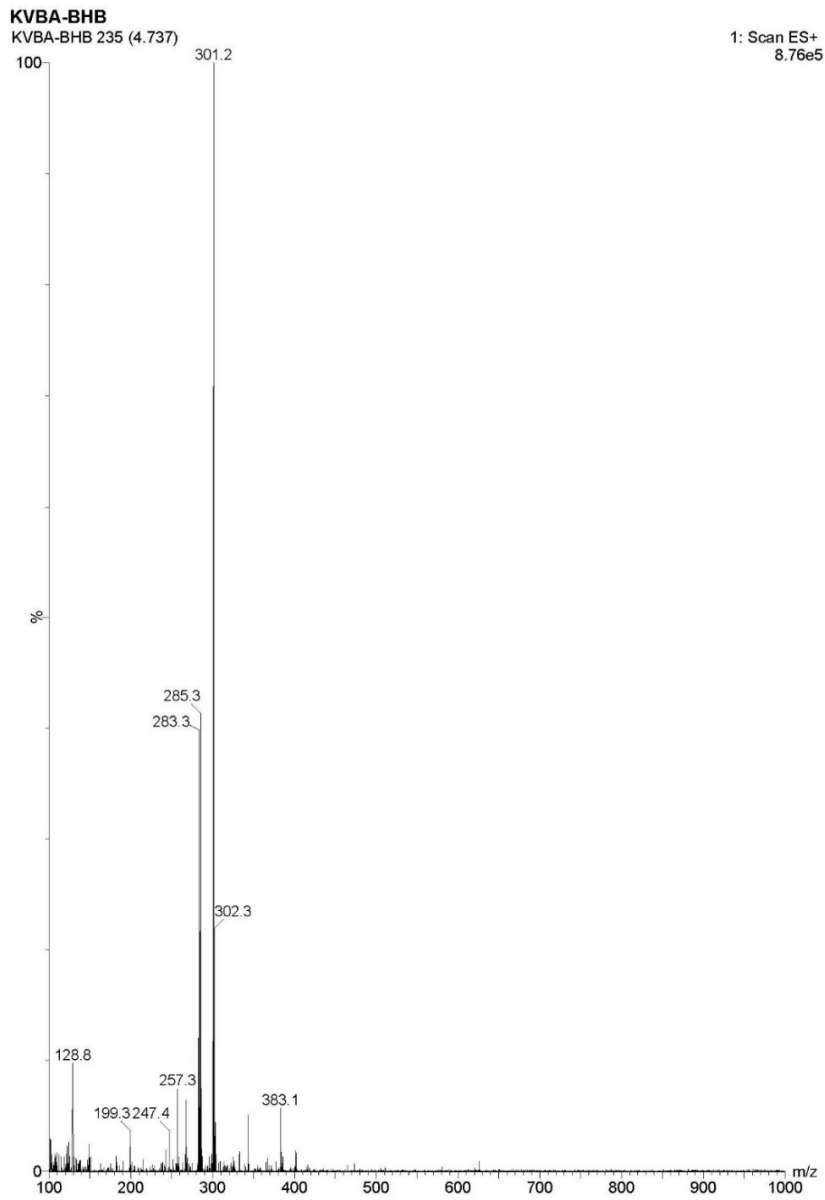
APPENDIX 2.0: ^{1}H NMR Spectrum of β-Stigmasterol (CD$_3$CN, 500 MHz)

KVP-3A_PROTON_01
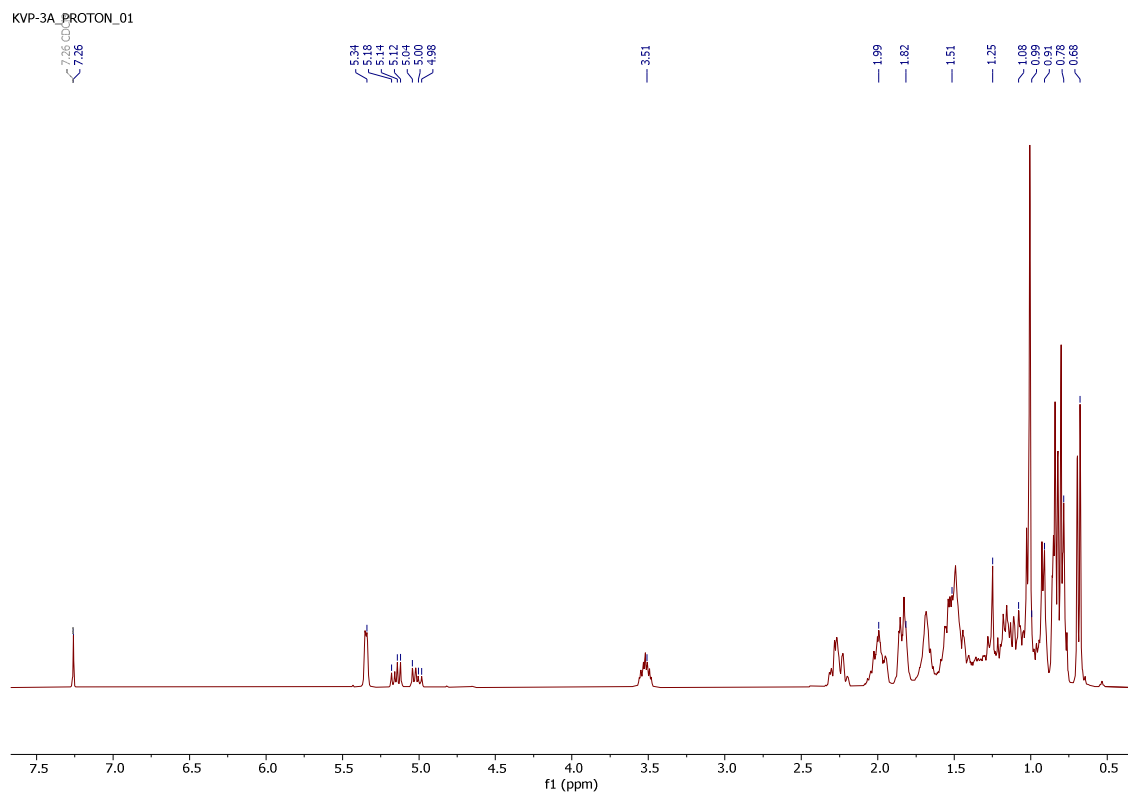
APPENDIX 2.1: ^{13}C NMR Spectrum of β-Stigmasterol (CD$_3$CN, 500 MHz)
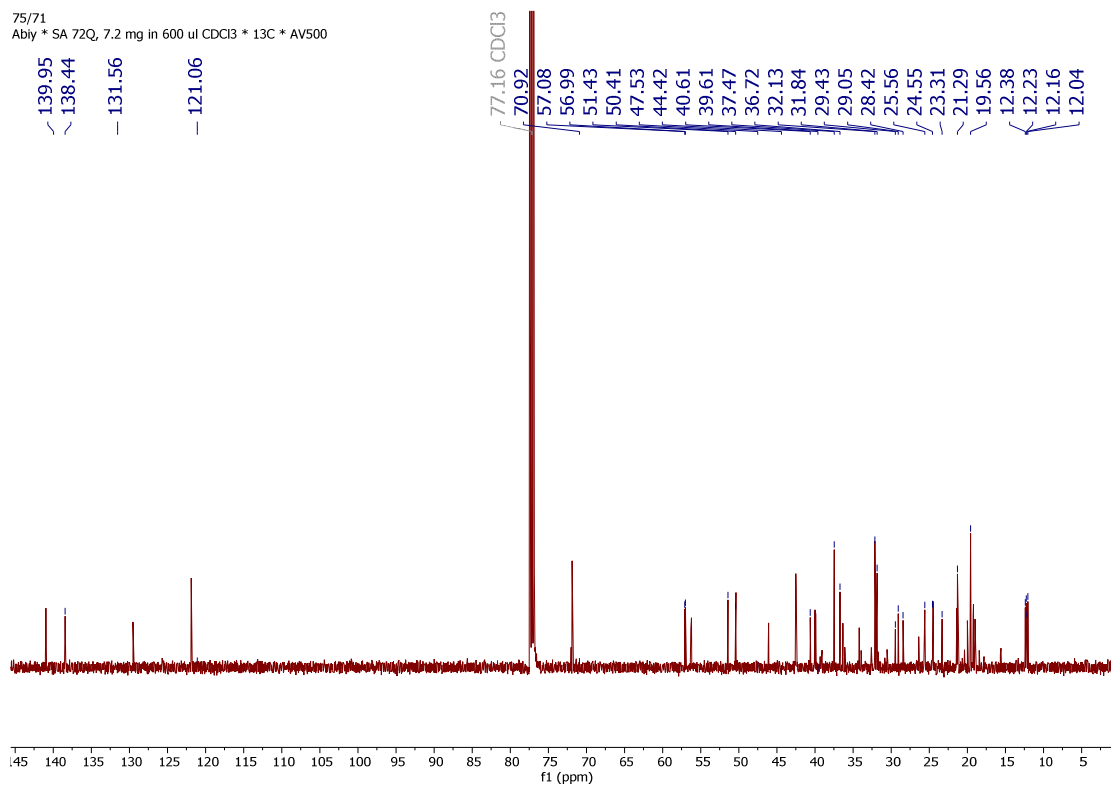
APPENDIX 3.0: ^{1}H NMR Spectrum of β-Amyrin (CDCl$_3$, 500 MHz)

AV500 Dec13-2019-ay/30
Abiy SA 72R, 6.9 mg in 550 ul CDCl3 * 1H * AV500
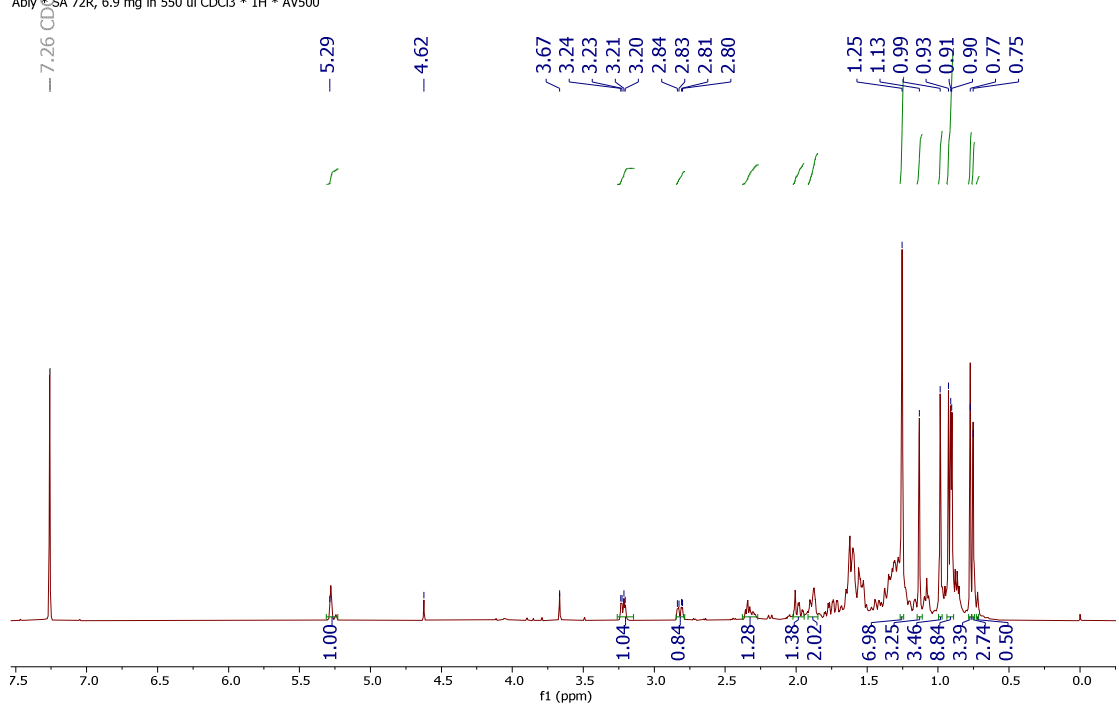
APPENDIX 3.1: ^{13}C NMR Spectrum of β-Amyrin (CDCl$_3$, 500 MHz)

AV500Dec13-2019-ay/34
Abiy * SA 72R, 6.9 mg in 550 ul CDCl3 * 13C * AV500
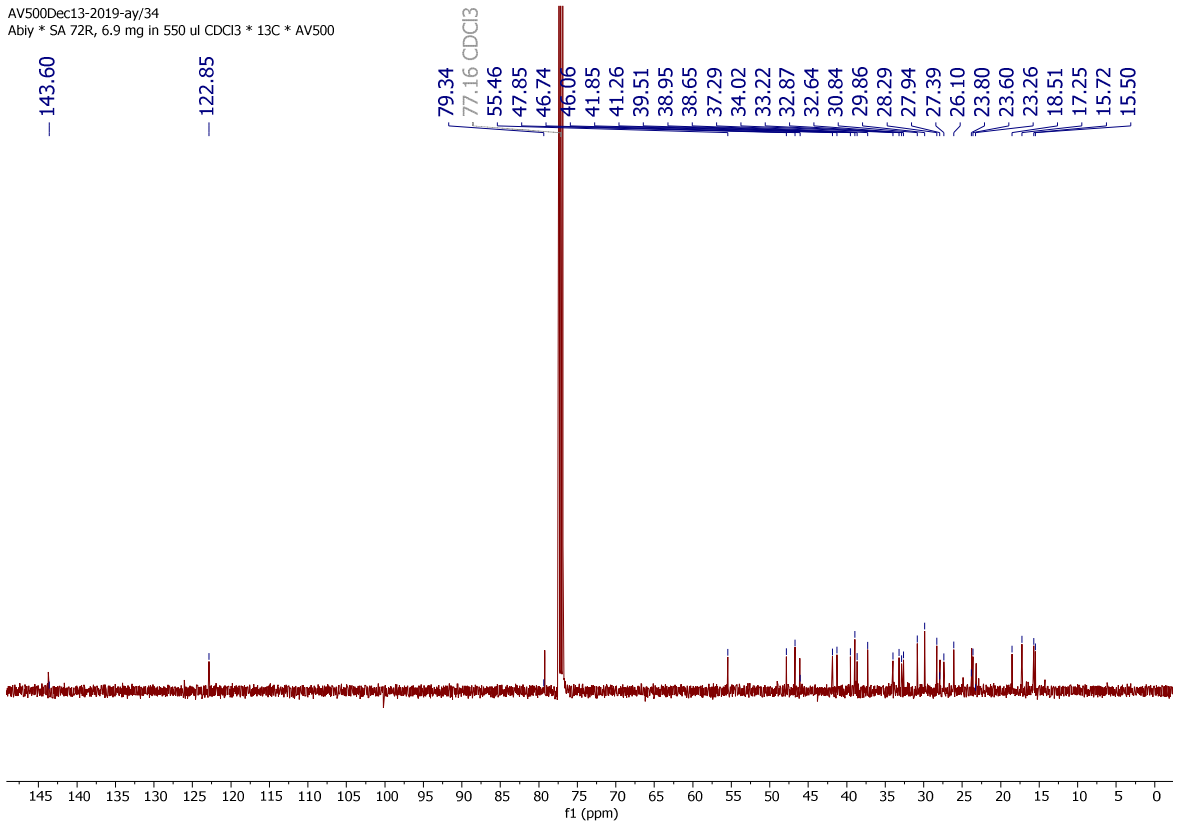
APPENDIX 4.0: ^{1}H NMR Spectrum of Busseihydroquinone A (CDCl$_3$, 500 MHz)

KVBA-38B_CDCl3_PROTON_01
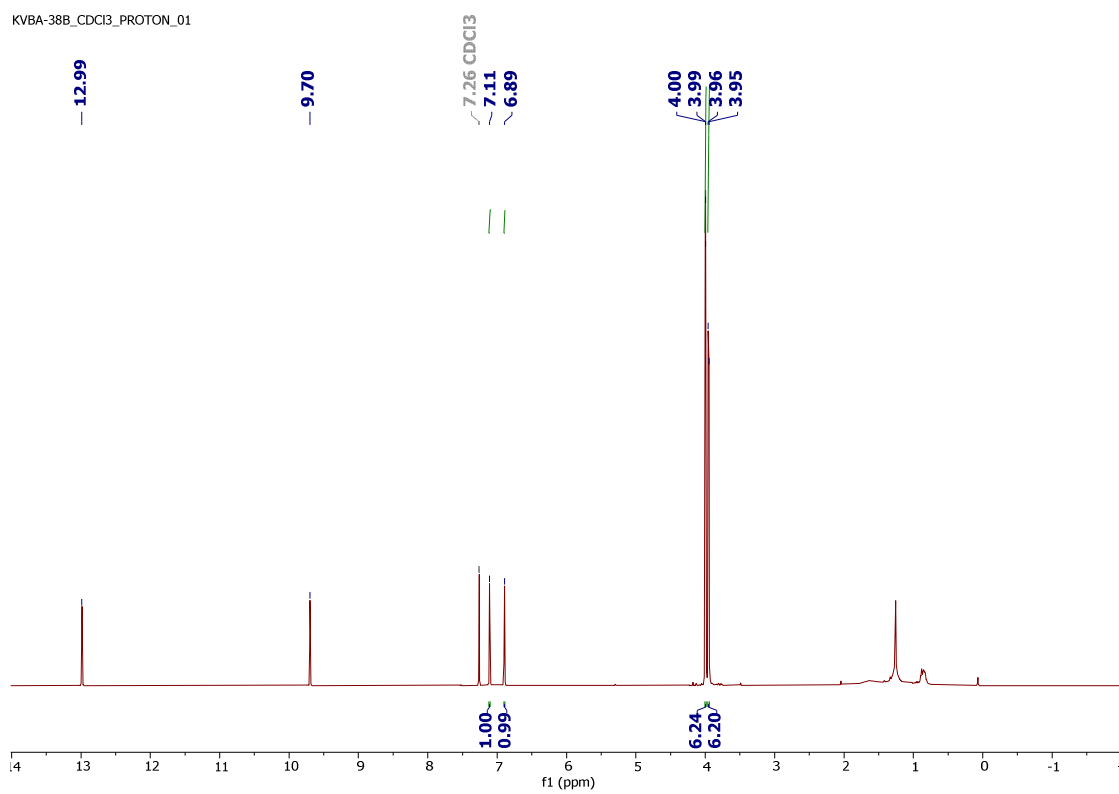
APPENDIX 4.1: ^{13}C NMR Spectrum of Busseihydroquinone A (Acetone-d$_6$, 500 MHz)

Win791
Abiy * SA 72P, 4.9 mg in 60ul acetone-d6 * 13C * AV500

206.26 (CD3)
206.26
172.61
157.53
150.57
148.40
136.53
128.87
111.10
102.99
100.86
95.85
94.87
60.61
56.32
56.29
53.20

f1 (ppm)
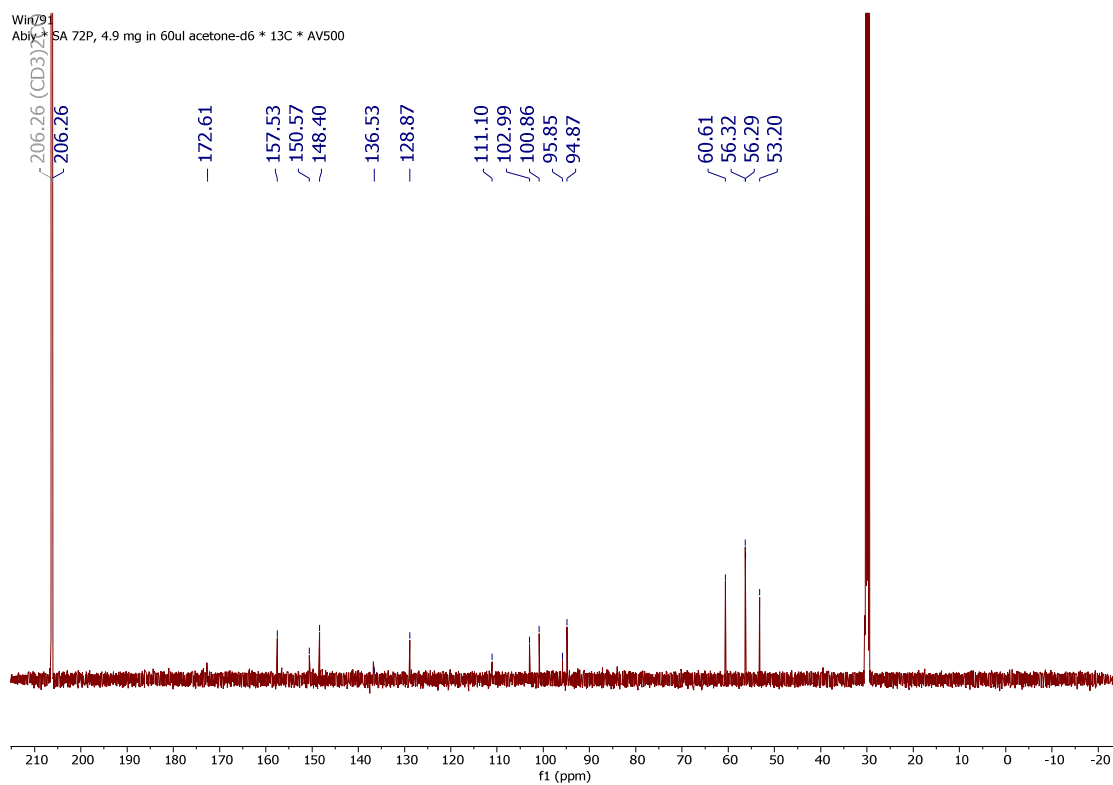
APPENDIX 4.1: ESI-MS Spectrum for Busseihydroquinone A
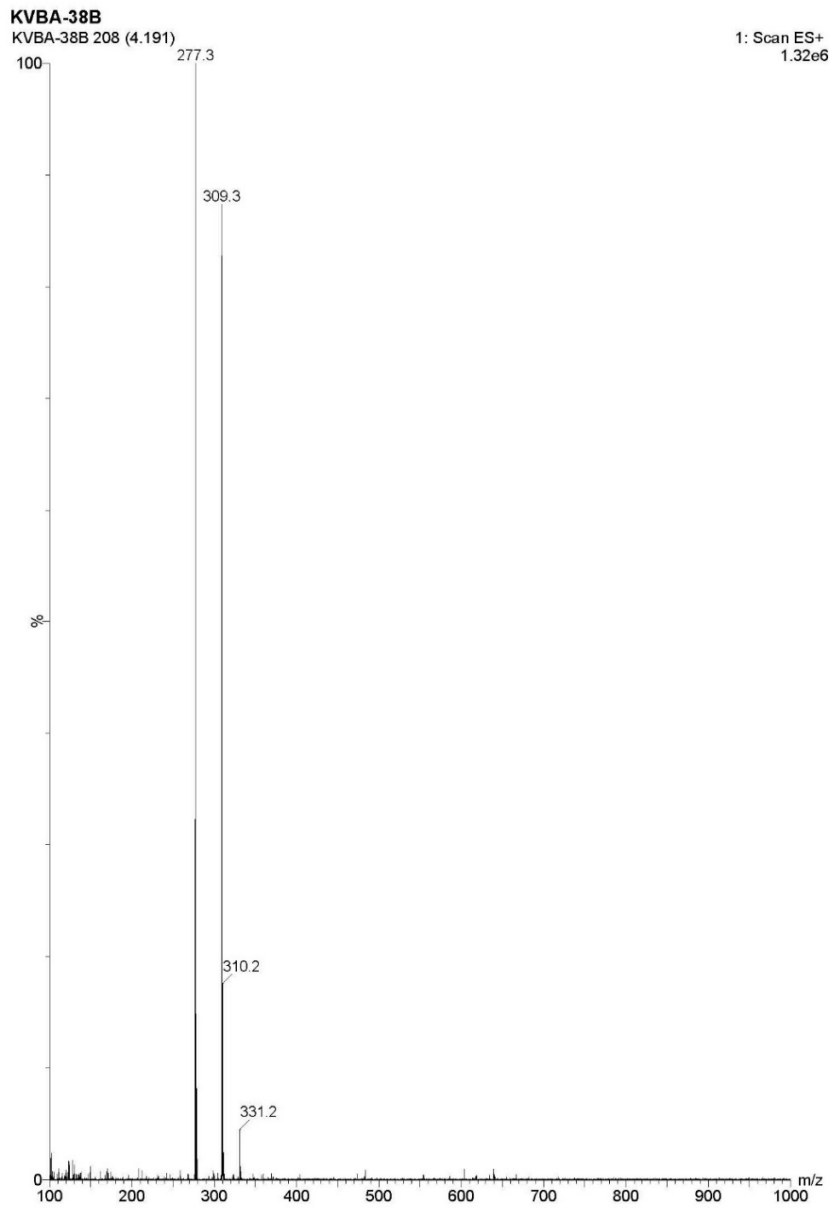
APPENDIX 5.0: ^{1}H NMR Spectrum of Vanillic acid (CD$_3$CN, 500 MHz)
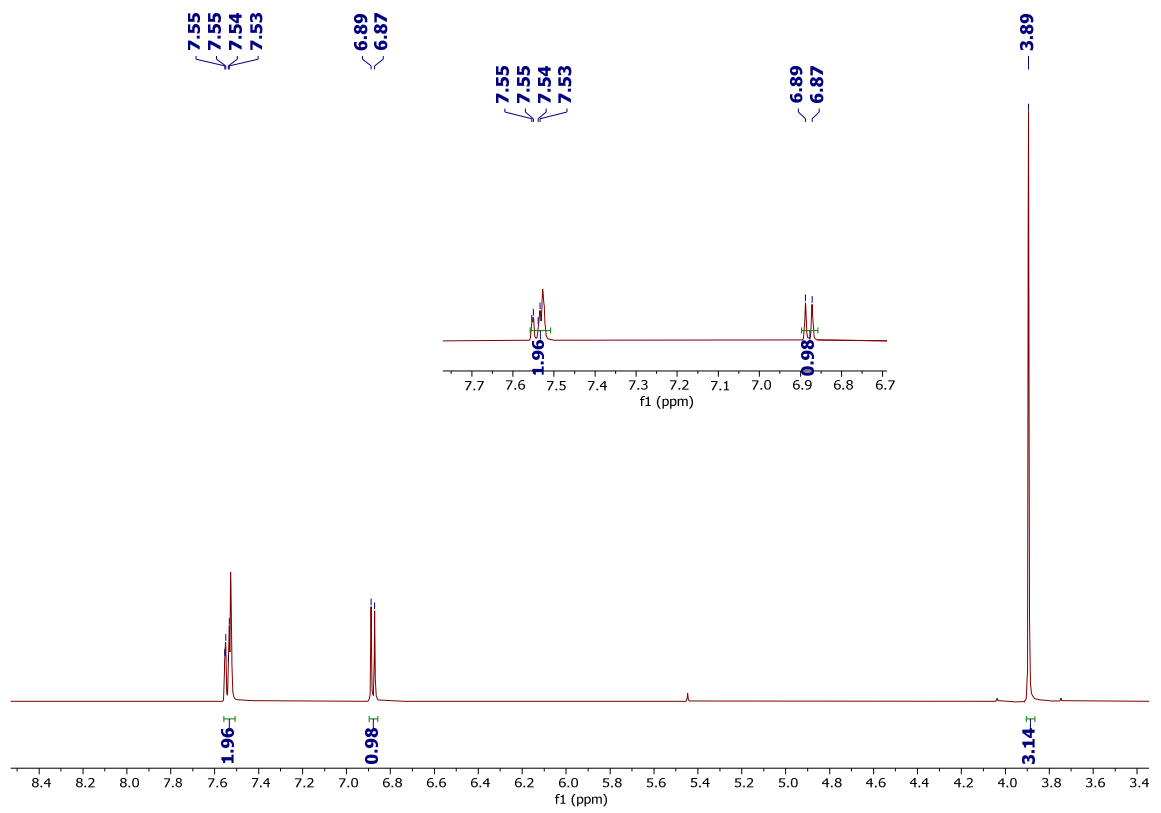
APPENDIX 5.1: ^{13}C NMR Spectrum of Vanillic acid (CD$_3$CN, 500 MHz)

KVPA-36A.2.fid
13C NMR for KVPA-36A 500 MHz
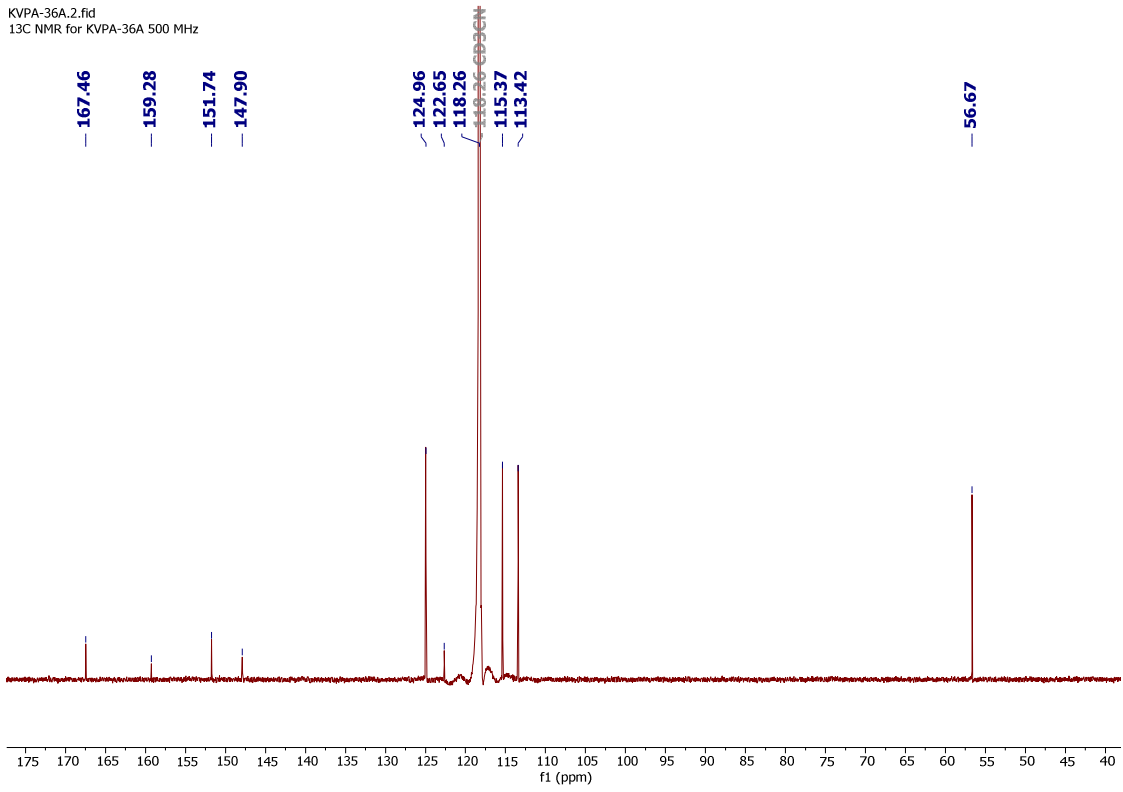
APPENDIX 5.2: ESI-MS Spectrum for Vanillic acid

KVPA-36A
KVPA-36A 37 (0.737)
1: Scan ES+
5.53e4

100 — 101.9

146.0

169.4

185.3

201.2
229.2

265.1
283.1
283.3

342.1 407.1 463.1 484.6 652.2 739.5 758.9 807.6 894.3 930.4 942.7 991.9

m/z
100   200   300   400   500   600   700   800   900   1000
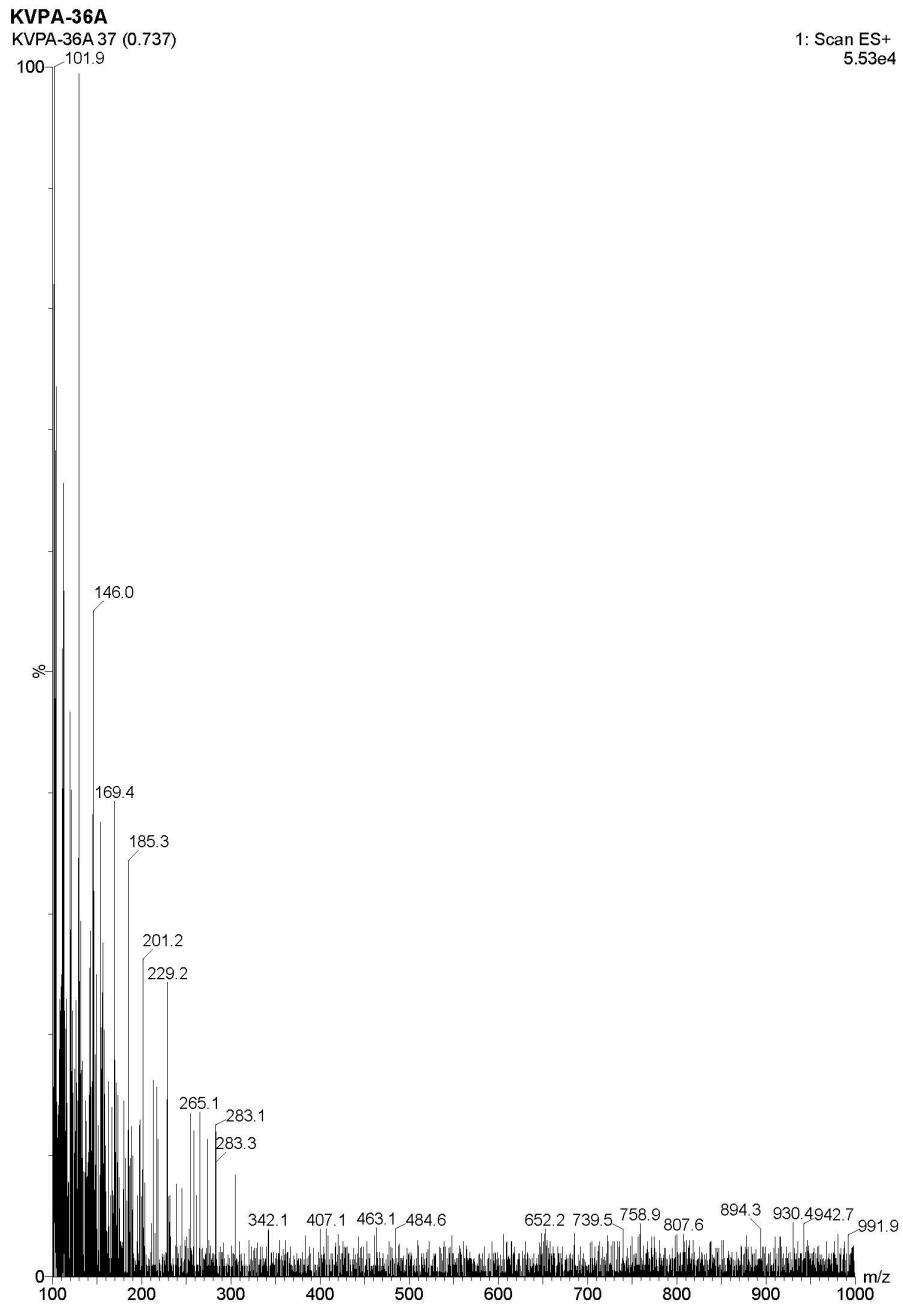
APPENDIX 6.0: ^{1}H NMR Spectrum of *p*-Hydroxybenzoic acid (CD$_3$CN, 500 MHz)

APPENDIX 6.1: ^{13}C NMR Spectrum of *p*-Hydroxybenzoic acid (CD$_3$CN, 500 MHz)

KVPA-36C.2.fid
13C NMR for KVPA-36C CD3CN 500 MHz

— 167.42
— 162.25
— 132.85
\ 125.15
/ 122.47
— 118.26 CD3CN
/ 115.63

f1 (ppm)
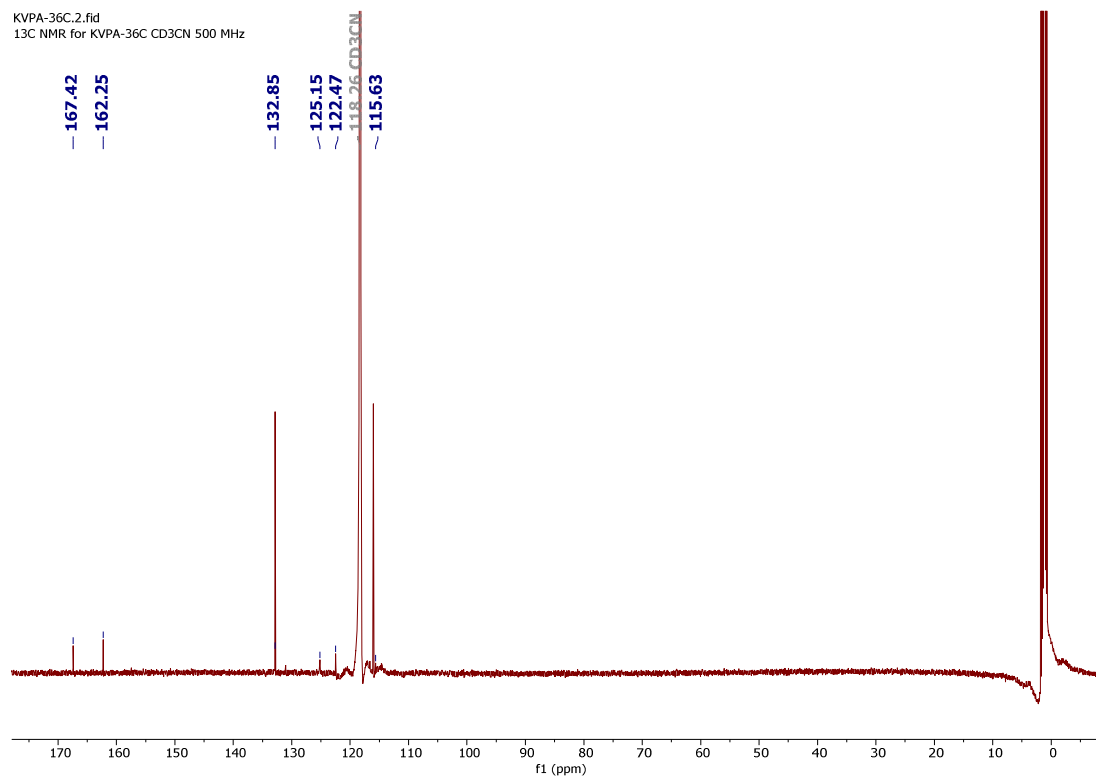
APPENDIX 6.2: ESI-MS Spectrum for *p*-Hydroxybenzoic acid

KVPA-36C
KVPA-36C 94 (1.889)

1: Scan ES+
5.46e4
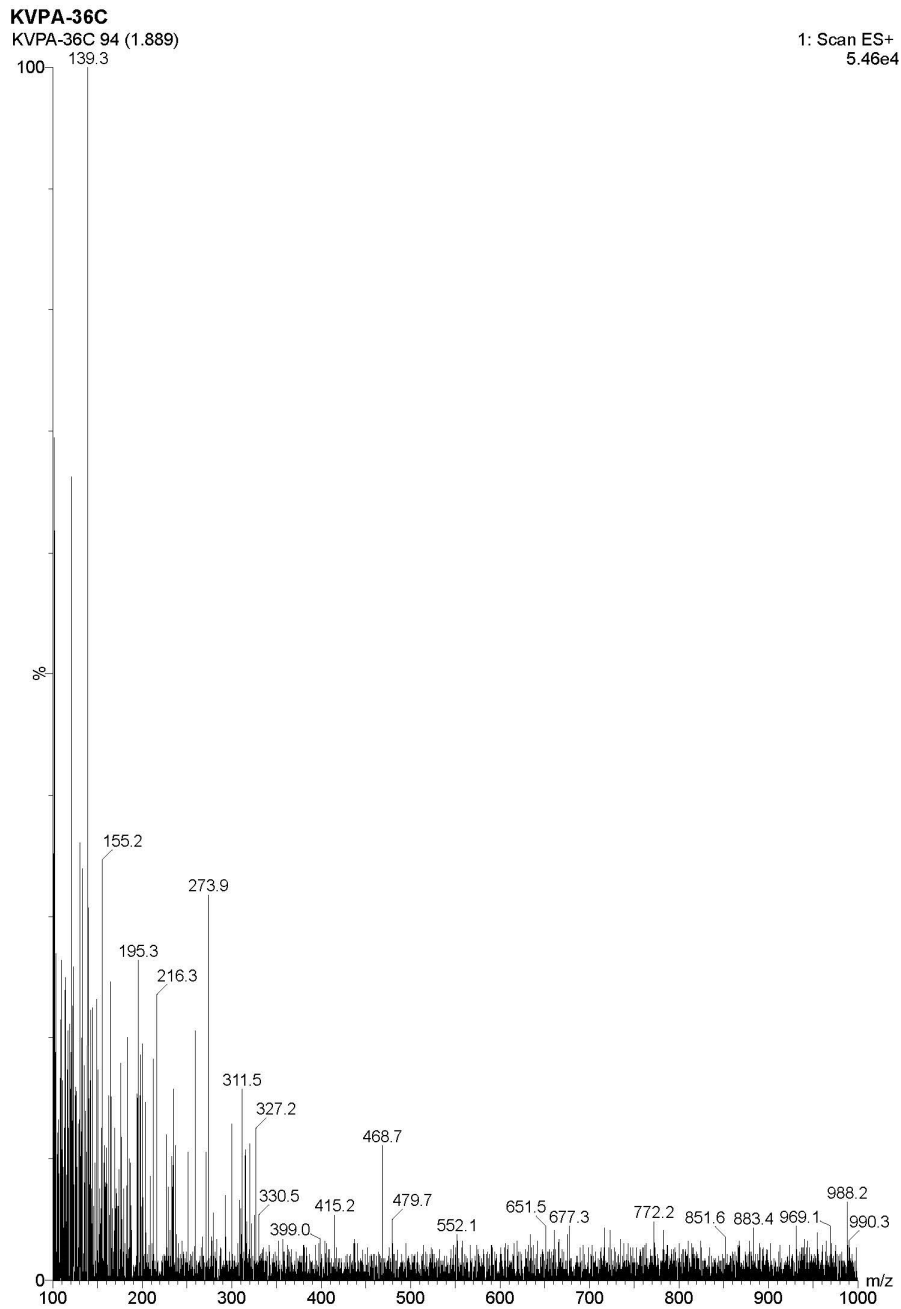
Appendix 7.0: ^{1}H NMR Spectrum of Protocatechuic acid (DMSO-d$_6$, 500 MHz)

KVBA-38K.1.fid
1H KVBA-38K DMSO-d6 500 MHZ

— 2.50 DMSO-d6

7.33
7.33
7.29
7.29
7.28
7.27
6.78
6.77
6.76

7.33
7.33
7.29
7.29
7.28
7.27

E (dd)
7.28

D (d)
7.33

6.78
6.77
6.76

F (d)
6.78

E (dd)
7.28

D (d)
7.33

F (d)
6.78

0.94
0.96
1.01

7.4 7.3 7.2 7.1 7.0 6.9 6.8 6.7 6.6
f1 (ppm)

0.94
0.96
1.01

10.0 9.5 9.0 8.5 8.0 7.5 7.0 6.5 6.0 5.5 5.0 4.5 4.0 3.5 3.0 2.5 2.0 1.5 1.0 0.5 0.0 -0
f1 (ppm)
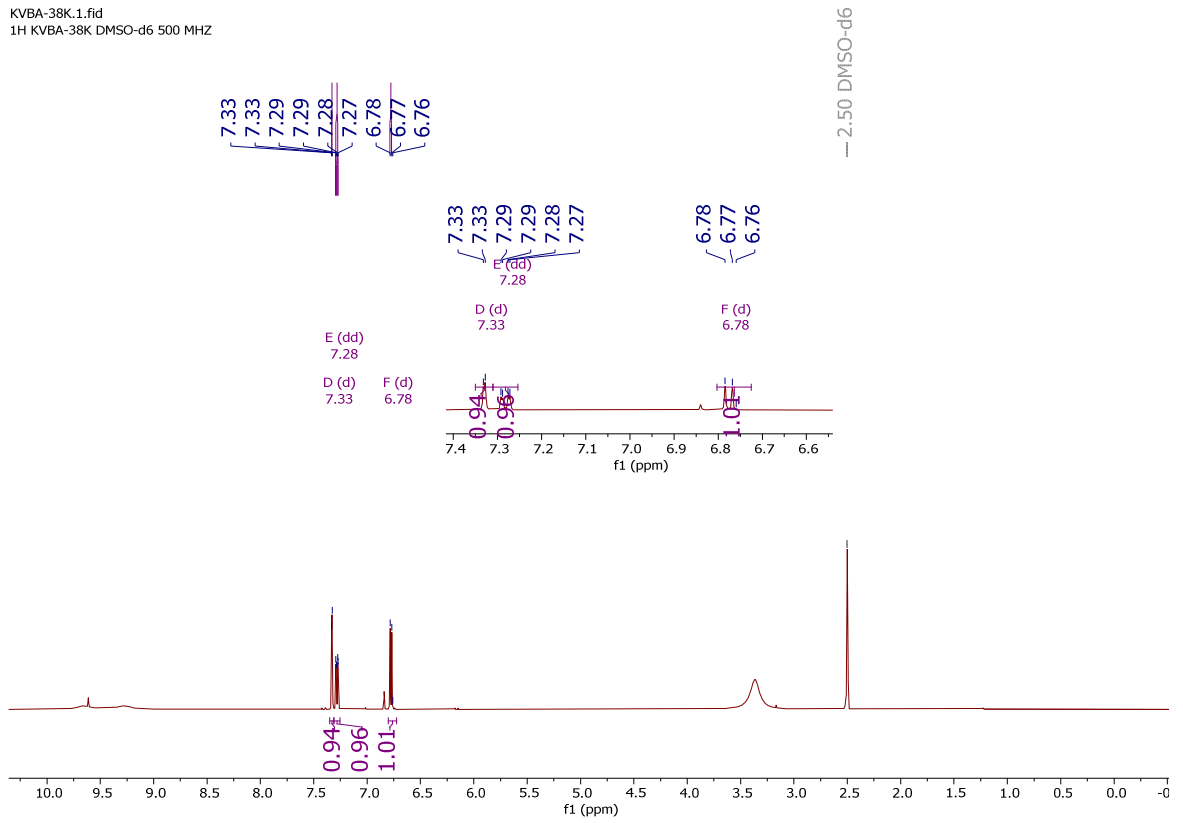
APPENDIX 7.1: ^{13}C NMR Spectrum of Protocatechuic acid (DMSO-d$_6$, 500 MHz)

— 167.31

\ 150.02
/ 144.89

⌐ 121.90
| 121.65
~ 116.55
\ 115.16

— 39.52 DMSO-d6

240 230 220 210 200 190 180 170 160 150 140 130 120 110 100 90 80 70 60 50 40 30 20 10 0 -10 -20 -30 -4C
f1 (ppm)

126

APPENDIX 7.2: ESI-MS Spectrum for Protocatechuic acid

127
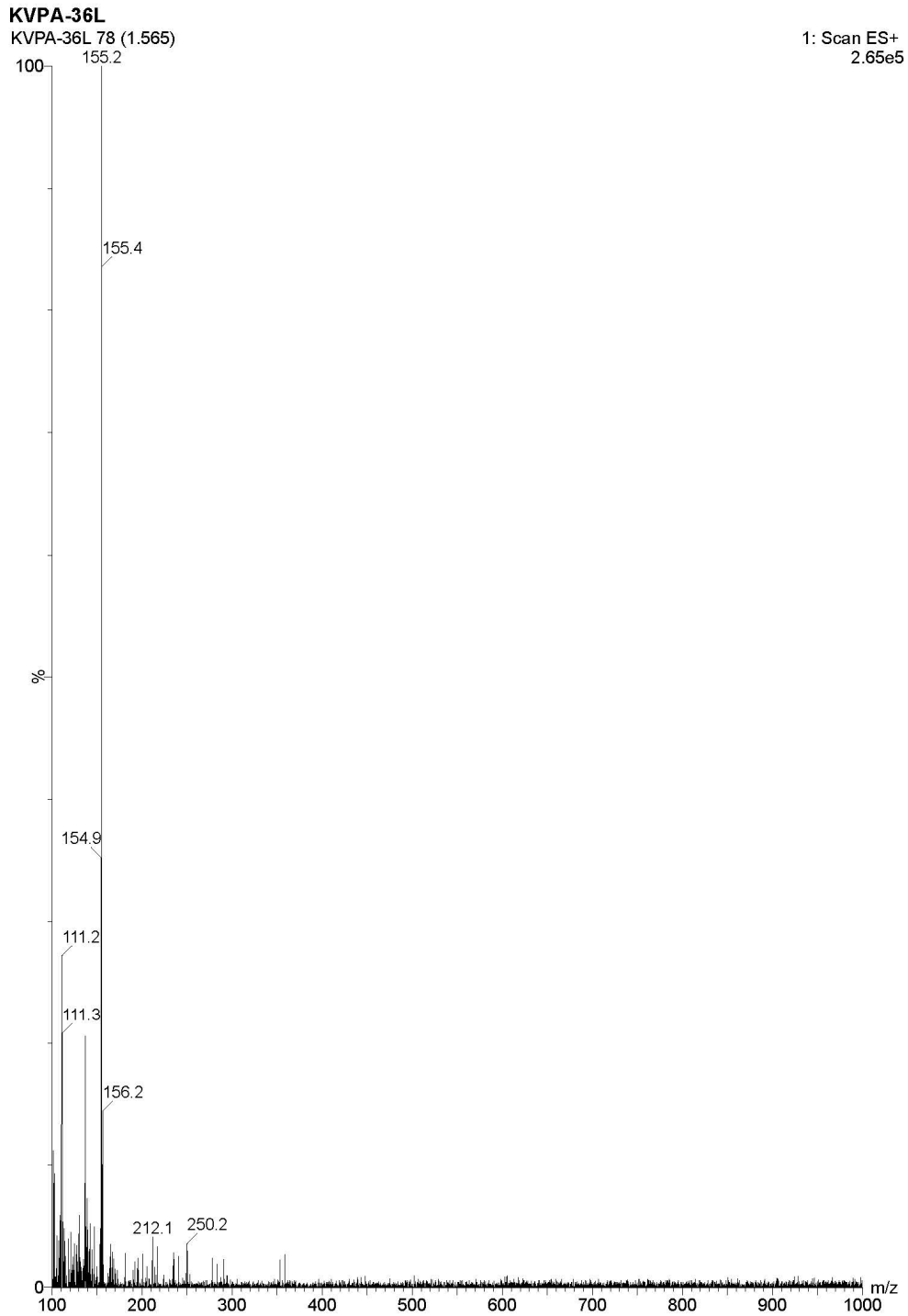
APPENDIX 8.0: ^{1}H NMR Spectrum of Compound **48** (CDCl$_3$, 500 MHz)

KVBA-38A.1.fid
1H NMR KVBA-8A CDCl3 500 MHz

7.26 CDCl3

G (s)
12.27

B (s)
7.61

A (d)
8.02

C (s)
6.92

E (d)
5.67

D (s)
6.06

F (tt)
5.10

I (s)
3.92

H (s)
3.97

N (s)
1.47

K (dd)
1.81

J (dt)
2.15

L (d)
1.66

M (s)
1.57

0.97

1.00
1.02
1.08
0.96
1.02
1.17
3.24
3.29
2.13
2.19
3.35
3.06
3.14

f1 (ppm)
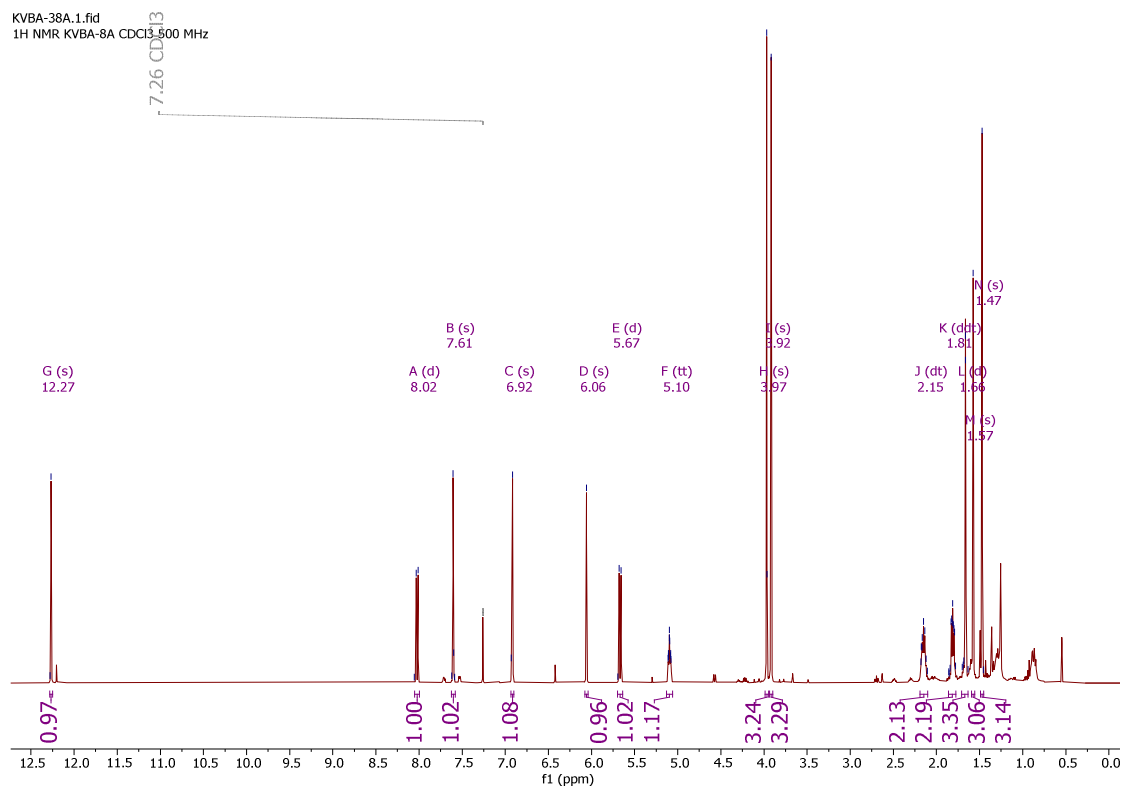
APPENDIX 8.1: ^{13}C NMR Spectrum of Compound **48** (CDCl$_3$, 500 MHz)

KVBA-38A.2.fid
13C NMR KVBA-8A CDCl3 500 MHz

172.12
157.72
147.44
147.07
141.13
132.12
127.97
127.30
123.95
123.50
117.49
116.10
105.46
103.66
99.67
79.04
77.16 CDCl3
55.96
52.32
40.45
25.78
25.70
22.93
17.78

f1 (ppm)
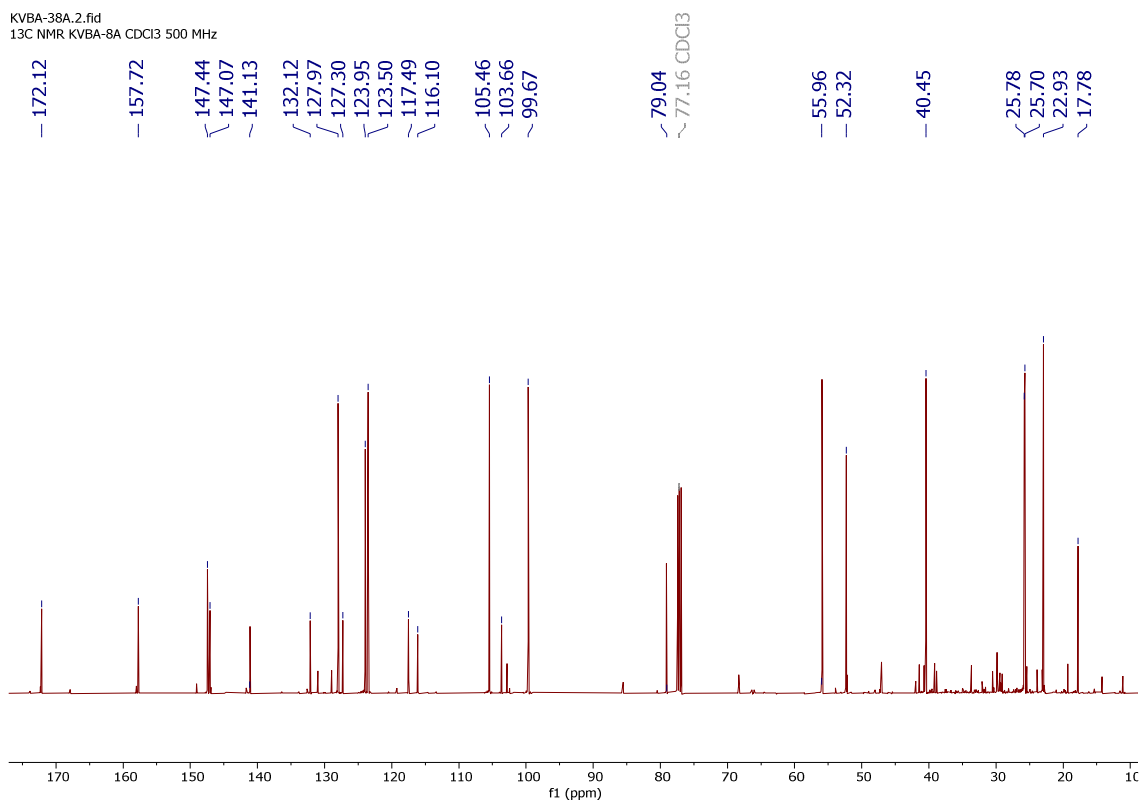
APPENDIX 8.2: H-H COSY Spectrum of Compound **48** (CDCl₃, 500 MHz)
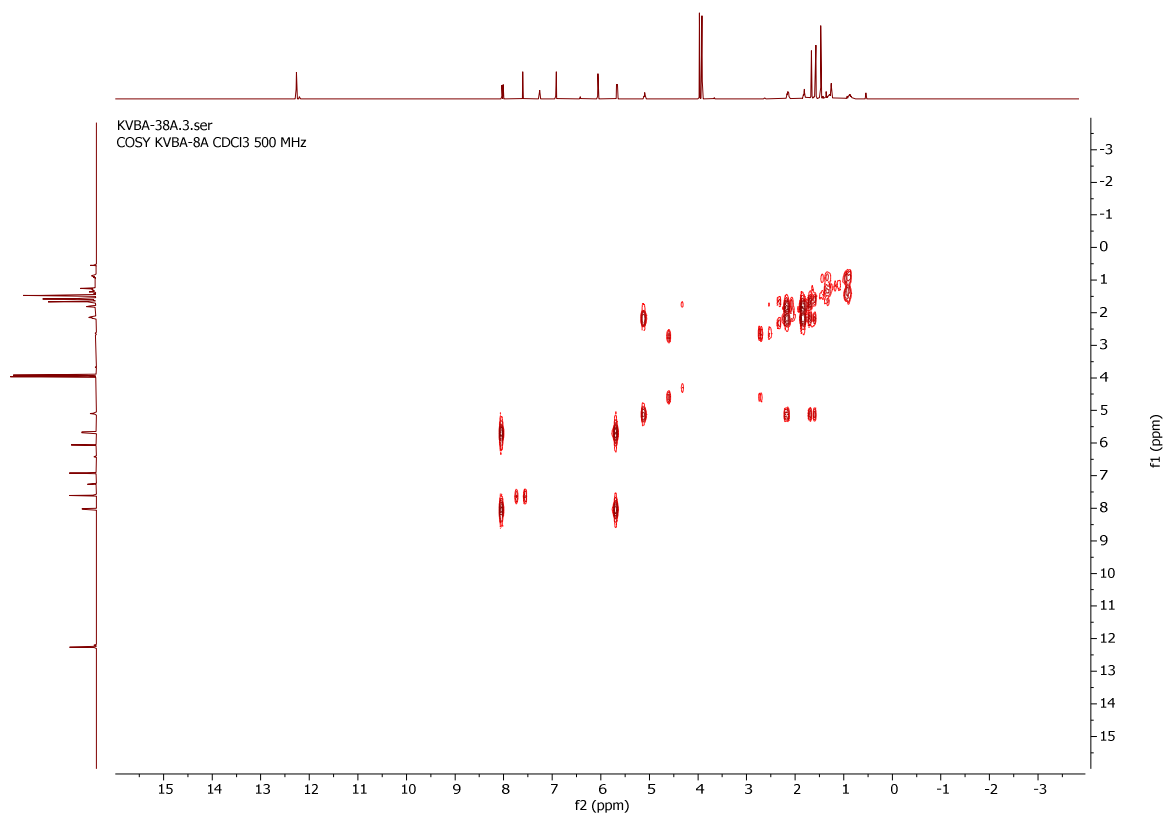
APPENDIX 8.3: HMBC Spectrum of Compound **48** (CDCl₃, 500 MHz)

KVBA-38A.5.ser
HMBC KVBA-8A CDCl3 500 MHz
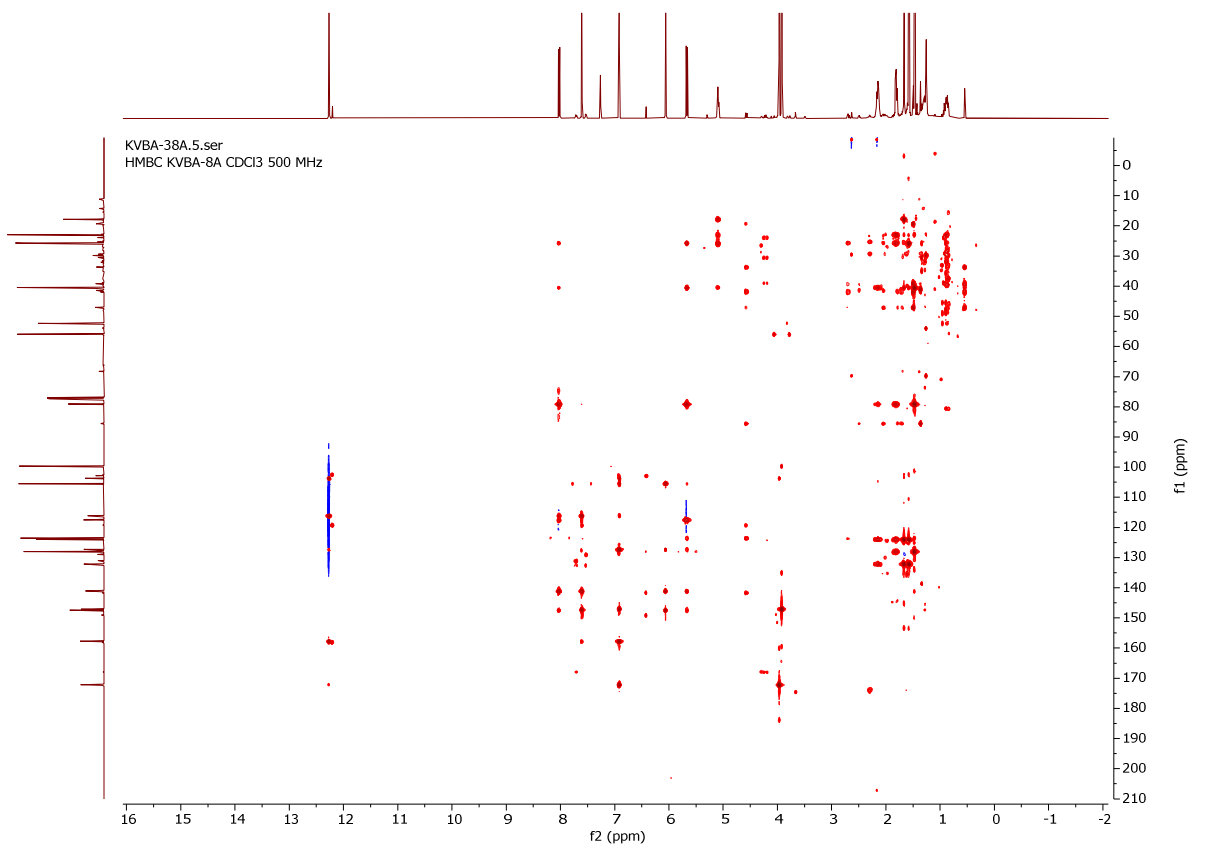
APPENDIX 8.4: NOESY Spectrum of Compound **48** (CDCl$_3$, 500 MHz)

KVBA-38A.6.ser
NOESY KVBA-8A CDCl3 500 MHz
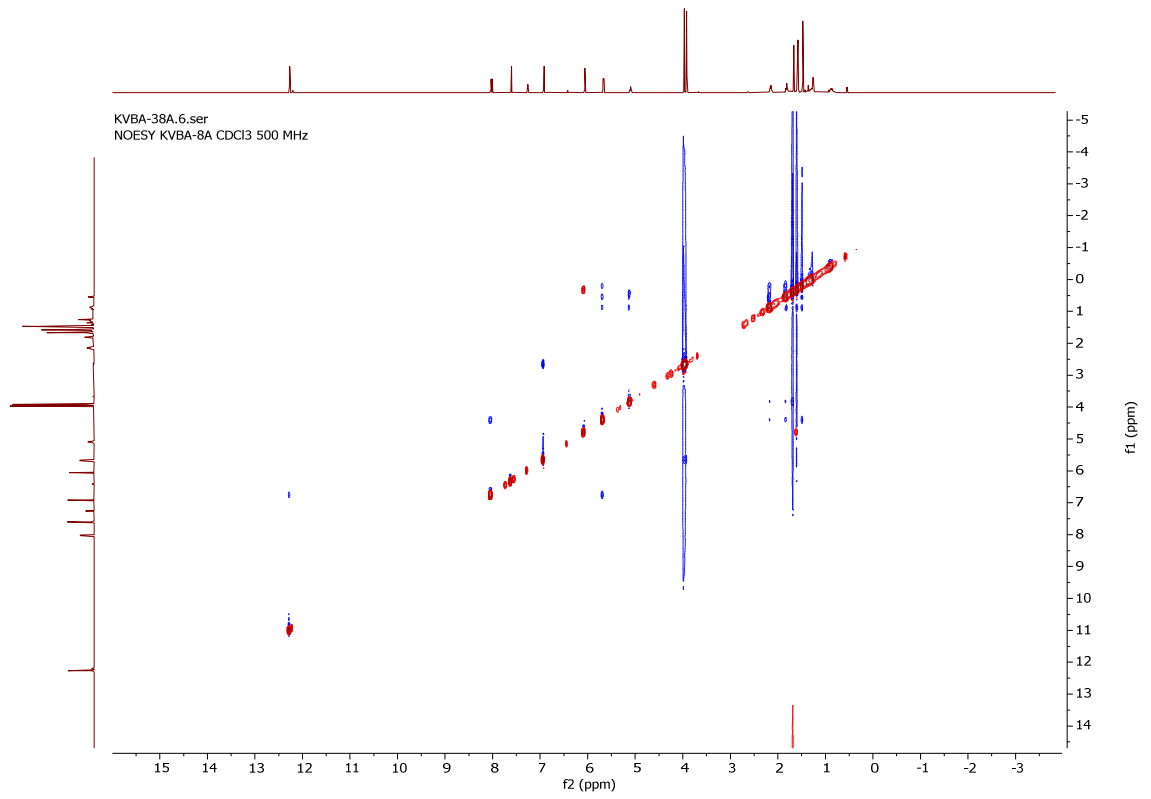
APPENDIX 8.5: ESI-MS Spectrum for Compound **48**

KVBA-38A
KVBA-38A 273 (5.504)
1: Scan ES+
2.40e4
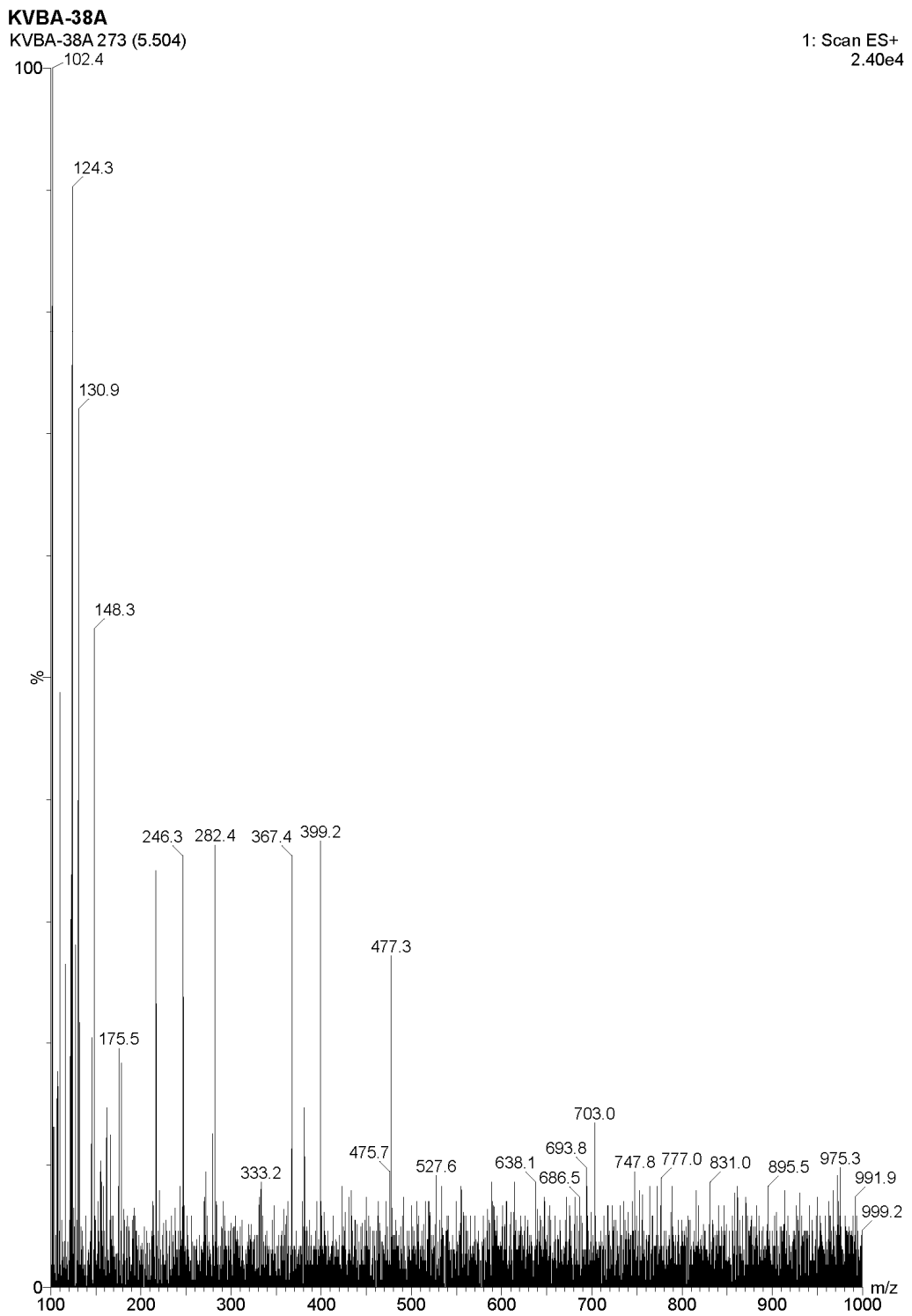
APPENDIX 9.0: 1H NMR Spectrum of Busseihydroquinone C (CDCl$_3$, 500 MHz)

KVBA-B44-J-13-2_PROTON_01
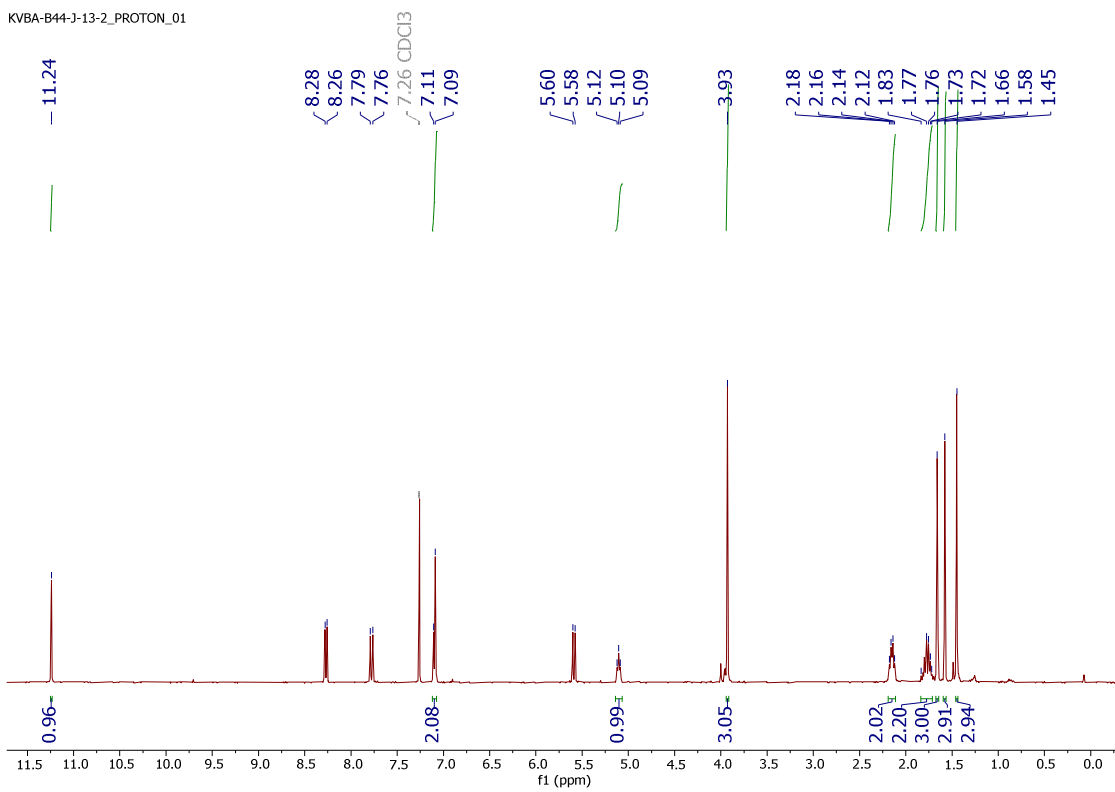
APPENDIX 9.1: ^{13}C NMR Spectrum of Busseihydroquinone C (CD$_3$CN, 500 MHz)

KVBA-38C.2.fid
13C NMR KVBA-38C CD3CN 500 MHz
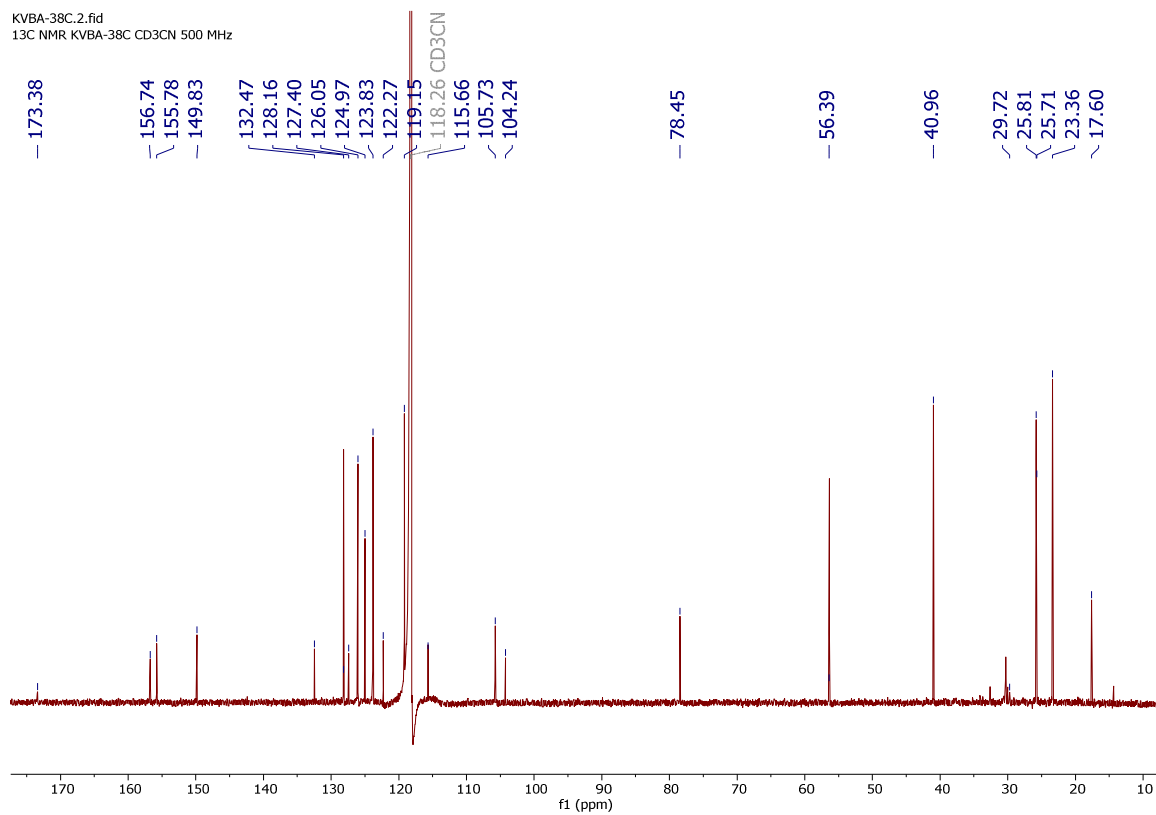
APPENDIX 9.2: ESI-MS Spectrum for Busseihydroquinone C

KVBA-38C
KVBA-38C 267 (5.383)   1: Scan ES+
                                                                                                         2.81e4

100 — 102.2

123.8

124.1

161.5
                        280.6 330.3
                223.2
        175.3   357.2
                272.1 329.3 369.1
                              383.0
                                        473.3   693.9
                              460.3   711.3
                                    552.4   853.9 876.6
                            497.2   567.9 690.7   887.6   989.0
                                                                                      990.7

0
   100   200   300   400   500   600   700   800   900   1000   m/z

136
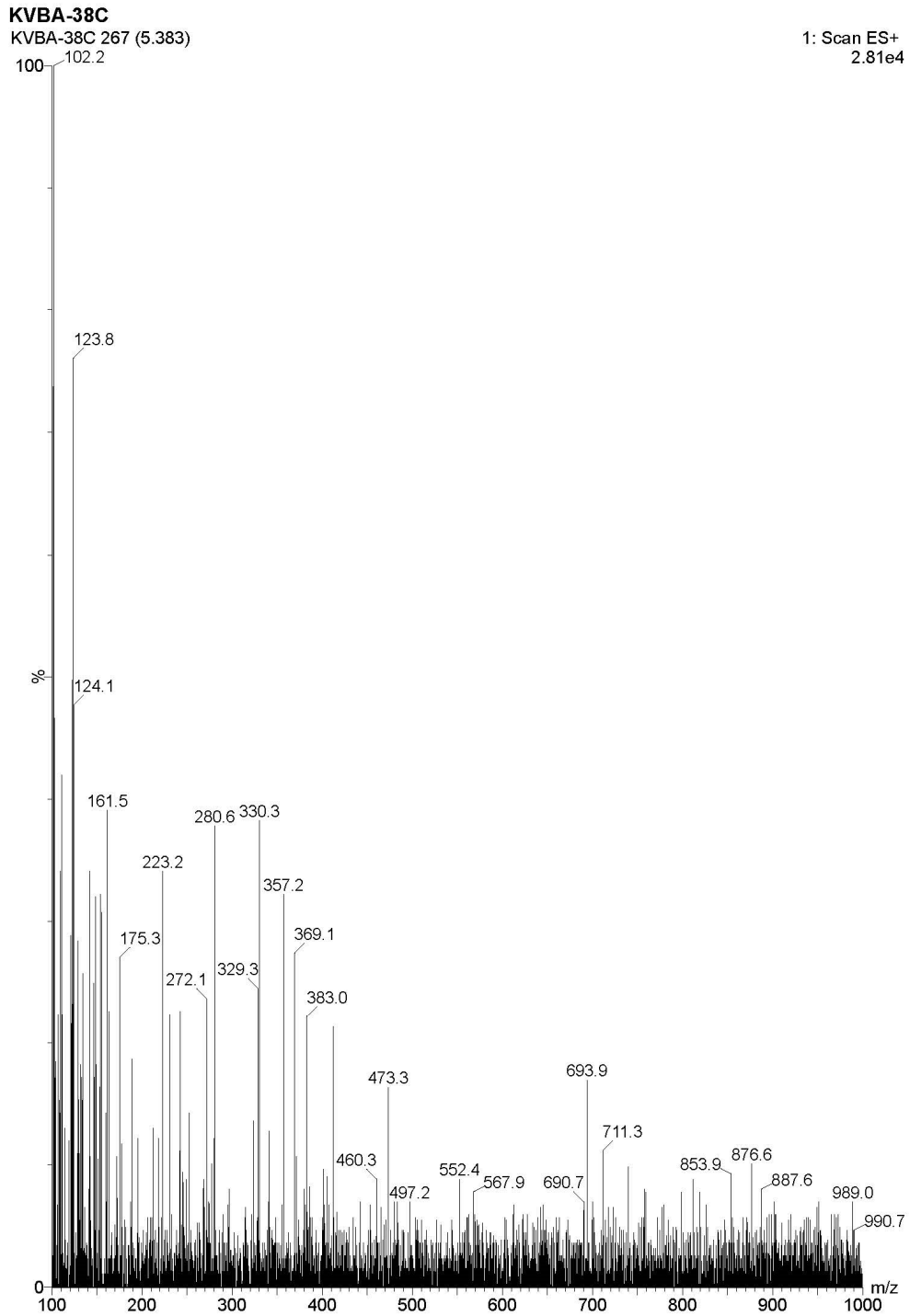
APPENDIX 10.0: ^{1}H NMR Spectrum of Compound **47** (CDCl$_3$, 500 MHz)
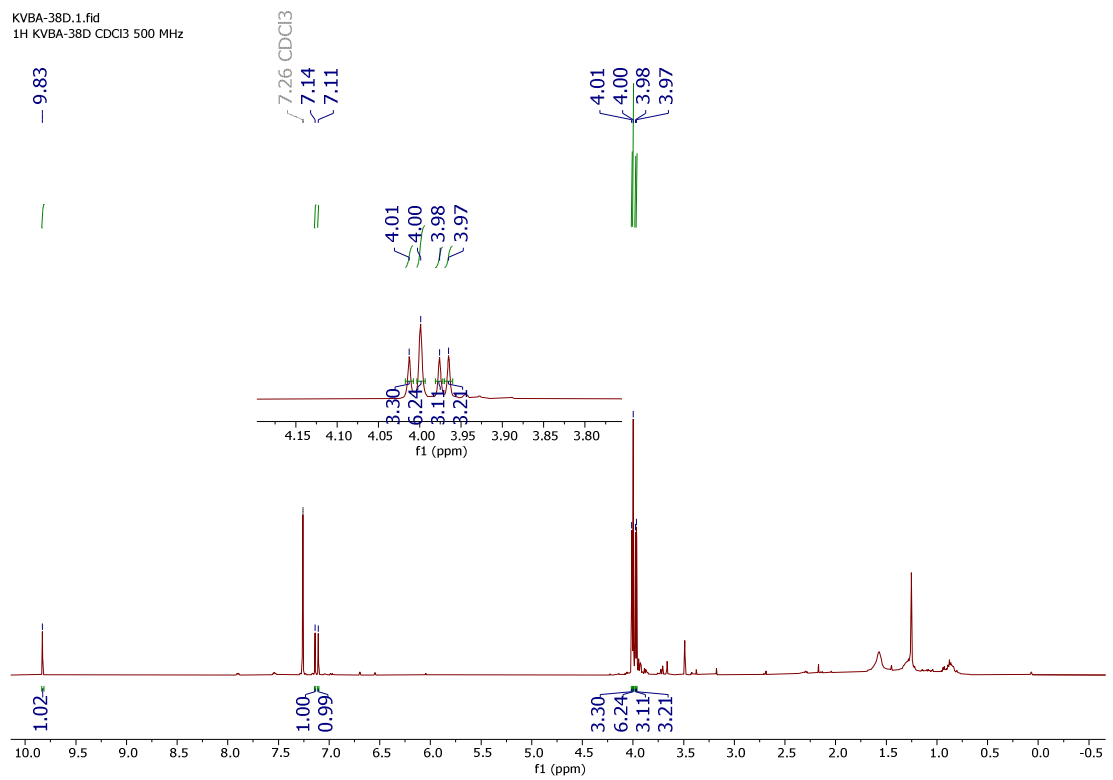
APPENDIX 10.1: ^{13}C NMR Spectrum of Compound **47** (CDCl$_3$, 500 MHz)

— 166.15
155.37
152.50
150.77
148.14
— 135.87
129.25
126.71
115.27
114.04
— 103.75
77.16 CDCl3
64.70
60.94
56.07
55.95
52.48

f1 (ppm)

138
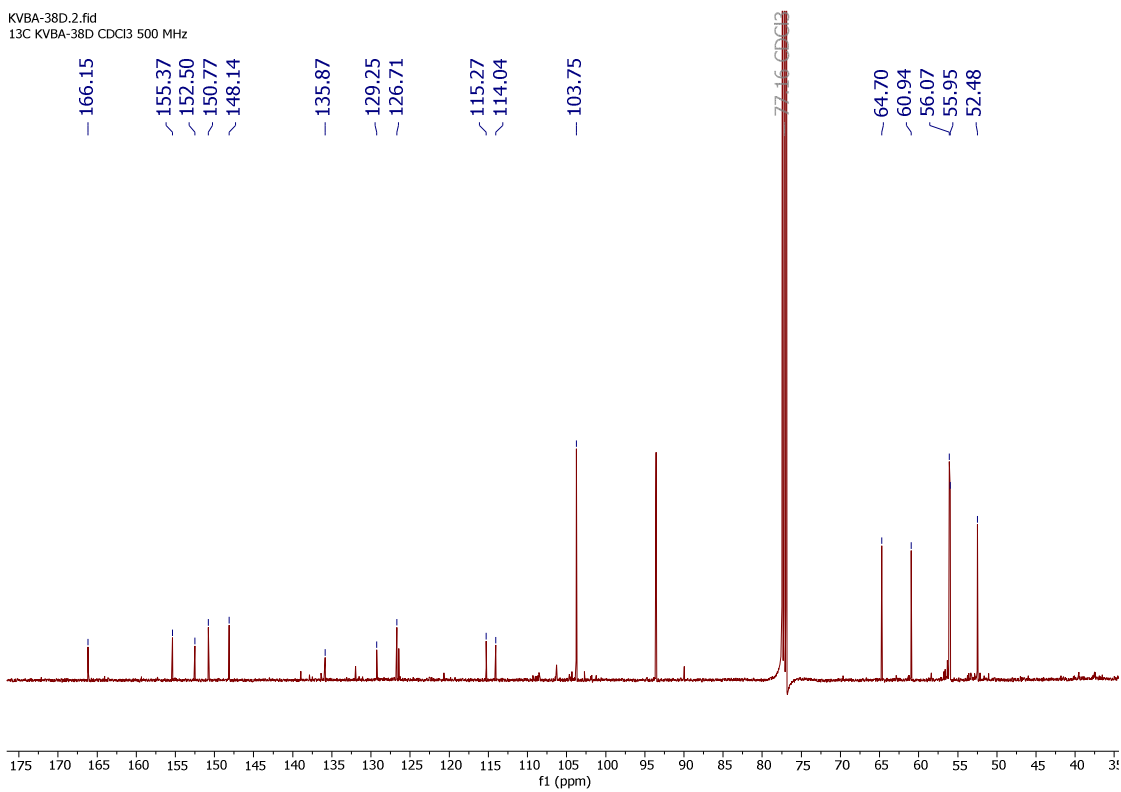
APPENDIX 11.0: ^{1}H NMR Spectrum of Compound **72** ((CD$_3$)$_2$CO, 500 MHz)

SA-74Y.1.fid
Proton

SA-74Y.2.fid
13C

206.26 ((CD3)...

183.56
181.30
162.19
136.02
135.01
133.98
129.19
127.70
126.98
109.88
61.31
9.31

f1 (ppm)
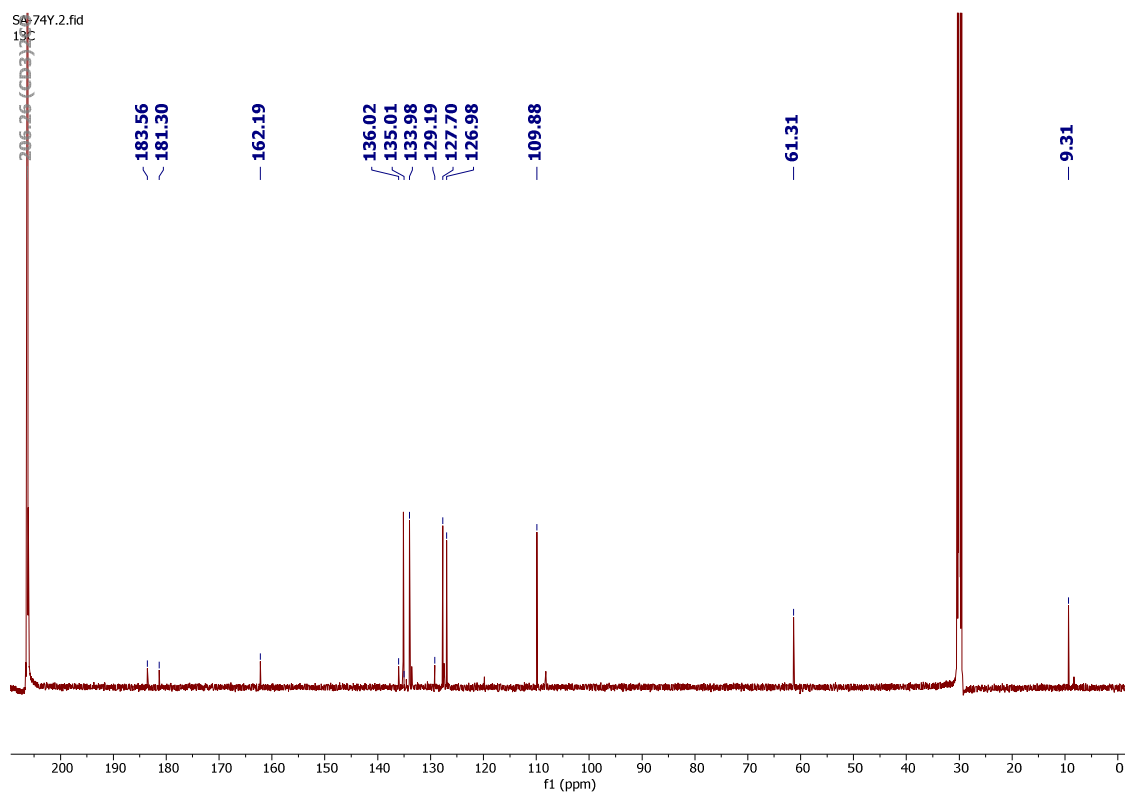
APPENDIX 11.2: HMBC Spectrum of Compound **72** ((CD₃)₂CO, 500 MHz)

SA-74Y.6.ser
HMBC
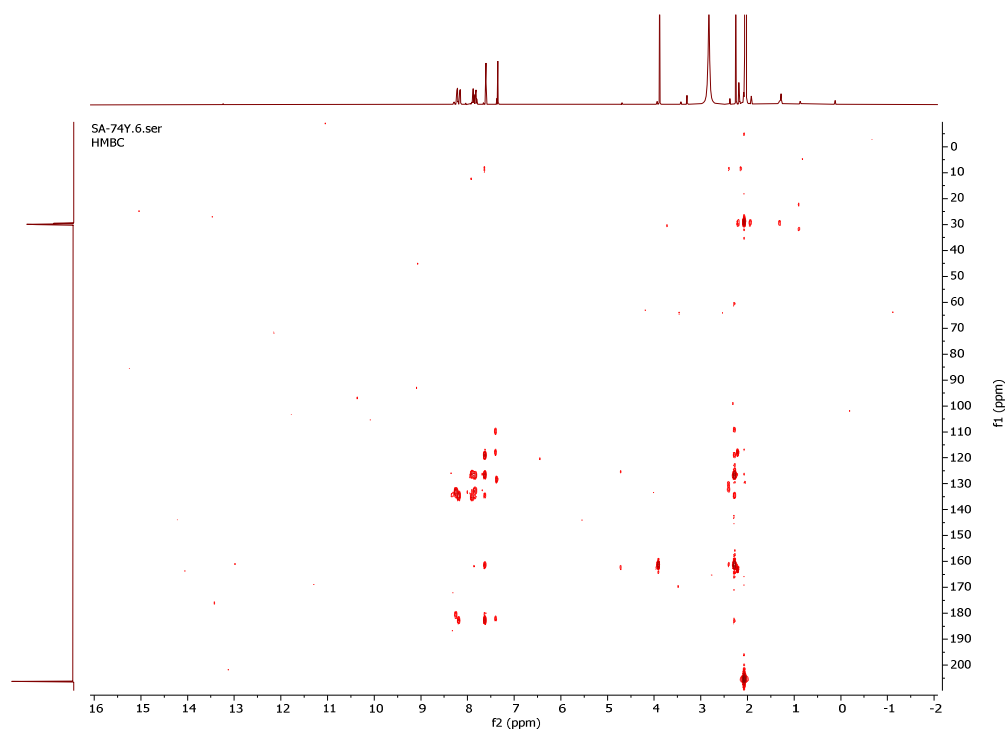
APPENDIX 12.0: ^{1}H NMR Spectrum of Rubiadin-1-methylether (DMSO-d$_6$, 500 MHz)

APPENDIX 12.1: ^{13} C NMR Spectrum of Rubiadin-1-methylether (DMSO-d$_6$, 500 MHz)

SA-74A.26.fid
13C-500MHz-DMSO

SA-74A.29.ser
HMBC-500MHz-DMSO
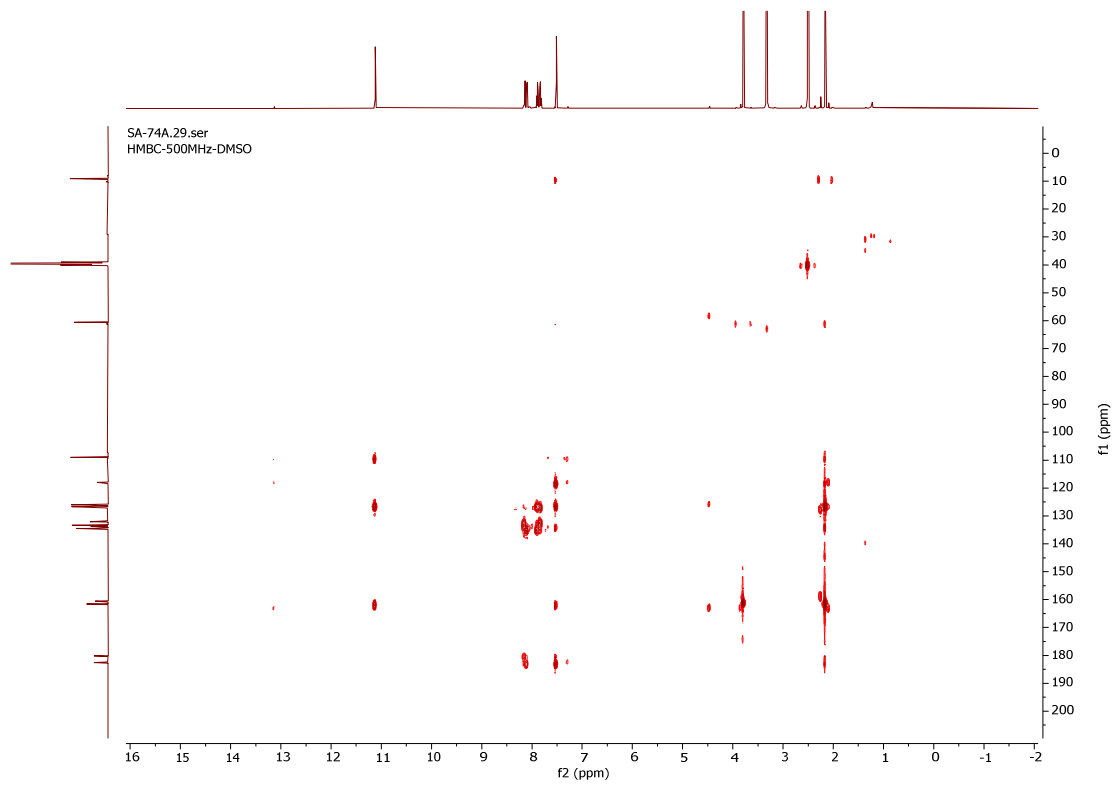
APPENDIX 12.3: ESI-MS Spectrum for Rubiadin-1-methyl ether

SA-74A
SA-74A 185 (3.727)

1: Scan ES+
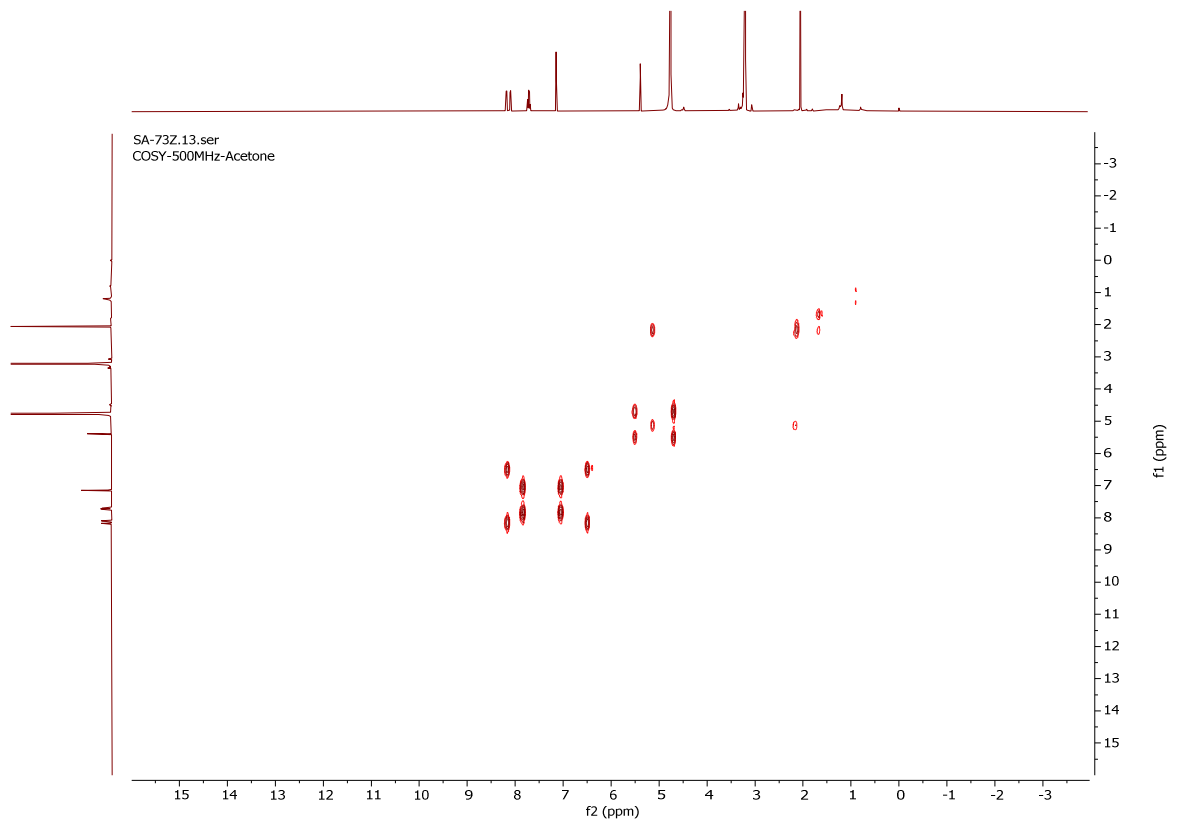2.03e5
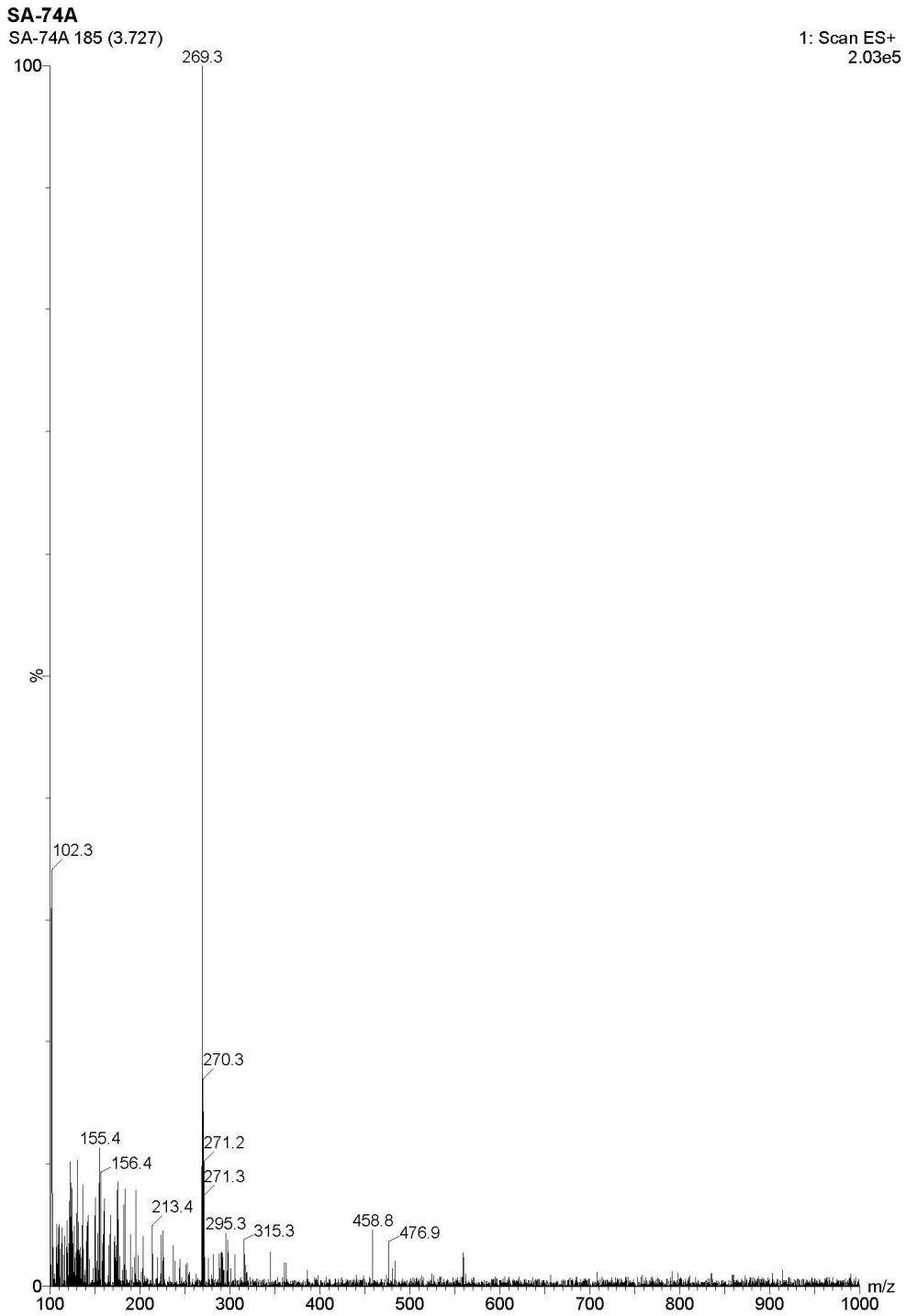
APPENDIX 13.0: ^{1}H NMR Spectrum of Rubiadin ((CD$_3$)$_2$CO, 500 MHz)

SA-73Z Proton.1.fid
1H SA-73Z Acetone 500 MHz
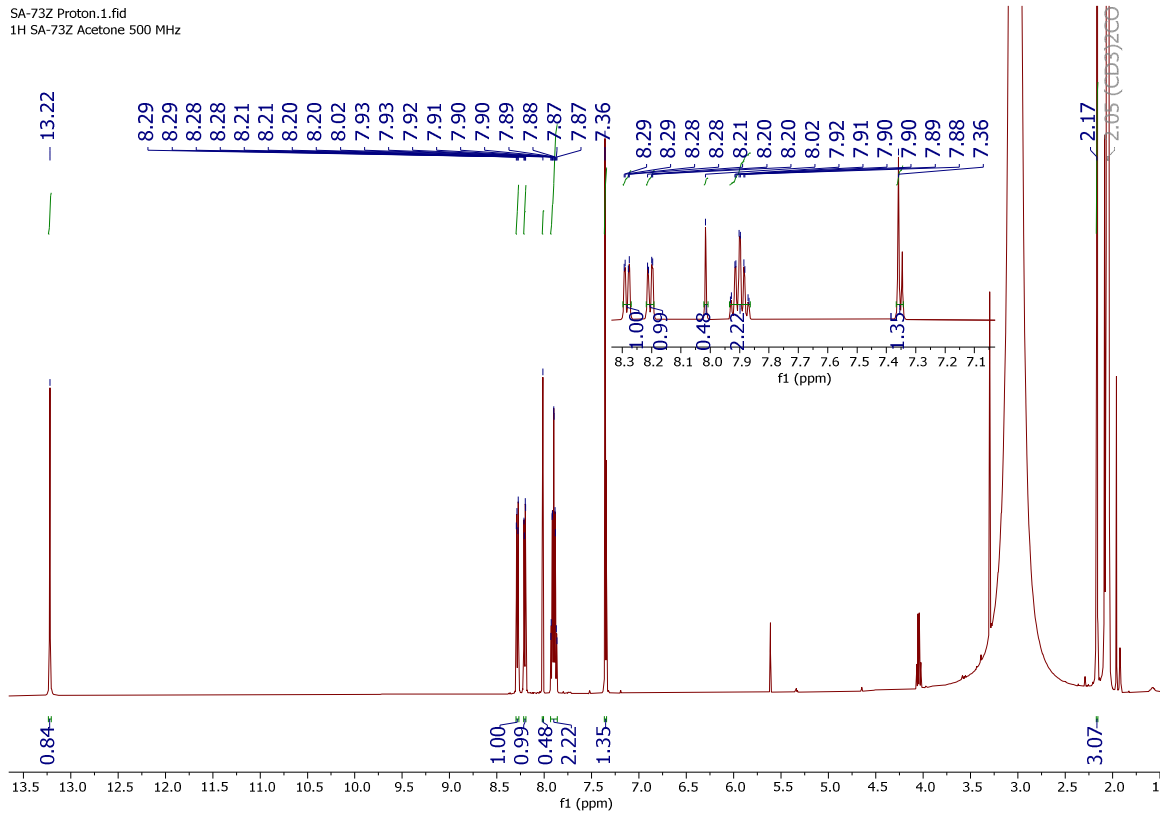
APPENDIX 13.1: ^{13}C NMR Spectrum of Rubiadin ((CD$_3$)$_2$CO, 500 MHz)

SA-73Z Acetone.1.fid
13C SA-73Z Acetone-d6 500 MHz

206.26 ((CD3)2CO)
187.44
182.55
163.81
163.49
134.88
134.80
134.13
134.05
132.90
127.33
127.04
118.51
110.14
107.91
60.28
7.92

f1 (ppm)
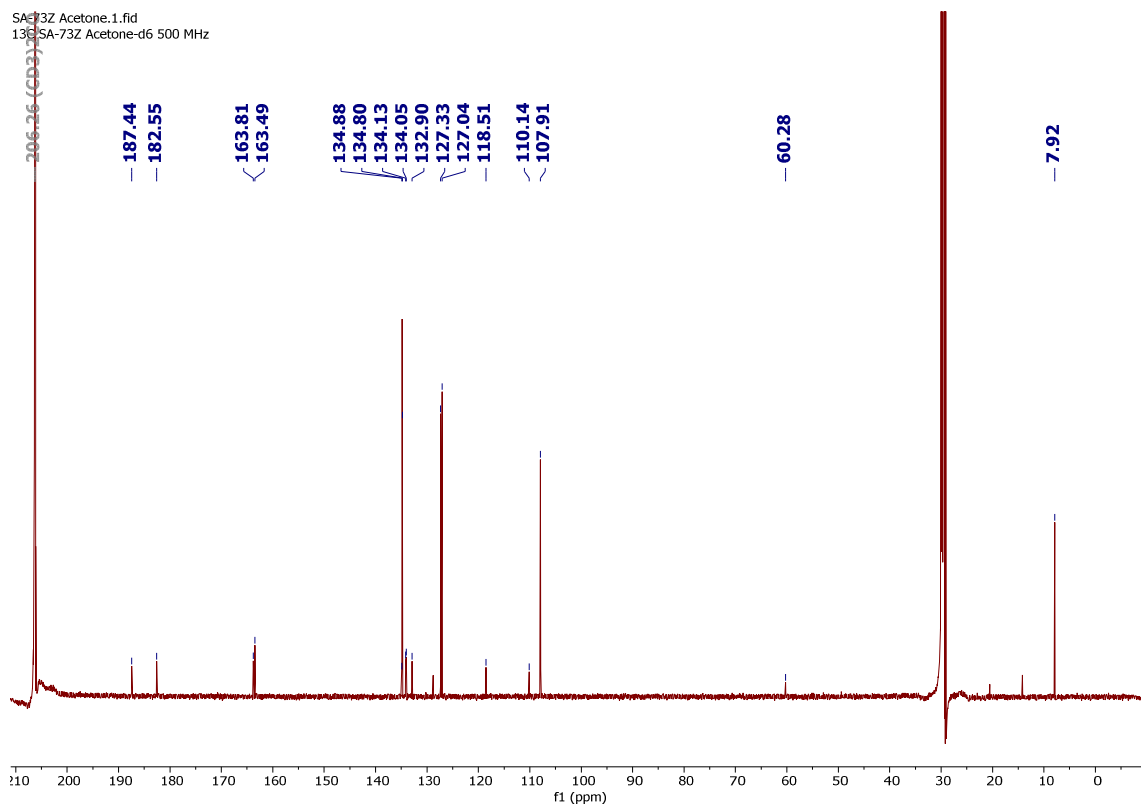
APPENDIX 13.2: COSY Spectrum of Rubiadin ((CD$_3$)$_2$CO, 500 MHz)

SA-73Z.13.ser
COSY-500MHz-Acetone

f1 (ppm)

f2 (ppm)

APPENDIX 13.3: HMBC Spectrum of Rubiadin ((CD$_3$)$_2$CO, 500 MHz)
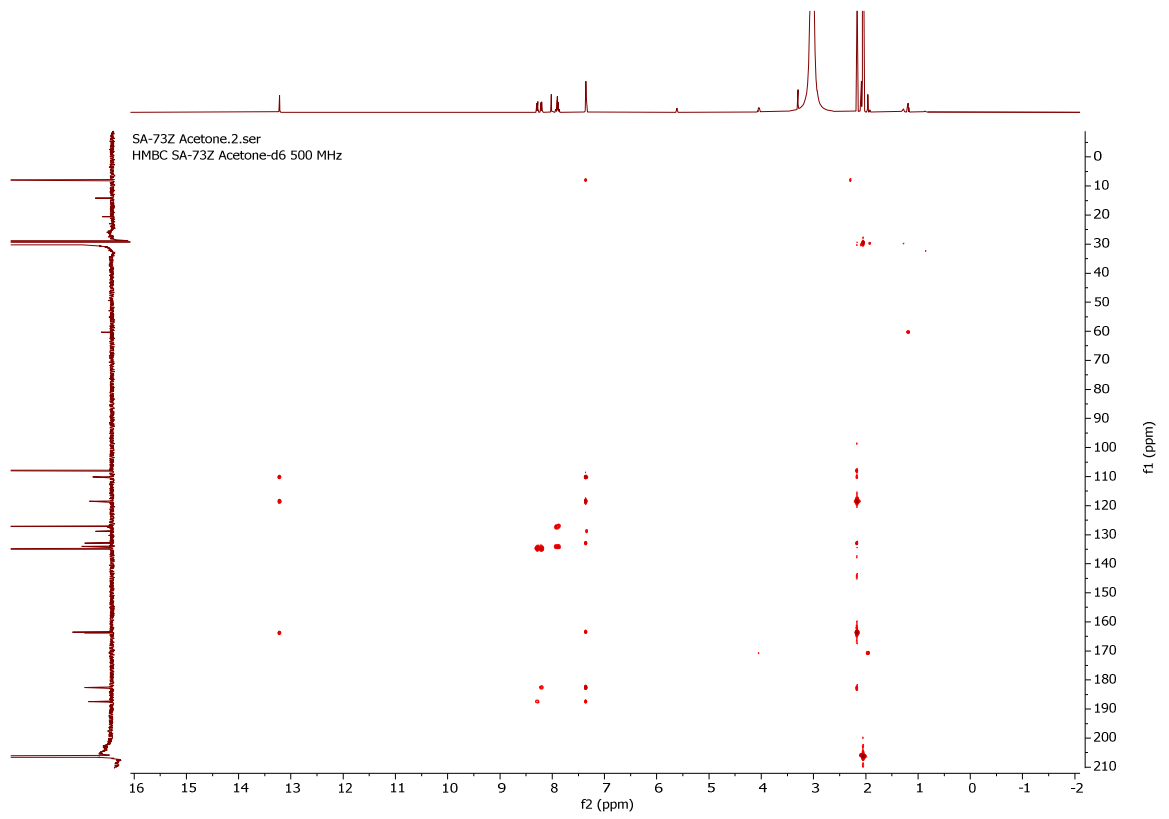
APPENDIX 13.4: ES-MS Spectrum for Rubiadin

150
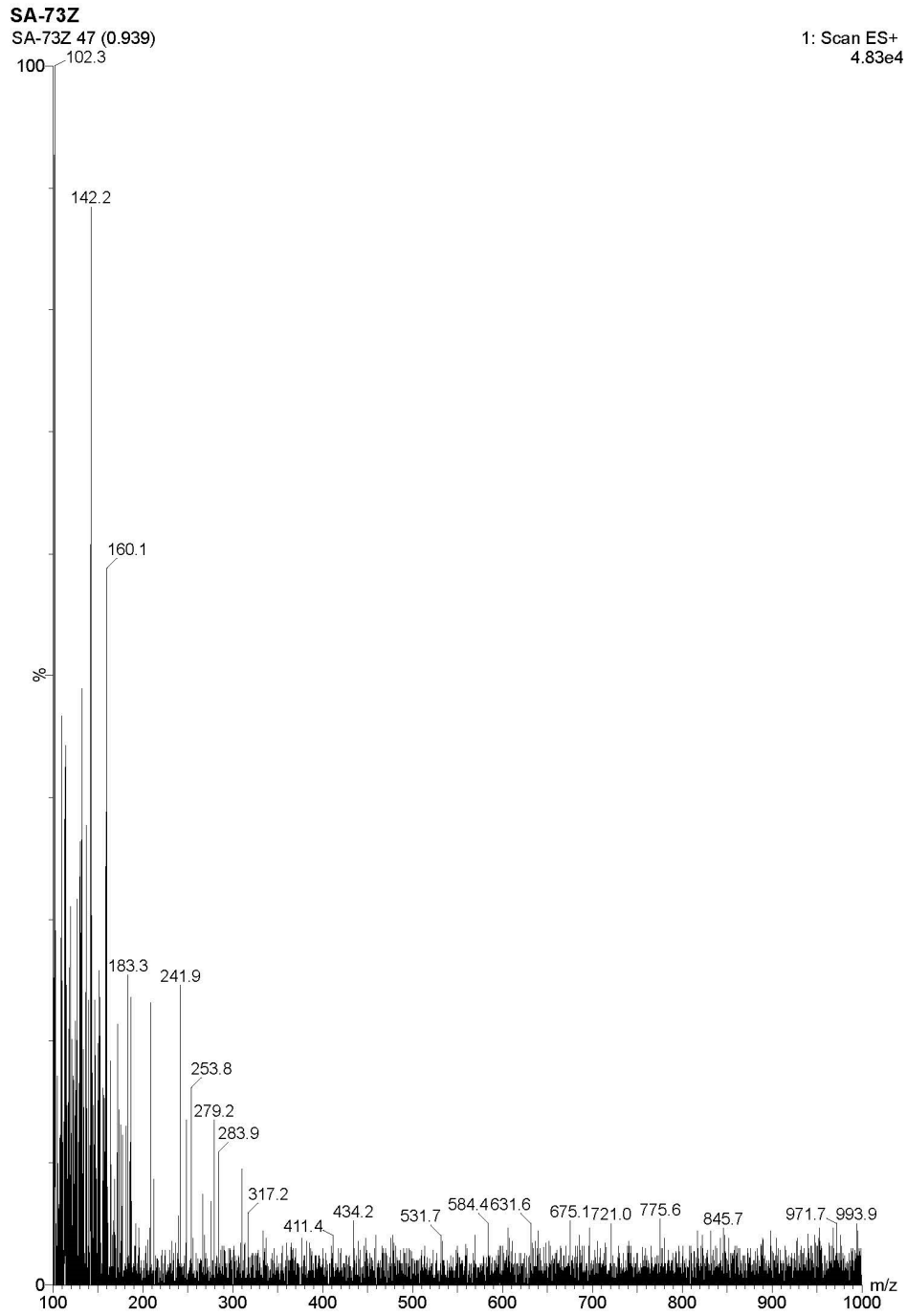
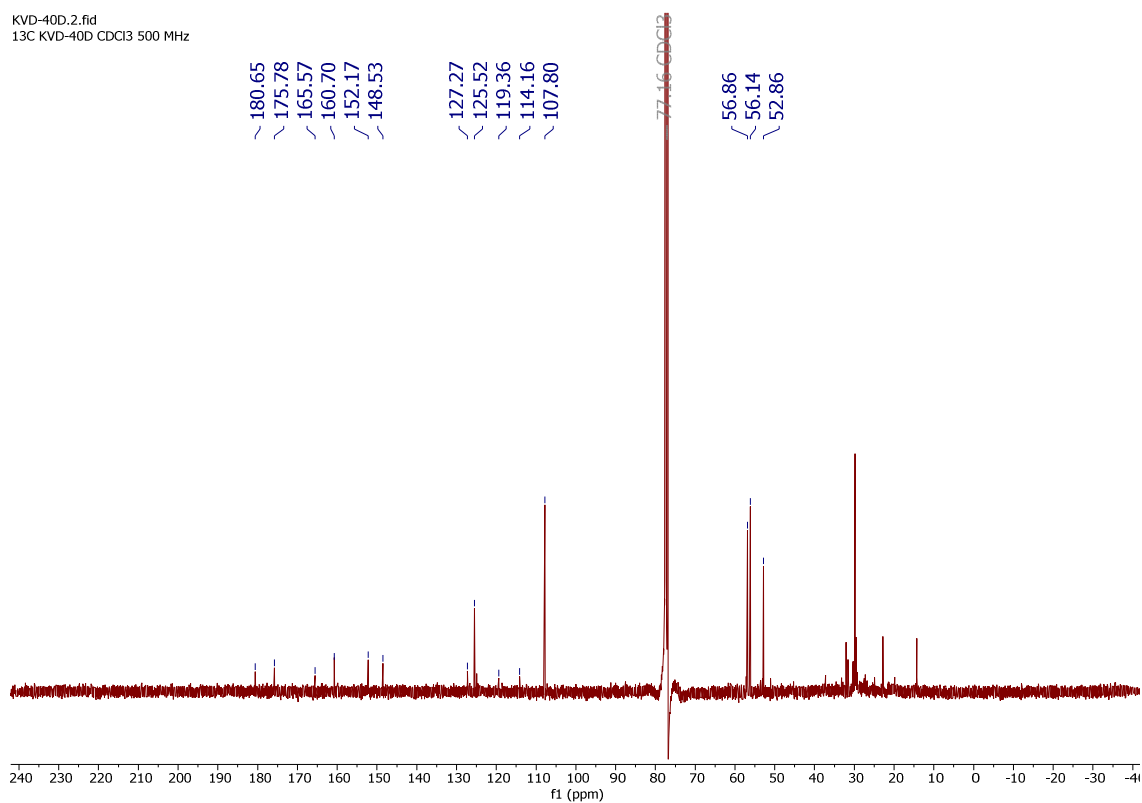APPENDIX 14.0: ^{1}H NMR Spectrum of Compound **99** (CDCl$_3$, 500 MHz)
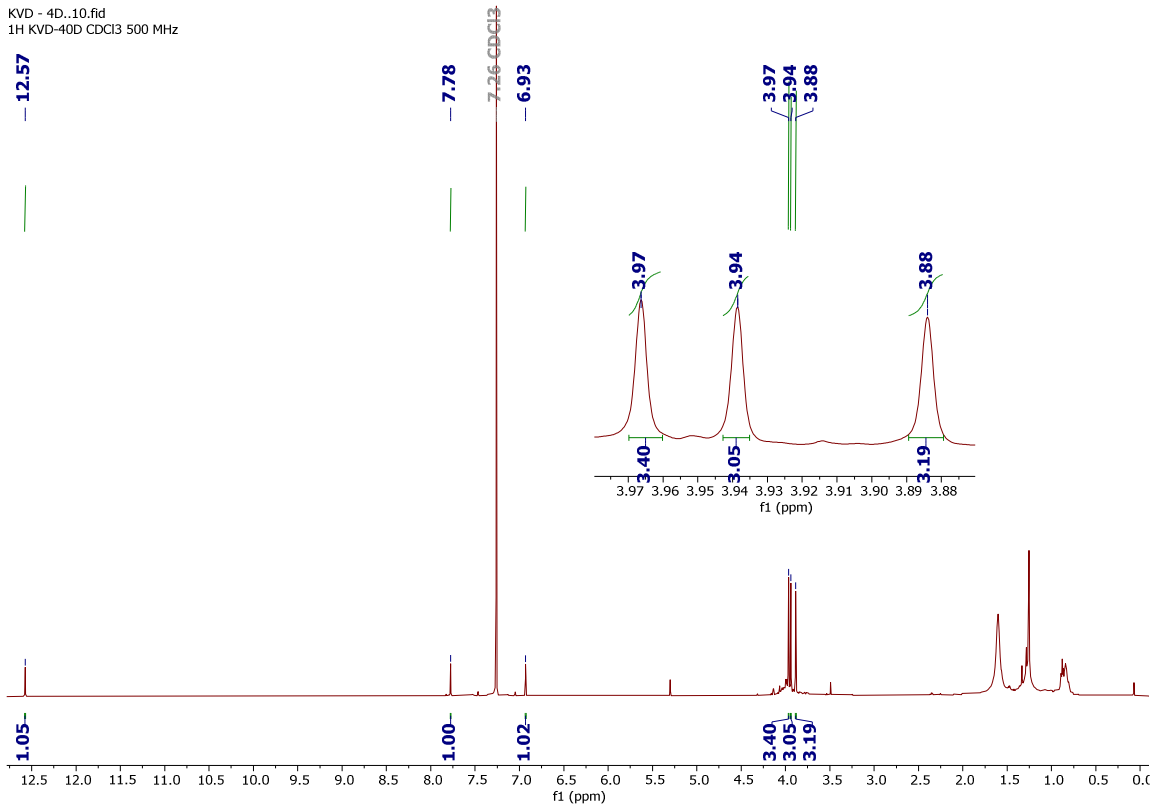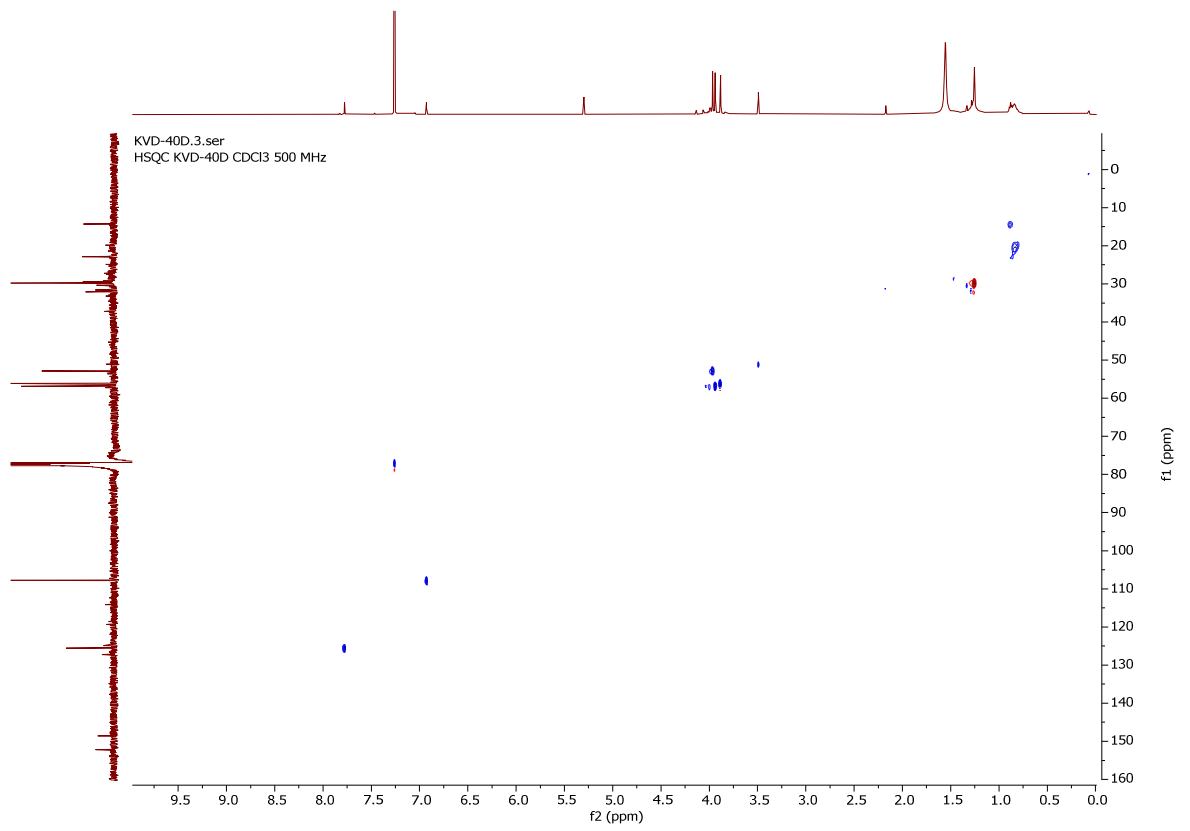
APPENDIX 14.1: ^{13}C NMR Spectrum of Compound **99** (CDCl$_3$, 500 MHz)

KVD-40D.2.fid
13C KVD-40D CDCl3 500 MHz

152

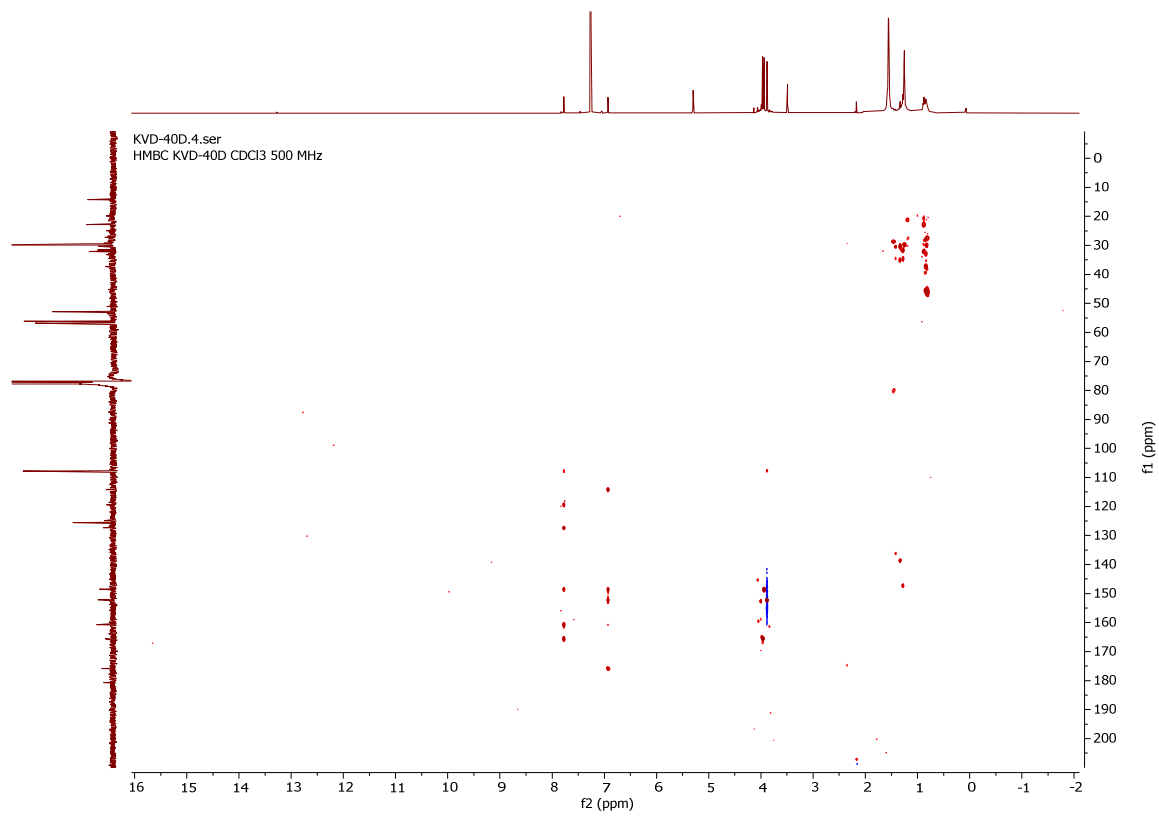APPENDIX 14.2: HSQC Spectrum of Compound **99** (CDCl$_3$, 500 MHz)
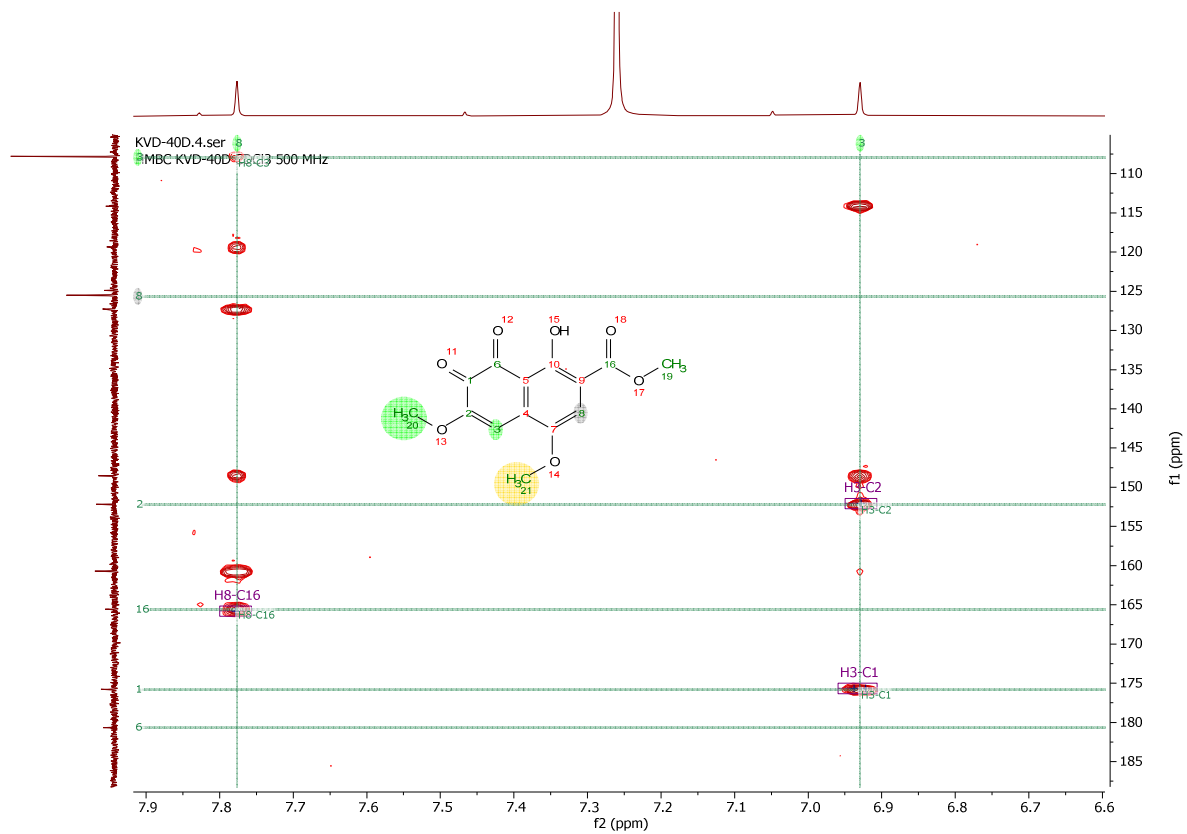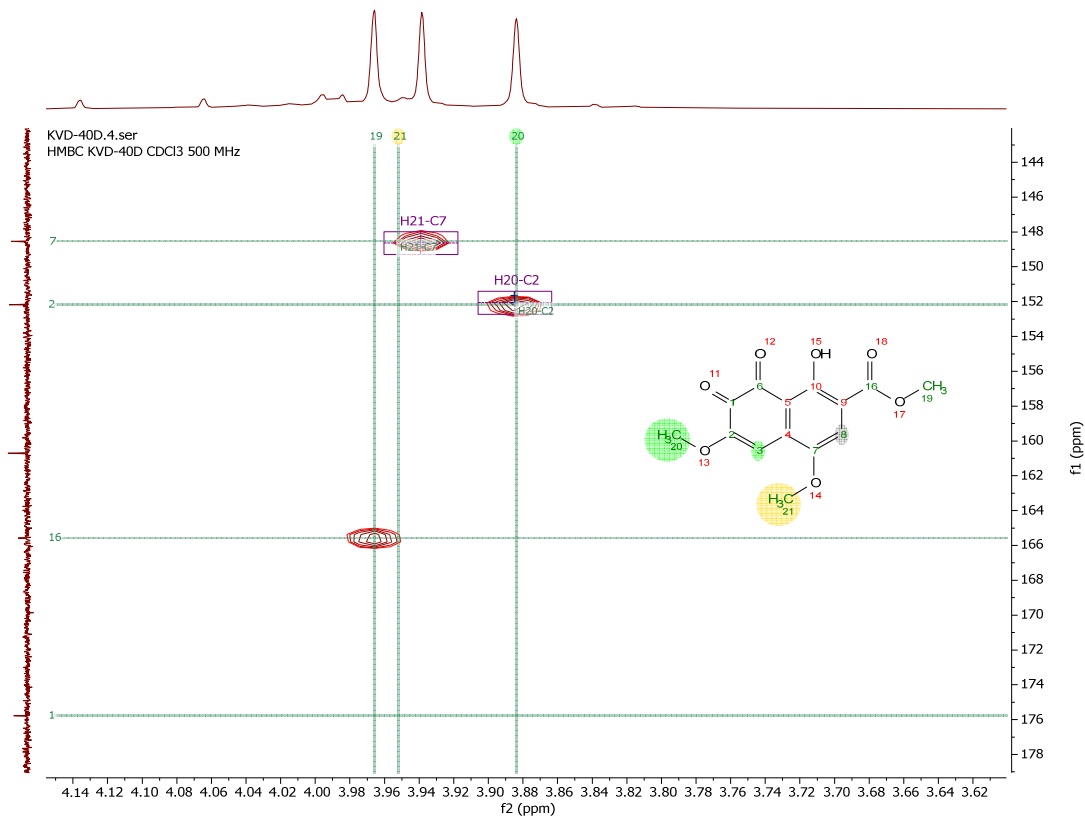

KVD-40D.3.ser
HSQC KVD-40D CDCl3 500 MHz

APPENDIX 14.3: HMBC Spectrum of Compound 99 (CDCl$_3$, 500 MHz)

APPENDIX 14.4: HMBC Spectrum of Compound **99** for Aromatic Region

APPENDIX 14.5: HMBC Spectrum of Compound **99** for Methoxy Groups

APPENDIX 14.6: ESI-MS Spectrum for Compound **99**

KVD-40D
KVD-40D 42 (0.838)   1: Scan ES+
                                                                                        5.84e4

100₁ 142.2

%

         159.0

              160.1
                 164.2
                    183.0   291.6
                 237.2
                        329.3
                           379.4   459.5   526.9   572.9   650.0   801.2 839.8 873.9   989.5
                                                                     761.9
0
    100   200   300   400   500   600   700   800   900   1000
                                                                      m/z

157